THEORETICAL STU[illegible]

OF THE ELECTRONIC NATURE

OF NON-STOICHIOMETRIC METAL HYDRIDES

by

Philip Anagnostaras

A thesis submitted to the Faculty of Science, University of the Witwatersrand, Johannesburg, for the degree of Doctor of Philosophy.

Johannesburg
March 1986

Ackrowledgements

First and foremost I wish to thank my supervisor Professor Ted Lowther for the consistency of his insight and wisdom, and especially his encouragement, without which this work would not have been possible. I am grateful to Dr. L. Schlapbach for valuable correspondence concerning his recent photoemission results, and also to Dr. Tony Andriotis for helpful and enthusiastic discussions, in particular those concerning the two-phase configurational entropy.

My thanks to Mrs. Tammy Main for her accurate typing, to Mr. Ray Smith for his extensive work on the figures, and to all those others whose encouragement has inspired me.

I finally wish to thank the CSIR (Pretoria) and the University of the Witwatersrand for the award of postgraduate bursaries.

DECLARATION

I declare that except where specifically acknowledged, this thesis is my own, unaided work. It is being submitted for the degree of Doctor of Philosophy at the University of the Witwatersrand, Johannesburg. It has not been submitted before for any degree or examination at any other University.

PHILIP ANAGNOSTARAS
(Name of Candidate)

P. Anagnostaras
(Signature)

7TH day of MARCH, 1986.

DECLARATION

I declare that except where specifically acknowledged, this thesis is my own, unaided work. It is being submitted for the degree of Doctor of Philosophy at the University of the Witwatersrand, Johannesburg. It has not been submitted before for any degree or examination at any other University.

PHILIP ANAGNOSTARAS
(Name of Candidate)

P Anagnostaras.
(Signature)

7TH day of MARCH, 1986.

ABSTRACT

A Cluster-Bethe-Lattice model is formulated which approaches non-stoichiometric transition metal hydrides from the viewpoint of local atomic environment and incorporates the short-range order characteristic of such systems. Analytic expressions for the Local Densities of States are derived, facilitating detailed examination of the band structure of the hydride as well as extensive charge and electronic energy calculations. This approach is developed to provide a physically sound and computationally practical alternative to existing theoretical techniques, which usually fall into one of two categories, viz. excessively simplistic on the one hand and physically inappropriate and computationally restrictive on the other. Our model is applied to non-stoichiometric palladium hydride (PdH_x, $0 < x < 1$), where good agreement is found between our computed Local Densities of States and sophisticated band structure calculations and photoemission experiments. Heats of formation evaluated using our Local Densities of States agree fairly well with experiment for $x \geq 0.5$ but not for lower concentrations. We therefore extend our model to a two-phase formalism which not only substantially improves upon our heats of formation for $x \leq 0.5$, but which also qualitatively predicts the higher concentration phase transition of the hydride. The physical validity of the two-phase model is confirmed by the fact that it significantly improves upon our original formalism in the experimentally-established two-phase region of the hydride ($0.01 \leq x \leq 0.6$ at room temperature). Consideration of the underlying physical assumptions of

our models indicates that the β-phase hydride ($x \geq 0.6$) consists of a random distribution of hydrogen in the palladium lattice whereas the two-phase region is characterized by phase segregation at a microscopic level.

Finally, both our formalisms are employed to model the pressure-composition isotherms of the palladium-hydrogen system. The one-phase model is only successful for $x \geq 0.7$, that is well within the β-phase region, whereas the two-phase formalism produces isotherms in good qualitative agreement with experiment for $x \geq 0.2$, that is over most of the two-phase region in addition to the β-phase regime.

CONTENTS

LIST OF TABLES

LIST OF FIGURES

[+] Local Density/ies of States

[‡] parameter set (a.1)

CHAPTER 1

INTRODUCTION, LITERATURE REVIEW AND AIMS

1.1 INTRODUCTION

The literature review which follows this introduction will focus mainly on the key words of the title of this work, viz. "electronic nature", "non-stoichiometric" and "metal hydrides". We have decided from the outset to concentrate our attention on *palladium* hydride, for the following reasons:-

1) it is fundamentally non-stoichiometric (PdH_x, $0 \leq x \leq 1$);

2) there is a rich theoretical literature for the electronic nature of both Pd and PdH (PdH_x with x = 0 and 1 respectively), which gives us two well-known extreme cases as reference points for a truly non-stoichiometric theory;

3) to quote Wicke and Brodowsky[1.1] p.73:"Palladium hydride represents one of the most transparent and instructive models for a metal-hydrogen system from structural, thermodynamic, and kinetic points of view... Nevertheless, *there are quite a number of details* in the mechanism of hydrogen diffusion as well as *in the behaviour of electronic states* in this system *not yet fully understood*" (our italics).

From this we appreciate the fact that a successful model for the palladium-hydrogen system is likely to give us important guidelines for understanding

a variety of other metal hydrides. It is also noteworthy that despite the considerable literature on the electronic nature of palladium hydride, there is still a distinct need for further contributions in this area.

It is for these reasons, in particular the understanding of palladium hydride as a "test case" for other metal hydrides, that we have been reluctant to entitle this work "Theoretical study of the electronic nature of non-stoichiometric *palladium hydride*"; we believe that the techniques developed here can easily be extended to other metal hydrides, at least to those of transition metals such as nickel and titanium. We nevertheless choose here to confine ourselves to palladium hydride so as not to obscure the main thrust of this work with excessive detail.

1.2 LITERATURE REVIEW

1.2.1 Introduction: A Polarization of Approaches

Interest in palladium hydride (PdH_x) goes back to the 1860s when palladium metal became available in sufficient quantities for experimentation. Graham[1,2] soon discovered that Pd absorbed large quantities of hydrogen. Since then a considerable experimental literature has accumulated concerning the absorption of hydrogen by palladium, with a particular interest being shown in hydrogen pressure versus hydrogen concentration (x) isotherms. These results have tended to be interpreted within simple semiempirical formalisms, and with the aid of physically transparent but rather simplistic electronic theories such as the Rigid Band Model (to be discussed below).

At the other extreme there is also a large theoretical literature, which approaches Pd and PdH (and occasionally, fairly simple intermediate cases, for example $PdH_{0.5}$) mainly from the viewpoint of sophisticated band structure calculations. These techniques are able to generate accurate band structure, charge and energy data for the limited cases of hydrogen concentration to which they are applied. However, three problems arise concerning band structure calculations: firstly, they require considerable computational resources; secondly, they make use of large numbers of fitting parameters which lack clear physical meaning; and thirdly, they are based on *periodic* crystal potentials and Bloch's theorem, which are physically inappropriate for non-stoichiometric (and hence essentially *disordered*) materials. This last drawback can to some extent be compensated for by using Bloch-like functions with finite decay-lengths[1,3], but this enhances the computational difficulties. The second problem will be

discussed in detail in Section 3.3 and Appendix 1; it is due in essence to the fitting of a large number of parameters to energy levels generated by, for example, the APW method. These energy parameters are by no means unique, and often bear little resemblance to atomic parameters (such as ionisation potentials and electron affinities).

Another theoretical approach involves the study of an isolated hydrogen "impurity" in the palladium lattice by means of a screened Coulomb or similar potential centred on the impurity. These techniques emphasize the localized electrostatic features of the system, and hence free one of the requirement of a periodic potential, but have limitations of their own: they are only good approximations for low concentrations of hydrogen (since the impurity is taken to be isolated); and they are highly sensitive to the techniques used in evaluating the screening parameter. Further, an accurate determination of this parameter can lead to a computationally-expensive self-consistent calculation.

In summary, then, we note a polarization in the theoretical study of PdH_x, with semiempirical and often simplistic theories being used on the one hand and sophisticated but cumbersome and often opaque techniques being applied on the other. In the light of this we can more fully appreciate a theory with the following attributes: it takes advantage of sophisticated calculations by incorporating a few simple parameters generated by them; it is based on a formalism which does not require a periodic lattice, with the result that it copes with non-stoichiometric compounds as naturally as with stoichiometric ones; it is more sophisticated than models such as the Rigid Band Model, yet simple enough to use for extensive energy calculations which can be compared directly with experiment. These are all features of the model which we will develop in subsequent chapters.

The literature review that follows is intended to provide the reader with a clear appreciation of the strengths and weaknesses of a selection of theoretical (mainly electronic) approaches that have been applied to PdH_x; the aim throughout is to emphasize the above-mentioned polarization of these approaches into essentially two camps. The topics and papers reviewed are for the most part in chronological order so as to give a feel for trends in the research; they have been chosen because of their relevance to the present work (themes to be taken up and foundational information). The relevant experimental papers have not been reviewed, but can easily be followed up through the references.

1.2.2 *Semiempirical Electronic Models*

Possibly the simplest model of the Pd/H system is the *pseudo-silver hypothesis* proposed by Oxley[1.4] and Vogt[1.5], based on the observation of similar decreases in the magnetic susceptibility of Pd as a function of both (substitutional) silver content and (interstitial) hydrogen content. Hence, this approach approximates a Pd/H pair to a single Ag atom (the Pd/H pair and the Ag atom being isoelectronic). The approximation is supported by certain X-ray crystallographic studies[1.6], and by evidence that hydrogen solubility in Pd/Ag decreases linearly with Ag content under certain circumstances[1.7]. However it has been shown[1.7] that this observation of linear dependence breaks down seriously over wide ranges of hydrogen pressure. In addition, Faulkner[1.8] has shown using his Coherent-Potential Approximation (CPA) calculations that the density of states of the (substitutional) Pd/Ag alloy is markedly different to that of the corresponding (interstitial) Pd/H system.

A modification of the pseudo-silver hypothesis is the so-called *proton model*. This model assumes that the hydrogen is centrally situated in interstitial sites in the Pd lattice, so that a hydrogen atom cannot be considered bound to any single Pd atom; rather, the hydrogen atoms

donate their electrons to the Pd band as a whole, leaving interstitial protons. There is some experimental evidence that hydrogen is present in a positively-charged form[1.9].

The proton model leads in a natural manner to the *Rigid Band Model*[1.10] (RBM). This is based on the observation that a number of electronic properties of PdH_x undergo significant changes for $x \approx 0.6$, for example the disappearance of paramagnetism[1.11]&[1.12] at this hydrogen concentration. The interpretation originally given to this phenomenon was that the Pd 4d band had 0.6 holes in it, so that by applying the proton model the 4d band would be filled at $x \approx 0.6$. The Rigid Band Model was then introduced to further quantify this concept; in the RBM formalism Pd is assumed to have two valence bands in its DOS, a high-density 4d band overlapping with a low-density 5s band at higher energies. It is further assumed that these bands do not change shape with addition of hydrogen electrons, that is, the bands are taken to be "rigid". As electrons are added, the Fermi energy (E_F) increases, at first slowly (in the high-density 4d band) and then rapidly (once E_F enters the low-density 5s band at $x \approx 0.6$). However, measurements of the de Haas-van Alphen effect on pure Pd performed by Vuillemin and Priestley[1.13] have shown that the 4d band contains only 0.36 ± 0.01 holes. This finding firstly undermines the proton model, as the following argument will reveal. Faulkner's CPA calculations[1.8] show that each hydrogen electron added to the palladium lattice is divided between a palladium and a hydrogen atom in the ratio of 3 to 2 respectively and that this ratio remains fairly constant with x. Therefore each Pd atom in PdH_1 gains roughly 0.6 electrons, and hence each Pd in $PdH_{0.6}$ gains approximately $0.6 \times 0.6 = 0.36$ electrons, in agreement with experiment[1.13]; it thus seems reasonable to assume that

Faulkner's 3:2 split of charge between Pd and H is a good approximation. We note however that the proton model requires that the entire electron be donated to Pd, that is it assumes a 1:0 split of charge between Pd and H, and hence this model becomes at least quantitatively incorrect.

Secondly, the occurrence of only 0.36 holes in the 4d band presents a problem for the RBM, which was formulated on the assumption of 0.6 hole in the palladium 4d band. By considering screening effects the RBM can be adapted to allow for this discrepancy[1.14]; the adaptation involves having a 5s band which is shifted downwards with increasing charge, so that this band "absorbs" the extra 0.24 (that is, 0.60 - 0.36) electron. In the resulting model the bands are no longer rigid relative to each other, so we now have a *Screening-Induced Band-Shift*[1.1] p.133 *Model* (SIBSM).

Although the SIBSM has had some success in explaining certain resistivity[1.15] and electronic heat capacity[1.16] experiments on Pd/Ag alloys, the CPA calculations of Faulkner[1.8] and the APW calculations of Switendick[1.17] and others have shown conclusively that not only do the palladium bands undergo distinct changes of shape with the addition of hydrogen electrons, but also that a hydrogen-induced band begins to form *beneath* the 4d band. Thus both the RBM and SIBSM are physically oversimplistic, as is reflected by their limited ability to consistently explain experimental data.

Summary: Semiempirical Electronic Models

We are led to the conclusion that the electronic structure of PdH_x requires more complex models than the four semiempirical approaches so far discussed. We shall therefore review some of the less phenomenological approaches that have been used.

1.2.3 *Switendick*[1.17] *(1972)*

We start with Switendick's APW calculations for palladium and some of its hydrides. He takes Pd to have the structure $4d^9 5s^1$ as opposed to the $4d^{10}5s^0$ configuration favoured by Mueller et al[1.18], so as to model the partially-filled 5s band ($4d^{9.64}5s^{0.36}$) revealed by experiment[1.13]. Pd metal has the fcc structure, and he uses the lattice constant a = 3.89 Å. The usual Muffin-Tin (MT) approximation is used for the potential, with the MT spheres touching. He obtains a fairly narrow 4d band (about 5 eV across) for pure Pd, overlapped by and hybridized with a wide plane-wave-like 5s-p band (≈ 10 eV across), with E_F in a high DOS region near the top of the d band. For PdH he makes the usual assumption of an NaCℓ-type structure (see Section 1.2.7) with a = 4.03 Å (the lattice constant for β-*phase* palladium hydride: see Section 1.2.4). The palladium MT spheres are no longer taken as touching in the stoichiometric hydride, since this would leave insufficient space for the hydrogen MTs; the Pd and H MTs are instead taken as touching, and have respective radii of 65% and 35% of the Pd/H separation. The resulting calculations reveal that the palladium d band is only slightly affected by hydride formation, whereas the s-p band changes significantly; in particular, states which allow s-like character in the hydrogen MT sphere are lowered considerably in energy, so that an s-like band is formed *below* the d bands.

Thirdly, Switendick has applied his APW model to the *ordered* structure Pd_4H_3; this is to approximate the behaviour of $PdH_{0.75}$, which in reality has *random* hydrogen occupation of the available interstitial sites. The difficulty here relates back to our observation in Section 1.2.1 concerning

the inapplicability of BS calculations to random (and hence disordered) systems; as Switendick comments:"we have assumed an ordered arrangement, since the disordered calculation is beyond any reasonable computational means"[1.17]p.538. In the same context he also indicates his belief in the importance of nearest-neighbour atoms (that is, *local environment*) in the determination of energy states; this is an important issue which will emerge more clearly later. For the case of Pd_4H_3 and then Pd_4H he again finds that states which are s-like around the hydrogen site are lowered, though less in the case of Pd_4H. On the basis of this he suggests that for infinite dilution part of an added hydrogen electron helps fill the d band and part goes to the lowered states.

Summary : Switendick (1972)

In his conclusion Switendick emphasizes that the significant qualitative differences he obtains in his various DOS show that the RBM does not apply. On the basis of the sophistication of his model we take this to be an accurate comment; however, we note in the context of model complexity (Section 1.2.1) that his approach makes use of 29 parameters which are used to fit 46 APW states (evaluated at high-symmetry points), in addition to MT radius parameters. Switendick points out that his calculations assume an ordered topology for PdH_x, since the disordered calculation would not be computationally feasible. He also comments on the importance of the local environment in determining the energy states of the system. A striking feature of his BS results is the appearance in the hydride of an s-like band below the d bands.

1.2.4 *Faulkner*[1.8] *(1976)*

We next consider Faulkner's CPA calculations for Pd, PdH and a number of substoichiometric compounds (PdH_x, $0 < x < 1$). He notes the essential randomness of the hydrogen sublattice at the outset; the CPA is in fact used because of its efficacy in modelling a class of essentially random systems viz. binary alloys[1.19]. Nevertheless, his model is still based on a *periodic* Hamiltonian; specifically, he has made use of the elaborate first-principles BS calculations of Papaconstantopoulos and Klein[1.20] (viz. self-consistent APW calculations including relativistic corrections). As is common practice, these BS calculations were carried out only for high-symmetry points in the Brillouin zone, and Faulkner thus follows the usual procedure of setting up an interpolation scheme between these points; specifically, he applies the well-known tight-binding scheme of Slater and Koster[1.21] (Switendick's 29 parameters mentioned above are the consequence of a related interpolation method). Faulkner uses 13 interpolation parameters for Pd and 17 for PdH, roughly half the number used by Switendick. The sacrifice of detail is to facilitate the CPA calculations, which require iterative solutions to a set of matrix equations.

His results confirm those of Switendick's in their essential features: firstly, a narrow ($\approx$ 5 eV), high-density d band for pure Pd and its hydrides; secondly, the lowering of the lowest-lying band in Pd to what Faulkner calls a palladium-hydrogen bonding band; and thirdly, E_F falls in a range of high DOS (at least in the cases below $x \approx 0.7$). Specifically, he points out from his DOS plots that no single band in his BS can be thought of as a purely hydrogenic band; also that the DOS is clearly

a function of hydrogen concentration. Hence he establishes the point (already emphasized by Switendick) that no RBM is acceptable for the Pd/H system.

He further addresses the issue of the *two-phase nature* of PdH_x: for $0.6 \leq x \leq 1$ this compound is in the so-called β-phase, which is usually described as having the NaCℓ structure, the vacancies being randomly-distributed on the hydrogen sublattice. His model is built upon this random one-phase concept; however, for $x \leq 0.6$, the β-phase is in equilibrium with the (much more dilute) α-phase, that is, we have a two-phase system. Faulkner concedes that his model is therefore suspect over this range of concentrations.

Summary: Faulkner (1976)

We see then that Faulkner's work has introduced the concept of randomness through application of the CPA, but that it is still bound within the framework of BS formalism and hence an implicitly ordered lattice. He addresses the issue of multiple phases in the Pd/H system, pointing out that strictly his model only holds in the β-phase region ($x \geq 0.6$). He has produced useful results for a range of Pd/H compounds, though we note again the large number of parameters (13 to 17) required by the BS interpolation scheme alone, as well as the need for iterative solution of the CPA equations in order to obtain the DOS. With specific reference to the application of the CPA to the disordered hydrogen sublattice, we note that Faulkner's formalism avoids the necessity of dealing with off-diagonal disorder[1,22]. We note however that the system does in fact have this kind of disorder, and hence a model which could comfortably

include it in its formalism would have enhanced physical value. It will be seen in subsequent chapters that our formalism results in just such a model.

Finally, Faulkner finds that in the hydride a band develops below the d bands, which he relates to the bonding of the hydrogen to the palladium ; this finding agrees closely with Switendick's results.

1.2.5 *Papaconstantopoulos et al*[1.23] *(1978)*

This work is an extension of Faulkner's CPA study (Section 1.2.4). The authors apply Faulkner's CPA technique as in his own work, but make better use of it by implementing a more sophisticated Slater-Koster Hamiltonian (see Section 3.3) with which to fit their APW band structure calculations for Pd and PdH.

They use the same basis functions as Switendick[1.17], viz. five d orbitals, three p orbitals and one s orbital for Pd, plus an extra hydrogen s orbital for PdH, but increase the sophistication and consequently the accuracy of the Slater-Koster interpolation scheme by including third-nearest neighbour interactions (cf Switendick, who considered second-nearest neighbours, and Faulkner, who only considered nearest neighbours). The consequence for PdH is that the number of parameters is increased from 29 in Switendick's case and 17 in Faulkner's case to 41 in their case. Using these 41 parameters the authors solve their CPA equations and hence generate the total DOS. They then drop the three Pd-H overlap parameters and find that the DOS change by no more than a few percent, so that they are left with 38 parameters for PdH (and 32 for pure Pd). The parameters are evaluated using a nonlinear least-squares technique, in which the

authors fit 111 and 127 energy values from their APW calculations for Pd and PdH respectively.

An important finding of this work is that the constituent DOS (s, p and d) are highly sensitive to the particular APW energy states fitted by the Slater-Koster scheme (though the *total* DOS is found to be much less sensitive in this regard). More specifically, they note the need for compatibility between the basis orbitals chosen and the APW states fitted; for example, the presence of higher-energy p orbitals in the basis set requires that the energies fitted include p states which are high in energy.

The authors calculate the constituent and total DOS, as well as the Fermi energy (E_F), for x = 0.0, 0.1, 0.2,....., 1.0; they also present a table of the various DOS, calculated at E_F, for these eleven x values. A striking feature is that the total DOS at E_F is dominated by contributions from the d bands, with the DOS of the s and p bands at E_F being small by comparison; in other words, E_F falls in an energy region of predominantly d-like character. This result is expected for pure transition metals, and hence their calculations indicate that even in the stoichiometric hydride the metallic behaviour dominates at E_F. The constituent and total DOS are also plotted as functions of energy for the cases x = 0.6, 0.8 and 1.0. As with both Switendick and Faulkner, we see the emergence of a hydrogen-related band below the palladium d bands.

The authors also comment on the subject of phases; they are confident of the accuracy of their model in the high-concentration, single-phase region (β-phase, $x \geq 0.6$). However they are less confident in the lower-concentration two-phase regime, for two reasons: firstly, they expect the two-phase regime to be dominated by *short-range order* phenomena, that is, by effects of *local environment* (cf their band structure approach, which is built on the principle of *long-range order* as found in crystals); and secondly, as x becomes smaller, the use of the PdH_1 Slater-Koster parameters becomes increasingly less valid.

Summary: Papaconstantopoulos et al (1978)

This paper is an extension of Faulkner's work and hence the summarizing comments at the end of Section 1.2.4 also apply here. The authors' results are more accurate than those of Faulkner, although we note that the number of energy parameters is more than doubled (38 parameters for PdH_1, as opposed to 17 in Faulkner's case).

The authors further extend Faulkner's work by calculating the constituent DOS (s, p and d) of PdH_x for $x = 0.0, 0.1, 0.2, \ldots\ldots, 1.0$. In particular, they tabulate the various DOS values at E_F, which gives us the result that E_F falls in a part of the band structure dominated by d bands. This is significant since it indicates that the electronic properties of the hydride at E_F are dominated by metallic contributions.

The two-phase behaviour of the hydride is also commented on, with a reminder that this model is only strictly valid in the high-concentration, single-phase regime. There are two reasons for this: firstly, the two-phase region is characterized by *short-range* (and hence *localized*) order

phenomena, whereas their BS-based approach assumes long-range crystalline order; and secondly, the use of the PdH_1 Slater-Koster parameters becomes increasingly less valid as x decreases.

1.2.6 *Gelatt et al*[1.24] *(1978)*

We now move on to the study of various transition metal hydrides by Gelatt et al, in which the authors focus their attention on Pd, PdH_1 and various substoichiometric compounds PdH_x ($0 < x < 1$). As with Switendick they use the APW method (though only for the metals and their stoichiometric hydrides), and like Faulkner and Papaconstantopoulos et al they treat the non-stoichiometric hydrides as disordered alloys with hydrogen distributed randomly over the one fcc sublattice, the other sublattice being entirely occupied by palladium atoms. Instead of the CPA they use the Average T-Matrix Approximation[1.25] (ATA) for the non-stoichiometric cases, in conjunction with the Korringa-Kohn-Rostoker (KKR) BS method (see Appendix 1.1 for a brief comparison of the CPA and ATA techniques). They note in this regard that although the correct *random* calculations could have been performed in the non-stoichiometric cases this would have resulted in an unwarranted increase in computational complexity.

Their BS results are similar to those of Switendick, Faulkner and Papaconstantopoulos et al; in particular, we note the following points: firstly, for small values of x a new band appears below the Pd d bands, which they associate with the formation of a Pd/H bond (this new band is in fact *flat*, that is it represents a discrete energy level, which

would show up as a delta function on a DOS plot. As x increases the level "broadens" into a true band); and secondly, the d bands are largely unaffected by increasing x, except that they are *shifted* slightly downwards in energy.

Gelatt et al are the first to have done *damping-of-states* calculations for the Pd/H system. Damping is essentially the "blurring" or broadening of energy bands as a result of electronic scattering from the randomly-occupied hydrogen sublattice. They observe that states having s-like symmetry about the interstitial hydrogen atom/proton (that is, the basis orbitals have finite amplitude at this point) are strongly damped, as well as shifted in energy, whereas orbitals with a node at this site are largely unperturbed by the introduction of hydrogen. This intuitively-sensible result is in agreement with Switendick's findings discussed above, and shall be further verified in Chapter 3.

This paper also contains work on the *heats of formation* (ΔH) of *stoichiometric* monohydrides, including PdH, where the aim is to reproduce trends across the 3d and 4d rows of the periodic table rather than to give precise results. They use the following equation:-

$$\Delta H_1 = \Delta E_1 - \tfrac{1}{2} E(H_2) \qquad (1.1)$$

where $E(H_2) = -2.266$ Ryd (hydrogen ionisation energy), and for PdH,

$$\Delta E_1 = 2(\langle\epsilon_{LB}^{PdH}\rangle - \langle\epsilon_{LB}^{Pd}\rangle) + 8(\langle\epsilon_{d}^{PdH}\rangle - \langle\epsilon_{d}^{Pd}\rangle) + \epsilon_{F}^{Pd} \qquad (1.2)$$

"$\langle\epsilon_{LB}^{PdH}\rangle$" is the *average* energy of the lowest band (LB) of PdH,

"$<\varepsilon_d^{PdH}>$" is the average energy of the four remaining d-bands of PdH (two electrons per band) and "ε_F^{Pd}" is an *absolute* number giving the contribution due to the addition of a hydrogen electron at E_F (this last term makes the resultant ΔH_1 values very sensitive to the choice of the crystal potential zero). Equations (1.1) and (1.2) successfully model the trends for ΔH_1 across the 3d and 4d rows, giving a reasonable estimate for PdH_1.

In addition, Gelatt et al made Coulomb corrections to these ΔH_1 values, and though these are considerable for the early transition metals such as Y, Zr and Nb (due to the presence of more than one electron per hydrogen site), the correction for PdH is minimal.

Summary: Gelatt et al (1978)

Like Faulkner and Papaconstantopoulos et al, Gelatt et al have appreciated the random nature of the Pd/H system but have nevertheless modelled it within the framework of BS (and hence ordered) theory; they also remind us of the computational restrictions on a truly random non-stoichiometric BS calculation, even with application of a non-self-consistent disorder model such as the ATA. Their calculations of the heats of formation of stoichiometric monohydrides, including PdH_1, are based on a physically transparent model which makes use of an average-energy concept; they have not here evaluated the heats of formation for non-stoichiometric hydrides. Again the formation of a new band below the d bands is reported, and again it is related to Pd/H bonding. It is further noted that for low concentrations x this band is flat, which gives rise to a delta function (bound state) in the DOS.

1.2.7 *Sholl and Smith*[1.26)-1.28)] *(1977-78)*

We turn now to isolated-impurity models for the Pd/H system, in which the hydrogen is treated as an isolated interstitial impurity in the host Pd lattice; such models take *electrostatic* effects into account, which are not considered in BS methods. We shall consider the work of Sholl and Smith[1.26)-1.28)], which also takes BS considerations into account; their model is based on the Green's function technique of Riedinger[1.29)] and the BS interpolation scheme of Hodges *et al*[1.30)]. Prior to Sholl and Smith all the applications of these techniques were to *substitutional* impurities in noble and transition metals; the extension to interstitial impurities gives a more complex formalism which requires further approximations[1.27)].

Sholl and Smith start by applying the parameterized expressions of Ehrenreich and Hodges[1.31)] to the APW BS calculations of Mueller *et al*[1.18)] and Switendick[1.17)] for pure Pd metal. The consequence in each case is a 14-parameter interpolation scheme, from which the integrated DOS (proportional to charge) of the *perturbed* system is determined by statistical techniques. By appropriate manipulation of the integrated DOS[1.26)], the change in *BS energy* (ΔE_{bs}) due to addition of the isolated hydrogen impurity, is calculated. They proceed to derive an expression for ΔE_{es}[1.26)], the change in *electrostatic energy* due to addition of chis impurity. This requires knowledge of $\Delta\rho(r)$, the change in charge density at the interstitial, and v(r), the Coulomb potential energy due to the addition of the impurity. $\Delta\rho(r)$ and v(r) are related via Poisson's equation, viz:-

$$\nabla^2 v(r) = -4\pi \Delta\rho(r) \qquad (1.3)$$

Sholl and Smith point out that equation (1.3) should be solved self-consistently to obtain both $v(r)$ and $\Delta\rho(r)$, but remark that this would not be computationally feasible. Hence they have approximated $v(r)$ to a screened Coulomb potential[1.26),1.27)], viz:-

$$v(r) = e \exp(-\beta r)/r \qquad (1.4)$$

where β is the inverse screening length and is evaluated[1.27)] so as to satisfy both the Friedel Sum Rule (which is essentially a charge conservation requirement) and the assumption that the hydrogen only interacts with its nearest neighbours (that is, β must be sufficiently large to "kill off" the potential before second-nearest neighbours are reached).

Their third and final energy-change term approximates the changes in *exchange and correlation energies* (ΔE_{xc}[1.27)]) due to introduction of hydrogen; its complexity is beyond the scope of this discussion.

We thus see that they express the change in energy (ΔE) of the interstitial site as a sum of three contributions, or more specifically, eight terms of comparable magnitude[1.27)]. Cancellation due to sign differences plays an important role in obtaining the final ΔE values; hence this model is sensitively dependent on accurate evaluation of several terms. The largest of these is $-e^2\beta/4$, so that the accuracy of the model depends largely on the validity of the β value used, or more fundamentally, the physical correctness of the screened Coulomb

potential. Sholl and Smith point out that their value of β is largely insensitive to the underlying Pd BS calculation used[1.26]. They nevertheless note that the *screened proton model* formula. d by Ebisuzaki and O'Keeffe[1.32] gives a β value about half the size of theirs; it can thus be seen that this important parameter needs ro be calculated with great caution. The considerable computational effort made by Sholl and Smith to determine β self-consistently[1.26] shows they have appreciated this point.

Before considering their energy calculations, we first comment on their integrated DOS curves[1.26]. Though the presence of hydrogen strongly perturbs the Pd valence band, they do not obtain the flat hydrogen-related band found by Gelatt et al for low hydrogen concentration ($PdH_{0.05}$). They attribute the absence of this band to the fact that they do not consider hydrogen-hydrogen interactions.

The main thrust of Sholl and Smith's energy calculations is to test their theory by the values it gives for ΔE. It has been well-established by NMR [illegible], neutron scattering[1.34] and neutron diffraction[1.35],[1.36] experiments that hydrogen occupies the sites in Pd which have *octahedral* symmetry. The only other likely site is that with tetrahedral symmetry[1.27]; hence they calculate ΔE for both the octahedral and tetrahedral configurations, and find (in agreement with experiment) that the former case has the lower energy. For a quantitative comparison with experiment, they evaluate the *heat of formation* ΔH, using the relation:-

$$\Delta H = \Delta E - \tfrac{1}{2} E(H_2) \qquad (1.5)$$

where $E(H_2)$ is given by equation (1.1). Their values for ΔH fluctuate considerably in sign and magnitude, depending on the underlying BS calculation used[1.27] and other details[1.28]. This inaccuracy is largely a consequence of cancellation effects in equation (1.5), which consists of the difference between two nearly-equal terms.

Summary: Sholl and Smith (1977-78)

As with Faulkner and Gelatt et al Sholl and Smith have modelled the Pd/H system within a BS formalism, which in their case requires the use of 14 interpolation parameters. They have also considered electrostatic interactions which are sensitively dependent on the screening parameter. Their integrated DOS is obtained by a computationally-intensive statistical approach; it lacks the low-lying hydrogen bonding band which characterizes the DOS of Faulkner and Papaconstantopoulos et al. Their expression for the heat of formation on addition of hydrogen to the Pd lattice is more sophisticated than that of Gelatt et al, and correctly predicts occupation of the octahedral interstitial sites by hydrogen; however, the corresponding values of the heat of formation are highly sensitive to the BS calculation used. Another limitation of their model is that it only holds for low concentrations of hydrogen; this is the case for all models of this class. Finally, we note that Sholl and Smith model the electrostatic contribution to the heat of formation within a nearest-neighbour formalism.

1.2.8 Oates[1.37] (1982)

We finally consider a review by Oates, which provides us with a link between some of the electronic models described above and the thermodynamics of the Pd/H system. He reviews semiempirical theoretical models of the pressure-composition isotherms of Pd/H. These models are all based on the following equation:-

$$\ln \sqrt{p_{H_2}} = \ln \frac{x}{b-x} + \frac{\Delta\mu_H^o}{RT} + \frac{\mu_H^E}{RT} \qquad (1.6)$$

where p_{H_2} is the hydrogen pressure, $\Delta\mu_H^o = \mu_H^o - \frac{1}{2}\mu_{H_2}^o$ is the change in chemical potential of hydrogen at infinite dilution and μ_H^E is the excess chemical potential of hydrogen and so tends to zero for small x; the first term on the right is the configurational entropy contribution (b is of order unity), and RT is the usual thermal energy factor. Equation (1.6) is convenient for comparison with experimental data, which are often expressed as isotherms of $\ln \sqrt{p_{H_2}}$ versus x. Most of the theoretical work on equation (1.6) has to do with modelling μ_H^E correctly; this quantity has been experimentally determined as a function of x by Kuji et al[1.38]. This excess potential can be analysed in various ways: for example it can be expressed in its explicitly thermodynamic form, viz. $\mu_H^E = H_H^E - T S_H^E$; the experiments of Kuji et al[1.38] strongly indicate that S_H^E, the excess partial *entropy*, is dominated by its configurational part (that is, vibrational and other contributions are small). This result, taken in conjunction with equation (1.6), would suggest that the total entropy of the Pd/H system is essentially *configurational*, and will be of use to us in Chapter 6.

One of the first theoretical applications of equation (1.6) was that of Lacher[1.39),1.40)], whose model considers interactions between dissolved (interstitial) hydrogen atoms only; assuming a constant, nearest-neighbour interaction energy W_{HH}, this model gives $\mu_H^E = W_{HH}\, x/b$. However, the experimental results of Kuji et al clearly indicate that μ_H^E is strongly nonlinear.

Wagner[1.41)] was the first to successfully model the nonlinearity of μ_H^E. By assuming the *proton model* for PdH_x, he expressed μ_H^E as a sum of a protonic term (μ_{H+}^E) and an electronic term (μ_e^E); then by applying the *Rigid Band Model* (RBM) to obtain μ_e^E and assuming a linear decrease in μ_{H+}^E with x, he obtained the correct form for μ_H^E. Brodowsky[1.42)] developed Wagner's model by replacing the linear μ_{H+}^E term with one derived using the Quasi-Chemical Approximation[1.43)] (QCA). He evaluated the electronic contribution μ_e^E by subtracting μ_{H+}^E from experimental values for μ_H^E, and found that the results were in agreement with the RBM. In addition he identified the protonic interaction (W_{HH} in Lacher's model) as being a short-range *elastic* interaction (note that the distance between H atoms in PdH_x is roughly 4 Å [1.27)], compared to the interatomic separation of the H_2 molecule of about 1 Å; hence we do not expect W_{HH} to have a significant electronic contribution).

Oates points out a number of weaknesses in the Wagner-Brodowsky models: firstly, μ_{H+} is inadequately described by a nearest-neighbour formalism (Lacher's approximation $\mu_{H+}^E = \mu_H^E = W_{HH}\, x/b$, the QCA[1.44)] and an exact calculation using Monte Carlo techniques[1.45)] all give phase diagrams that disagree with experiment); secondly, dilation of the lattice by

hydrogen is ignored; thirdly, W_{HH} is assumed constant, though one would expect it to change with increasing x (as the H atoms are forced closer together); and fourthly, both the protonic model and the RBM are too simplistic, as we have seen before.

In addressing some of these problems, the following refinements have been made to the Wagner-Brodowsky models: firstly, the other two possible (pairwise) interactions have been included, viz. W_{PdH} and W_{PdPd}; secondly, these interaction parameters have been given x-dependence; and thirdly, lattice-expansion terms have been included, giving rise to a near-neighbour contribution to μ_H^E (as opposed to solely nearest-neighbour terms). One such improved model is that formulated by Horner and Wagner[1.46], which is the basis for Monte Carlo calculations performed by Dietrich and Wagner[1.47]. These calculations are in fair agreement with experimental isotherms, though noticeable shortcomings show up in the *phase diagram* (which is basically a plot of temperature versus concentration). The Horner-Wagner model is essentially phenomenological; two of its shortcomings are that it lacks configuration-independent terms (the existence of which are predicted by first-principle calculations), and that it does not take into account change of *electronic structure* as a function of x. It and similar models are often able to provide satisfactory results for low and high x, but not for intermediate ranges of concentration. This implies that they are essentially one-phase models, and hence not very effective in the two-phase region of the Pd/H phase diagram.

Summary: Oates (1982)

The models reviewed by Oates are basically phenomenological, relying on experimental observations and ideal-case theory. The non-ideal (real) behaviour of the Pd/H system is approximated by the *excess chemical potential* μ_H^E, which has been modelled with varying degrees of success; the approach has generally been to reproduce the experimentally-known μ_H^E isotherms via semiempirical theories, rather than to provide a fundamentally-correct model.

Because it is known that μ_H^E has a significant *electronic* contribution (μ_e^E), these theories constitute a link between easily-measurable thermodynamic quantities (such as the pressure-composition isotherms) and less-accessible electronic features; they hence provide at least a *qualitative* means of testing electronic models (bearing in mind that the non-electronic contributions to μ_H^E are also imperfectly known). In conclusion, we note firstly that these models are all based on nearest- or near-neighbour formalisms (that is they emphasize the importance of the local environment of an atom in PdH_x); and secondly, that they only give accurate results in the one-phase regions of the Pd/H system.

1.3 SUMMARY OF LITERATURE REVIEW AND AIMS OF PRESENT WORK

The following points have emerged from this review:-

- electronic theories for PdH_x tend either to be *too simplistic* on the one hand or *computationally restrictive* on the other;
- the more sophisticated theories are almost invariably locked within *ordered-crystal formalisms* which are *physically incorrect* for substoichiometric (and hence disordered) systems such as PdH_x. In particular the concensus of opinion is that such formalisms make the correct modelling of disorder *computationally impractical*;
- the importance of *nearest neighbours* in modelling electronic properties has been a recurring theme;
- *heats of formation* have been theoretically estimated for stoichiometric palladium hydride and for palladium containing very low concentrations of hydrogen, but not for the wide range of concentrations between these limits;
- the *multiphase nature* of the Pd/H system is widely accepted; however, semiempirical approaches are unable to model this feature with clarity and accuracy; furthermore, multiphase modelling is computationally prohibitive from the point of view of band structure techniques, while being beyond the range of physical applicability in the case of isolated-impurity models.

The aim of the present work is to provide more flexible alternatives to the above-mentioned shortcomings of existing models, and thereby to investigate the applications which up to now have been computationally unfeasible. We proceed as follows: in Chapter 2 we present a formalism which approaches a binary solid in a way radically different to band structure techniques; in Chapter 3 we provide links that will allow this formalism to make use of existing band structure results for Pd and PdH_1; then in Chapter 4 the model is applied in detail to PdH_x, leading up to a *one-phase model* for the *heat of formation* of this system; in Chapter 5 we rectify the anticipated shortcomings of the one-phase approach by developing a physically more correct *two-phase model*, which we again apply to the heat of formation; in Chapter 6 our models are further applied, this time in a semi-qualitative manner, to examine some important *thermodynamic aspects* of the Pd/H system; and finally in Chapter 7 we summarize our findings and provide direction for the development of our formalism.

APPENDIX 1.1

THE CPA AND ATA[1.25)]

These are two of the principal approximations used in the calculation of electronic properties of binary alloys (which are disordered systems). They are both derived via a general multiple scattering formalism, with configurational averages of physical observables (such as the total energy) playing a vital part in the theory. Expressions for these averages are most easily obtained using Green's function techniques from which the DOS can be obtained directly, by taking the imaginary part of the trace of the Green's function matrix.

However, useful results can only be obtained once certain approximations are made, the most important being the "single site" approximation: this involves the decoupling of a particular site from its neighbours in an average/effective medium. Because this effective medium is described by a non-Hermitian Hamiltonian, the eigenvalues are complex, with the imaginary part related to the lifetimes of single-electron states. From this effective Hamiltonian one is then able to calculate the self-energy in one of two ways: self-consistently, which gives the CPA; and non-self-consistently, which gives inter alia the ATA.

The CPA is a mean field theory, analogous to the Random Phase Approximation (RPA) which models Coulomb interactions in a many-electron system. Although these models are strictly only applicable for limited ranges of their characteristic parameters, they are nevertheless often effective

well outside these strict limits, making them quite versatile approximations. The lack of self-consistency makes the ATA less accurate than the CPA; but it gains on the CPA because of its greater simplicity and hence lower computational demands. The ATA has another advantage, viz. the convenience with which it can be formulated in terms of the Muffin-Tin approach to band theory.

We therefore conclude that the CPA and ATA are complementary techniques, the choice between them being made on the basis of the accuracy requirements of a particular problem, the structure of the formalism and the computational resources available.

REFERENCES (CHAP. 1)

1.1) Wicke E and Brodowsky H 1978 *Hydrogen in Palladium and Palladium Alloys* in *Topics in Appl. Phys.* 29 73 (Ed.s: Alefeld G and Völkl J; publ.: Springer-Verlag)

1.2) Graham T 1866 *Phil. Trans. R. Soc.* 156 415

1.3) Heine V 1980 *Electronic Structure from the Point of View of the Local Atomic Environment* in *Solid State Phys.* 35 1 (Ed.s: Ehrenreich H, Seitz F and Turnbull D ; publ.: Academic Press)

1.4) Oxley A E 1922 *Proc. R. Soc.* 101A 264

1.5) Vogt E 1932 *Annln Phys.* 14 1

1.6) Rosenhall G 1935 *Annln Phys.* 24 297

1.7) Lewis F A 1967 *The Palladium/Hydrogen System* 153 (Academic, New York)

1.8) Faulkner J S 1976 *Phys. Rev. B* 13 2391

1.9) Wagner C and Heller C 1940 *Z. Phys. Chem.* 46B 242

1.10) Mott N F and Jones H 1936 *The Theory of the Properties of Metals and Alloys* (Oxford University Press, London)

1.11) Husemann H and Brodowsky H 1968 *Z. Naturforsch.* 23a 1693

1.12) Brodowsky H, Husemann H and Mehlmann R 1973 *Ber. Bunsenges. Physik. Chem.* 77 36

1.13) Vuillemin J J and Priestley M G 1965 *Phys. Rev. Lett.* 14 307

1.14) Brodowsky H 1968 Habilitationsschrift, Münster

1.15) Dugdale J S and Guénault A M 1966 *Phil. Mag.* 13 503

1.16) Montgomery H, Pells G P and Wray E M 1976 *Proc. Roy. Soc. London* A301 261

REFERENCES (CHAP. 1) continued

1.17) Switendick A C 1972 *Ber. Bunsenges. Phys. Chem.* 76 535

1.18) Mueller F M, Freeman A J, Dimmock J O and Furdyna A M 1970 *Phys. Rev. B* 1 4617

1.19) Kirkpatrick S, Velicky B and Ehrenreich H 1970 *Phys. Rev. B* 1 3250

1.20) Papaconstantopoulos D A and Klein B M 1975 *Phys. Rev. Lett.* 35 110

1.21) Slater J C and Koster G F 1954 *Phys. Rev.* 94 1498

1.22) Blackman J A, Esterling D M and Berk N F 1971 *Phys. Rev. B* 4 2412

1.23) Papaconstantopoulos D A, Klein B M, Faulkner J S and Boyer L L 1978 *Phys. Rev. B* 18 2784

1.24) Gelatt C D Jr, Ehrenreich H and Weiss J A 1978 *Phys. Rev. B* 17 1940

1.25) Ehrenreich H and Schwartz L M 1976 *The Electronic Structure of Alloys* in *Solid State Phys.* 31 149 (Ed.s: Ehrenreich H, Seitz F and Turnbull D; publ.: Academic, New York)

1.26) Sholl C A and Smith P V 1977 *J. Phys. F: Met. Phys.* 7 789

1.27) Sholl C A and Smith P V 1977 *J. Phys. F: Met. Phys.* 7 799

1.28) Sholl C A and Smith P V 1978 *J. Phys. F: Met. Phys.* 8 775

1.29) Riedinger R 1971 *J. Phys. F: Met. Phys.* 1 392

1.30) Hodges L, Ehrenreich H and Lang N D 1966 *Phys. Rev.* 152 505

REFERENCES (CHAP. 1 continued

1.31) Ehrenreich H and Hodges L 1968 *Methods in Comp. Phys.* 8 149

1.32) Ebisuzaki Y and O'Keeffe M 1967 *Prog. Solid St. Chem.* 4 187

1.33) Seymour E F W, Cotts R M and Williams W D 1976 *Phys. Rev. Lett.* 35 165

1.34) Nelin G and Skold K 1975 J. *Phys. Chem. Solids* 36 1175

1.35) Worsham J E Jr, Wilkinson M K and Shull C G 1957 *J. Phys. Chem. Solids* 3 303

1.36) Bergsma J and Goedkoop J A 1960 *Physica* 26 744

1.37) Oates W A 1982 *J. Less-Comm. Metals* 88 411

1.38) Kuji T, Oates W A, Bowerman B S and Flanagan T B 1983 *J. Phys. F: Met. Phys.* 13 1785

1.39) Lacher J R 1937 *Proc. Roy. Soc. London* A161 525

1.40) Lacher J R 1938 *Proc. Camb. Philos. Soc.* 34 518

1.41) Wagner C 1944 *Z. Phys. Chem.* 193 386

1.42) Brodowsky H 1965 *Z. Phys. Chem. N.F.* 44 129

1.43) Wicke E and Brodowsky H 1978 *Hydrogen in Palladium and Palladium Alloys* in *Topics in Appl. Phys.* 29 99 (Ed.s: Alefeld G and Völkl J; publ.: Springer-Verlag)

1.44) Li Y Y 1949 *J. Chem. Phys.* 17 447

1.45) Binder K, Lebowitz J L, Phani M K and Kalos M H 1981 *Acta Met.* 29 1655

1.46) Wagner H 1978 *Elastic Interaction and Phase Transition in Coherent Metal-Hydrogen Alloys* in *Topics in Appl. Phys.* 28 5 (Ed.s: Alefeld G and Völkl J; publ.: Springer-Verlag)

1.47) Dietrich S and Wagner H 1979 *Z. Phys. B* 36 121

CHAPTER 2

CLUSTER-BETHE-LATTICE TECHNIQUE

2.1 INTRODUCTION

In this chapter we will present a formalism which is fundamentally different in concept to band structure (BS) techniques. The latter are essentially methods for the solution of the one-electron Schrödinger equation with a periodic potential; chey have proved highly successful in obtaining the energy levels and hence Densities of States (DOS) of perfect crystalline solids. This success is due to the physical compatibility of the periodic model potential and the potential of the actual crystal. However, when we consider a substoichiometric hydride such as PdH_x, in which one crystal sublattice is *randomly* occupied, we realize that the real system can no longer be described in terms of a periodic potential. In physical terms, the solid ceases to have the long-range order which is a fundamental requirement for a successful band structure calculation. It is still possible to model such a system within a band structure formalism by using finite decay lengths for the lattice wave functions, but the problem becomes physically opaque and computationally unwieldy.

It is physically sounder to search for a formalism which suits this random, disordered state of affairs rather than to adapt a proven tool to tasks unsuited to it. An alternative approach to BS techniques would most logically consider the random solid from the viewpoint of *local*

environment, since there is now no motivation for looking at the solid as a whole (because of the lack of long-range order). Having taken this fundamental conceptual step, it would seem sensible to deal with as small a local environment as can give physically meaningful results. At this point we are encouraged by the continual emphasis in Chapter 1 of the importance of near-neighbour interactions in understanding the behaviour of PdH_x.

The most immediately obvious idea is to consider a *finite cluster* of atoms in the solid, with some sort of boundary condition to allow for the surrounding atoms. This approach has been applied in practice[2.1], and experience shows that it has one major drawback, viz. that *large* clusters must be considered before physically realistic results are obtained.

Another concept that has been implemented approximates the random solid by means of *infinite, branching chains* of atoms which lack periodicity; examples of this technique are the Husumi cacti method[2.2] and the Cayley tree or Bethe lattice approach (see below). Although this is not a localized concept, it certainly overcomes the problem of periodicity, and has the added advantage of producing analytically soluble models. However, this approach has an important limitation, viz. it generates DOS which tend to be rather featureless and hence unhelpful.

In the present work we consider a formalism which is basically a hybrid of the above two approaches and which incorporates the best features of both: a cluster of atoms is removed from the solid as in the finite cluster approach, but instead of using standard boundary conditions the

dangling bonds on the surface of the cluster are attached to infinite Bethe lattices. This is the *Cluster-Bethe-Lattice* (CBL) *approach*, developed by Yndurain and coworkers[2.3)-2.5)]. It generates the detail of the finite cluster approach, but with considerably smaller clusters; it also has the important attribute of the Bethe Lattice approach of being analytically soluble.

The rest of this chapter is divided up as follows: in Section 2.2 we define the Bethe Lattice more precisely, and expand briefly upon its appeal from a physical point of view; in the following three sections (2.3 - 2.5) we provide insight into the CBL formalism by considering two extreme cases and one intermediate case. More specifically, in Section 2.3 we consider a CBL consisting of only one type of atom (referred to as the *homopolar case*[2.3)]), which will reveal the essential features of the CBL technique; then in Section 2.4 we examine the opposite extreme, viz. a CBL consisting of two atomic species present in equal amounts (the *heteropolar case*[2.4)]); and thirdly in Section 2.5 we look at the case midway between these extremes (the *random case*[2.5)]); in the next section of the chapter, Section 2.6, we tie together the expressions resulting from the special cases by means of suitable interpolation formulae[2.5)], leaving us with a highly versatile analytical expression for the Local Density of States (LDOS). This will allow us to evaluate the LDOS for any ratio of the two types of atom, and thus to study non-stoichiometric binary alloys. Finally in Section 2.7 we summarize some of the important findings of this chapter.

2.2 THE BETHE LATTICE

This consists of an infinite "tree" of atomic chains, branching in such a way that no rings of bonds are formed: see Figure 2.1. It can also be seen from this figure that the coordination of every atom in the tree is constant, allowing us to model local or short-range order to some degree. We use Bethe Lattices in place of more traditional boundary conditions for the following three reasons:-

- firstly, they give rise to Densities of States (DOS) which are analytically soluble;
- secondly, they are physically appealing because they maintain the connectivity and coordination of the real system;
- and thirdly, the DOS of the Bethe Lattice is smooth and featureless, so that it does not impose upon the electronic structure of the cluster itself.

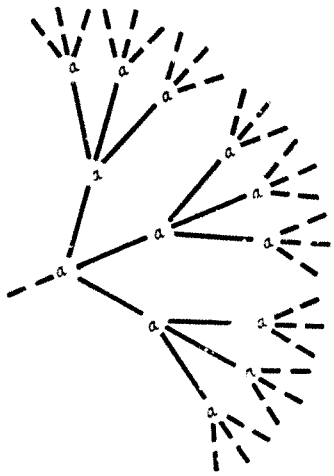

Figure 2.1 Schematic representation of a homopolar Bethe Lattice with coordination number m = 4. The letters "a" refer to atoms and the lines to interatomic bonds.

2.3 FIRST EXTREME CASE: HOMOPOLAR LATTICE

2.3.1 *Basic Topography*

We start by removing a *cluster* of atoms from the complete lattice (represented by the symbols a_i, i = 0,...3 in Figure 2.2). We then attach each "dangling" bond to a Bethe Lattice (represented by ϕ_a in Figure 2.3). Now that we have the topography of the homopolar CBL, we need suitable mathematical tools to take advantage of it.

2.3.2 *Dyson's Equation and Local Density of States*

With reference to Figure 2.2, let us denote the wave function of the central atom by $|a_0>$, and that of each atom in near-neighbour shell i by $|a_i>$; let us assume that these wave functions form an orthonormal basis set $\{|a_i>\}$. Let H be the Hamiltonian of the system and ε the associated eigenenergy. We can then define the *Green's function* to be:-

$$G = \frac{1}{\varepsilon - H}$$

Thus $G(\varepsilon - H) = I$ and so

$$\varepsilon G = I + HG \qquad (2.1)$$

When expressed in terms of the set of basis functions $\{|a_i>\}$, equation (2.1) becomes:-

$$\varepsilon <i|G|j> = <i|j> + <i|HG|j> ,$$

that is:-

$$\varepsilon <i|G|j> = \delta_{ij} + \sum_k <i|H|k><k|G|j> \qquad (2.2)$$

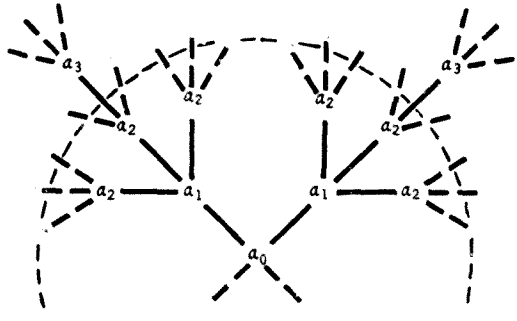

Figure 2.2 Schematic representation of the environment about atom "a_0" in a homopolar lattice. Atoms within broken curve are removed to form a cluster centred on atom "a_0" (see Figure 2.3).

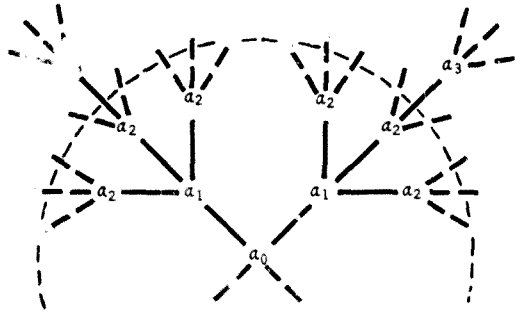

Figure 2.2 Schematic representation of the environment about atom "a_0" in a homopolar lattice. Atoms within broken curve are removed to form a cluster centred on atom "a_0" (see Figure 2.3).

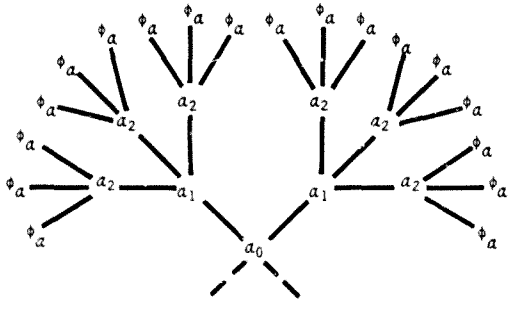

Figure 2.3 Homopolar cluster with Bethe Lattices ϕ_σ attached to the dangling bonds.

which is a form of *Dyson's equation*. The *Density of States* (DOS) is given by the following standard expression:-

$$n(\varepsilon) = -\frac{1}{\pi}\,\mathrm{Im}\,\mathrm{Tr}\,G$$

$$= -\frac{1}{\pi}\,\mathrm{Im}\sum_i \langle i|G|i\rangle \qquad (2.3)$$

We are now able to give concrete meaning to the useful concept of *Local Density of States* (LDOS). This is the DOS of a *particular atom* a_i, and is defined as follows:-

$$n_i(\varepsilon) = -\frac{1}{\pi}\,\mathrm{Im}\,\langle i|G|i\rangle \qquad (2.4)$$

It follows from equations (2.3) and (2.4) that:-

$$n\ (\text{or DOS}) = \sum_i n_i\ (\text{or LDOS})$$

In the next section we shall examine the LDOS of the central atom in our cluster.

2.3.3 *LDOS at the centre of the Cluster*

2.3.3.1 Parametrization

We introduce the following notation to simplify our expressions:-

$$\langle a_i|H|a_j\rangle \equiv \begin{cases} U \text{ for } i = j \\ V \text{ for } i \neq j \text{ (nearest neighbours)} \\ 0 \text{ for } i \neq j \text{ (2nd, 3rd,... neighbours)} \end{cases}$$

Let the coordination of each atom be m (that is, each atom has m nearest neighbours).

2.3.3.2 Lattice Equations; Transfer Matrix Technique

We now apply equation (2.2) to Figure 2.2 to obtain the following set of equations:-

$$
\begin{aligned}
(\varepsilon-U)\langle a_0|G|a_0\rangle &= 1 + mV\,\langle a_1|G|a_0\rangle,\\
(\varepsilon-U)\langle a_1|G|a_0\rangle &= V\,\langle a_0|G|a_0\rangle + (m-1)V\,\langle a_2|G|a_0\rangle,\\
(\varepsilon-U)\langle a_2|G|a_0\rangle &= V\,\langle a_1|G|a_0\rangle + (m-1)V\,\langle a_3|G|a_0\rangle,\\
(\varepsilon-U)\langle a_3|G|a_0\rangle &= V\,\langle a_2|G|a_0\rangle + (m-1)V\,\langle a_4|G|a_0\rangle,\\
&\vdots\\
(\varepsilon-U)\langle a_n|G|a_0\rangle &= V\,\langle a_{n-1}|G|a_0\rangle + (m-1)V\,\langle a_{n+1}|G|a_0\rangle,\\
&\vdots
\end{aligned}
\qquad (2.5a)
$$

We now make use of the *transfer matrix technique*[2.6] by defining the following ratio:-

$$
T = \frac{\langle a_{N+1}|G|a_0\rangle}{\langle a_N|G|a_0\rangle} \qquad ,N \geq 2 \qquad (2.6)
$$

The transfer matrix T is a useful construct which will allow us to model the connection of our finite central cluster to the infinite Bethe Lattices. We will see its purpose once we have substituted equation (2.6) into equations (2.5a). We do so bearing in mind that for $N \geq 2$ equation (2.6) gives us:-

$$
\frac{\langle a_{N+2}|G|a_0\rangle}{\langle a_N|G|a_0\rangle} = \frac{\langle a_{N+2}|G|a_0\rangle}{\langle a_{N+1}|G|a_0\rangle} \times \frac{\langle a_{N+1}|G|a_0\rangle}{\langle a_N|G|a_0\rangle} = T^2
$$

or

$$
\langle a_{N+2}|G|a_0\rangle = T^2\,\langle a_N|G|a_0\rangle
$$

Hence equations (2.5a) become:-

$$
\begin{aligned}
N = 0 :\quad & (\varepsilon-U)\langle a_0|G|a_0\rangle = 1 + mV\,\langle a_1|G|a_0\rangle, \\
N = 1 :\quad & (\varepsilon-U)\langle a_1|G|a_0\rangle = V\,\langle a_0|G|a_0\rangle + (m-1)V\,\langle a_2|G|a_0\rangle, \\
N = 2 :\quad & (\varepsilon-U)\langle a_2|G|a_0\rangle = V\,\langle a_1|G|a_0\rangle + (m-1)VT\,\langle a_2|G|a_0\rangle, \\
N = 3 :\quad & (\varepsilon-U)T\langle a_2|G|a_0\rangle = V\,\langle a_2|G|a_0\rangle + (m-1)VT^2\langle a_2|G|a_0\rangle \\
& \vdots \qquad\qquad\qquad\qquad \vdots \\
N = n :\quad & (\varepsilon-U)T\langle a_{n-1}|G|a_0\rangle = V\,\langle a_{n-1}|G|a_0\rangle + (m-1)VT^2\langle a_{n-1}|G|a_0\rangle \\
& \vdots \qquad\qquad\qquad\qquad \vdots
\end{aligned}
\tag{2.5b}
$$

or more simply:-

$$
\begin{aligned}
N = 0 :\quad & (\varepsilon-U)\langle a_0|G|a_0\rangle = 1 + mV\,\langle a_1|G|a_0\rangle, \\
N = 1 :\quad & (\varepsilon-U)\langle a_1|G|a_0\rangle = V\,\langle a_0|G|a_0\rangle + (m-1)V\,\langle a_2|G|a_0\rangle, \\
N = 2 :\quad & (\varepsilon-U)\langle a_2|G|a_0\rangle = V\,\langle a_1|G|a_0\rangle + (m-1)VT\,\langle a_2|G|a_0\rangle, \\
N \geq 3 :\quad & (\varepsilon-U)T = V + (m-1)VT^2
\end{aligned}
\tag{2.5c}
$$

Thus we see that the condition $N \geq 2$ in equation (2.6) for the introduction of the transfer matrix T causes the central atom to be equally affected by all nearest-neighbour shells from the third outwards. That is, the "true" lattice is removed from third-nearest neighbours outwards, leaving us with a cluster including only first- and second-nearest neighbours of the central atom.

We next consider the cases $N \geq 1$ and $N \geq 3$ in equation (2.6), and write down the resulting equations to bring out an important feature of the transfer matrix technique.

a) $T = \dfrac{\langle a_{N+1}|G|a_0\rangle}{\langle a_N|G|a_0\rangle}$, $N \geq 1$ gives:-

$N = 0$: $(\varepsilon-U)\langle a_0|G|a_0\rangle = 1 + mV\langle a_1|G|a_0\rangle$,

$N = 1$: $(\varepsilon-U)\langle a_1|G|a_0\rangle = V\langle a_0|G|a_0\rangle + (m-1)VT\langle a_1|G|a_0\rangle$,

$N \geq 2$: $(\varepsilon-U)T = V + (m-1)VT^2$

(2.7a)

b) $T = \dfrac{\langle a_{N+1}|G|a_0\rangle}{\langle a_N|G|a_0\rangle}$, $N \geq 3$ gives:-

$N = 0$: $(\varepsilon-U)\langle a_0|G|a_0\rangle = 1 + mV\langle a_1|G|a_0\rangle$,

$N = 1$: $(\varepsilon-U)\langle a_1|G|a_0\rangle = V\langle a_0|G|a_0\rangle + (m-1)V\langle a_2|G|a_0\rangle$,

$N = 2$: $(\varepsilon-U)\langle a_2|G|a_0\rangle = V\langle a_1|G|a_0\rangle + (m-1)V\langle a_3|G|a_0\rangle$,

$N = 3$: $(\varepsilon-U)\langle a_3|G|a_0\rangle = V\langle a_2|G|a_0\rangle + (m-1)VT\langle a_3|G|a_0\rangle$,

$N \geq 4$ $(\varepsilon-U)T = V + (m-1)VT^2$

(2.7b)

The important feature is that the Bethe Lattice contribution is modelled by *the same* equation for *all* cluster sizes. Thus the effect of increasing the cluster size is reflected in the cluster equations only, which is a physically reasonable and indeed pleasing feature.

Specifically, we note that the complexity of the cluster's mathematics is increased by one equation per addition of one near-neighbour shell; also that the equations are analytically soluble for $\langle a_0|G|a_0\rangle$, and hence the LDOS can be derived analytically provided that T as well as the parameters m, U and V are known.

2.3.3.3 Cluster Size

We should now briefly address the issue of cluster size before proceeding with the formalism. Appendix 2.1 contains details of a *first*-nearest neighbour cluster, the salient feature of which is a lack of interesting structure. A cluster extending to the second-nearest neighbours of the central atom does however produce quite rich structure in the LDOS. Going to third-nearest neighbours would create even richer structure, but it will be appreciated from Section 2.6.3 and also from later chapters that this would lead to a computationally intractable problem. The spirit of this work has been to derive an analytical LDOS function which can be conveniently and rapidly employed in a variety of charge and energy calculations, rather than to obtain excellence of detail of the LDOS, which has been the emphasis of other workers[2.5]. We have thus settled for the case implied by equation (2.6), viz. a *second-nearest neighbour cluster*.

2.3.3.4 Solution of Transfer Matrix Equation

We now consider the last of equations (2.5c), (2.7a) and (2.7b), viz:-

$$(\varepsilon-U)T = V + (m-1)VT^2 \tag{2.8}$$

We note that the equation is quadratic in T; we will discuss the choice of the physically-correct root below. The solutions of equation (2.8) are:-

$$T = \frac{1}{2(m-1)V}\left[(\varepsilon-U) \pm \sqrt{(\varepsilon-U)^2 - 4(m-1)V^2}\right] \tag{2.9}$$

We recall that the LDOS is given by $-\frac{1}{\pi}\,\mathrm{Im}\,\langle a_0|G|a_0\rangle$. Examining equations (2.5) and (2.7) we see that they contain no explicitly imaginary terms, but that they do have T as a variable. Hence we will introduce imaginary terms by rewriting equation (2.9) as follows:-

$$T = \frac{1}{2(m-1)V}\left[(\varepsilon-U) \pm i\sqrt{4(m-1)V^2 - (\varepsilon-U)^2}\right] \qquad (2.10)$$

Now the criterion for choosing the correct root is clarified: we will choose the sign of the imaginary part of T such that the LDOS is *positive*.

We are now in a position to crystallize out a physical concept which will save us much tedious application of the transfer matrix technique in deriving equations for binary and other Cluster-Bethe-Lattices.

2.3.3.5 Physical Insights into Transfer Matrix

Consider the *last cluster equation* in equations (2.5c):-

$$(\varepsilon-U)\ \langle \quad |a_0\rangle = V\ \langle a_1|G|a_0\rangle + (m-1)VT\ \langle a_2|G|a_0\rangle$$

The factor VT is seen to represent the link between the cluster and the Bethe Lattice. By considering the corresponding equations in equations (2.7a) and (2.7b) we obtain the following general equation for the outermost shell of a given cluster:-

$$(\varepsilon-U)\ \langle a_N|G|a_0\rangle = V\ \langle a_{N-1}|G|a_0\rangle + (m-1)VT\ \langle a_N|G|a_0\rangle \qquad (2.11)$$

where N is the number of the outermost shell. We recall that V is the interatomic interaction parameter ($V = \langle a_i|H|a_j\rangle$ for nearest neighbours, V = 0 otherwise). Hence we see that VT is a *modified* interaction parameter, representing the interaction between an atom on the outer surface of the cluster and its corresponding Bethe Lattice. For convenience we shall call this parameter ϕ, so that equation (2.10) becomes:-

$$\phi = VT = \frac{1}{2(m-1)}\left[(\epsilon-U) \pm i\sqrt{4(m-1)V^2 - (\epsilon-U)^2}\right] \qquad (2.12)$$

and equation (2.11) becomes:-

$$(\epsilon-U)\langle a_N|G|a_0\rangle = V\langle a_{N-1}|G|a_0\rangle + (m-1)\phi\langle a_N|G|a_0\rangle \qquad (2.13)$$

where N = 2 in our case.

Because ϕ represents the interaction of an entire Bethe Lattice with a cluster surface atom, we shall henceforth refer to it as the *mean field function*, that is, the mean external field experienced by the surface atom. Figure 2.3 provides a schematic representation of the homopolar CBL system.

We are now in a position to evaluate an expression for the LDOS of a *homopolar lattice* within our CBL formalism.

2.3.3.6 I.DOS

We write the first three of equations (2.5c) in the following condensed form:-

$$\left.\begin{aligned} \epsilon_1 g_0 &= 1 + mVg_1 \\ \epsilon_1 g_1 &= Vg_0 + nVg_2 \\ \epsilon_1 g_2 &= Vg_1 + n\phi g_2 \end{aligned}\right\} \qquad (2.14)$$

where $\epsilon_1 \equiv \epsilon - U$

$n \equiv m-1$

$g_i \equiv \langle a_i | G | a_0 \rangle$

Solving for g_0 gives:-

$$g_0 = \cfrac{1}{\epsilon_1 - \cfrac{mV^2}{\epsilon_1 - \cfrac{nV^2}{\epsilon_1 - n\phi}}} \qquad (2.15)$$

Equation (2.15) is in the form of a *truncated continued fraction*. Notice that it is truncated at the third level of "nesting" by means of the mean field function ϕ. If we were to have one more near-neighbour "shell" in our cluster it would also be terminated by ϕ, only one level lower down. As can be seen from Appendix 2.1, g_0 for a first-nearest neighbour cluster follows the same mathematical trend.

We now evaluate the LDOS ($n(\epsilon)$) at the centre of our cluster; this is done by writing $\phi = \mathrm{Re}\phi + i\ \mathrm{Im}\ \phi$, and then evaluating Im g_0, where g_0 is given by equation (2.15). We obtain the following formulae:-

$$n(\varepsilon) = \frac{1}{\pi} \frac{\eta}{\delta^2 + \eta^2} \tag{2.16a}$$

where:-

$$\left.\begin{aligned} \delta &= \varepsilon_1 - \frac{mV^2\beta}{\beta^2 + \gamma^2} \\ \eta &= \frac{mV^2\gamma}{\beta^2 + \gamma^2} \end{aligned}\right\} \tag{2.16b}$$

$$\left.\begin{aligned} \beta &= \varepsilon_1 - \frac{nV^2\,(\varepsilon_1 - n\mathrm{Re}\phi)}{\alpha^2} \\ \gamma &= \frac{n^2V^2\,\mathrm{Im}\,\phi}{\alpha^2} \end{aligned}\right\} \tag{2.16c}$$

and

$$\left.\begin{aligned} \alpha^2 &= (\varepsilon_1 - n\,\mathrm{Re}\,\phi)^2 + (n\,\mathrm{Im}\,\phi)^2 \\ \mathrm{Re}\phi &= \frac{(\varepsilon - U)}{2(m-1)} \\ \mathrm{Im}\,\phi &= + \frac{\sqrt{4(m-1)V^2 - (\varepsilon - U)^2}}{2(m-1)} \end{aligned}\right\} \tag{2.16d}$$

We note that the only place where Im ϕ does not appear in the form $(\mathrm{Im}\,\phi)^2$ is as a factor in the numerator of $n(\varepsilon)$ (see equations (2.16)); hence our choice of the *positive* sign in front of the Im ϕ expression. We are now able to consider a more complex CBL topology.

2.4 SECOND EXTREME CASE: HETEROPOLAR LATTICE

2.4.1 *Basic Topography*

In this case our lattice consists of *two* atomic species in equal quantities, and with bonds only between unlike atoms. We shall label the two species with subscripts a and b. We again remove a cluster of atoms from the real lattice, and attach the dangling bonds to Bethe Lattices. The latter are represented by the mean fields ϕ_a and ϕ_b, depending on whether they are linked to a- or b- type atoms respectively (cf Figure 2.3). It is clear that there are now two types of cluster to consider, viz. atom a at the centre and atom b at the centre.

2.4.2 *Mean Field*

Bearing in mind the concept of the *mean field function* for a *homopolar* Bethe Lattice (Section 2.3.3.5) we are now in a position to extend this concept to a *heteropolar* Bethe Lattice (BL). As in the case of the heteropolar cluster, each atom in the heteropolar BL is surrounded entirely by atoms of the other kind, as illustrated in Figure 2.4; the coordination m is kept the same for both kinds of atom (m = 4 in our figures). We determine the mean field functions by considering four "cuttings" from our Bethe Lattice (Figures 2.5), two with a-type and two with b-type atoms at the centre.

Consider firstly Figure 2.5a : here we have removed an a-type atom and its m neighbouring b-type atoms from the BL. We now proceed to reattach this "cutting" to the BL by treating it as a cluster. We obtain the following equations:-

$$(\varepsilon-U)\langle a_0|G|a_0\rangle = 1 + mV\,\langle b_1|G|a_0\rangle \qquad (2.17a)$$

$$(\varepsilon+U)\langle b_1|G|a_0\rangle = V\,\langle a_0|G|a_0\rangle + (m-1)V\,\langle a_2|G|a_0\rangle \qquad (2.17b)$$

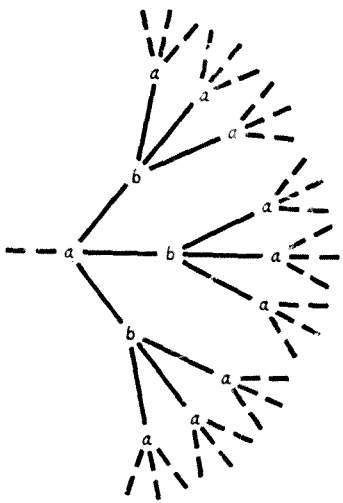

Figure 2.4 Schematic representation of a [illegible] topolar Bethe Lattice with coordination number m = 4.

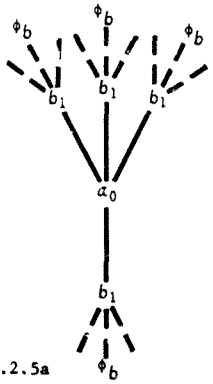

Fig.2.5a

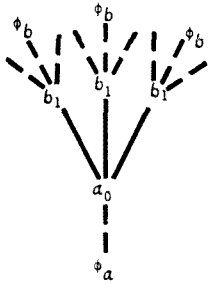

Fig.2.5b

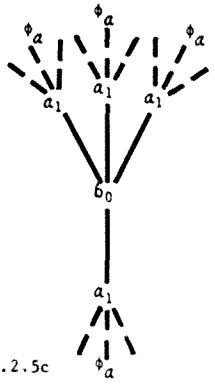

Fig.2.5c

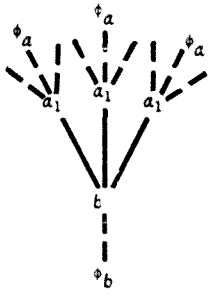

Fig.2.5d

Figures 2.5a-d Four "cuttings" from the heteropolar Bethe Lattice of Figure 2.4. Br[illegible] indicate the bonds broken in the "cutti[illegible] Figures 2.5a and b: a-type atom at centre o[illegible]g; Figures 2.5c and d: b-type atom at centre of cutting.

We notice that the a_2 atoms are outside the "cluster" and hence we can proceed along the lines of Section 2.3.3.2 by introducing a suitable transfer matrix, viz.:-

$$T_b = \frac{\langle a_2|G|a_0\rangle}{\langle b_1|G|a_0\rangle} \tag{2.18}$$

so that equation (2.17b) becomes:-

$$(\varepsilon+U)\langle b_1|G|a_0\rangle = V\langle a_0|G|a_0\rangle + (m-1)VT_b\langle b_1|G|a_0\rangle \tag{2.17c}$$

which is an equation in the form of equation (2.11). By comparing equations (2.17c) and (2.11) we can write $\phi_b = VT_b$, where ϕ_b is the mean field function which links a b-type "surface" atom to its BL.

We next consider Figure 2.5b; again an a-type atom is removed from the BL, but this time with only (m-1) of its nearest neighbours. The "reattachment" equations i this case are:-

$$(\varepsilon-U)\langle a_0|G|a_0\rangle = 1 + (m-1)V\langle b_1|G|a_0\rangle + VT_a\langle a_0|G|a_0\rangle \tag{2.19a}$$

$$(\varepsilon+U)\langle b_1|G|a_0\rangle = V\langle a_0|G|a_0\rangle + (m-1)VT_b\langle b_1|G|a_0\rangle \tag{2.19b}$$

where $T_a = \frac{\langle b_1|G|a_0\rangle}{\langle a_0|G|a_0\rangle}$.

These two cases leave us with three equations, which we express in our simplified notation (Table 2.1) as follows:-

Quantity	Symbol
m-1	n
ε-U	ε_1
ε+U	ε_2
$\langle a_i \vert G \vert a_0 \rangle$	g_{a_i}
$\langle b_i \vert G \vert a_0 \rangle$	g_{b_i}

Table 2.1 Abbreviations used in CBL equations.

Matrix element		Parameter
$\langle a_i \vert H \vert a_i \rangle$	=	+U
$\langle b_i \vert H \vert b_i \rangle$	=	-U
both $\langle a_i \vert H \vert b_j \rangle$ and $\langle b_i \vert H \vert a_j \rangle$	=	V for nearest neighbours 0 for 2nd, 3rd,... neighbours

Table 2.2 Parameters for the heteromolar CBL.

$$\left.\begin{aligned} \varepsilon_1 \, g_{a_0} &= 1 + mV g_{b_1} \\ \varepsilon_2 \, g_{b_1} &= V g_{a_0} + n\phi_b \, g_{b_1} \\ \varepsilon_1 \, g_{a_0} &= 1 + nV g_{b_1} + \phi_a \, g_{a_0} \end{aligned}\right\} \qquad (2.20)$$

solving equations (2.20) gives:-

$$\phi_a = \frac{V^2}{\varepsilon_2 - n\phi_b} \qquad (2.21)$$

where:-

$$\left.\begin{aligned} \phi_a &= VT_a = V \frac{\langle b_1|G|a_0\rangle}{\langle a_0|G|a_0\rangle} \\ \phi_b &= VT_b = V \frac{\langle a_2|G|a_0\rangle}{\langle b_1|G|a_0\rangle} \end{aligned}\right\} \qquad (2.22)$$

The above process is now repeated for "cuttings" with b-type atoms at the centre (see Figures 2.5 c and d). This gives rise to the following results:-

$$\phi_b' = \frac{V^2}{\varepsilon_1 - n\phi_a'} \qquad (2.23)$$

where:-

$$\left.\begin{aligned} \phi_a' &= VT_a' = V \frac{\langle b_2|G|b_0\rangle}{\langle a_1|G|b_0\rangle} \\ \phi_b' &= VT_b' = V \frac{\langle a_1|G|b_0\rangle}{\langle b_0|G|b_0\rangle} \end{aligned}\right\} \qquad (2.24)$$

ϕ_a' is the mean field function which connects an a-type "surface" cluster atom to its BL, and similarly ϕ_b' connects a b-type atom to its BL. Now we have seen for the *homopolar lattice* that the mean field is independent of the cluster details (Section 2.3.3.2);

transferring this concept to our heteropolar lattice, we are then able to say that:-

$$\left.\begin{aligned}\phi_a &= \phi'_a \\ \phi_b &= \phi'_b\end{aligned}\right\} \tag{2.25}$$

This amounts to the physically sensible concept that an a-type atom on the surface of a cluster experiences a mean field ϕ_a due to its BL, regardless of whether the atom at the centre of the cluster is a-type or b-type. Hence we are left with the following pair of equations (equations (2.21) and (2.23)):-

$$\left.\begin{aligned}\phi_a &= \frac{V^2}{(\varepsilon+U)-(m-1)\phi_b} \\ \phi_b &= \frac{V^2}{(\varepsilon-U)-(m-1)\phi_a}\end{aligned}\right\} \tag{2.26}$$

The solutions are:-

$$\left.\begin{aligned}\phi_a &= \frac{(\varepsilon-U)}{2(m-1)} \pm i\,\frac{1}{2(m-1)}\sqrt{\frac{4(m-1)V^2(\varepsilon-U)}{(\varepsilon+U)} - (\varepsilon-U)^2} \\ \phi_b &= \frac{(\varepsilon+U)}{2(m-1)} \pm i\,\frac{1}{2(m-1)}\sqrt{\frac{4(m-1)V^2(\varepsilon+U)}{(\varepsilon-U)} - (\varepsilon+U)^2}\end{aligned}\right\} \tag{2.27}$$

cf equation (2.12) for the homopolar lattice (a-type atoms):-

$$\phi = \frac{(\varepsilon-U)}{2(m-1)} \pm i\,\frac{1}{2(m-1)}\sqrt{4(m-1)V^2 - (\varepsilon-U)^2} \tag{2.12}$$

From equations (2.27) we see that ϕ_a and ϕ_b differ only in the sign of the parameter U.

2.4.3 LDOS

Consider an infinite *heteropolar* lattice (cf Figure 2.2), and remove a suitable cluster of atoms (cf Figure 2.3). Now "saturate" the "dangling" bonds with mean field functions, as in Figure 2.6. Recalling equation (2.2), viz.:-

$$\varepsilon\langle i|G|j\rangle = \delta_{ij} + \sum_k \langle i|H|k\rangle\langle k|G|j\rangle \qquad (2.2)$$

and referring to Table 2.2, we are able to write down the following cluster equations:-

$$\left.\begin{aligned}(\varepsilon-U)\langle a_0|G|a_0\rangle &= 1 + mV\,\langle b_1|G|a_0\rangle \\ (\varepsilon+U)\langle b_1|G|a_0\rangle &= V\,\langle a_0|G|a_0\rangle + (m-1)V\,\langle a_2|G|a_0\rangle \\ (\varepsilon-U)\langle a_2|G|a_0\rangle &= V\,\langle b_1|G|a_0\rangle + (m-1)V\,\langle b_3|G|a_0\rangle\end{aligned}\right\} \qquad (2.28)$$

that is, 3 equations in 4 unknown matrix elements. So we return to the first of equations (2.22):-

$$\phi_a = V\,\frac{\langle b_1|G|a_0\rangle}{\langle a_0|G|a_0\rangle} \qquad (2.22a)$$

With reference to equation (2.6) and the arguments that follow it (Section 2.3.3.2), we may reasonably extend equation (2.22a) to a more general form:-

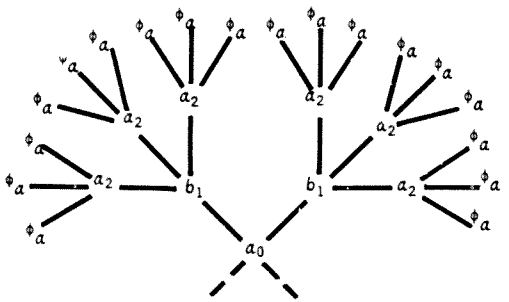

Figure 2.6 Heteropolar cluster with Bethe Lattices ϕ_a attached to the dangling bonds.

$$\phi_a = V \frac{\langle b_{N+1}|G|a_0\rangle}{\langle a_N|G|a_0\rangle}, \quad N \geq \text{(some integer n)} \tag{2.29}$$

In the case of the last of equations (2.28) we have n = 2. Thus we may rewrite equations (2.28) (in the condensed notation of Table 2.1) as:-

$$\left.\begin{aligned} \varepsilon_1 g_{a_0} &= 1 + mVg_{b_1} \\ \varepsilon_2 g_{b_1} &= Vg_{a_0} + nVg_{a_2} \\ \varepsilon_1 g_{a_2} &= V\varepsilon_{b_1} + n\phi_a g_{a_2} \end{aligned}\right\} \tag{2.30}$$

Solving equations (2.30) for g_{a_0} gives:-

$$g_{a_0} = \frac{1}{\varepsilon_1 - \dfrac{mV^2}{\varepsilon_2 - \dfrac{nV^2}{\varepsilon_1 - n\phi_a}}} \tag{2.31}$$

Then using $n_a(\varepsilon) = -\frac{1}{\pi} \text{Im } g_{a_0}$ we obtain the LDOS for the case of a heteropolar system (with a-type atom at centre of cluster):-

$$n_a(\varepsilon) = -\frac{1}{\pi} \frac{B}{A^2+B^2} \tag{2.32a}$$

where

$$\left.\begin{aligned} A &= \varepsilon_1 - \frac{mV^2\alpha}{\alpha^2+\beta^2} \\ B &= \frac{mV^2\beta}{\alpha^2+\beta^2} \end{aligned}\right\} \tag{2.32b}$$

$$\left.\begin{aligned} \alpha &= \varepsilon_2 - \frac{nV^2(\varepsilon_1 - n\text{Re}\phi_a)}{(\varepsilon_1 - n\text{Re}\phi_a)^2 + n^2\text{Im}\phi_a^2} \\ \beta &= \frac{n^2V^2\text{Im}\phi_a}{(\varepsilon_1 - n\text{Re}\phi_a)^2 + n^2\text{Im}\phi_a^2} \end{aligned}\right\} \tag{2.32c}$$

$$\left.\begin{aligned} \varepsilon_1 &= \varepsilon - U \\ \varepsilon_2 &= \varepsilon + U \end{aligned}\right\} \qquad (2.32d)$$

For the case of a b-type atom at the centre of the cluster, an expression for the LDOS ($n_b(\varepsilon)$) can be obtained by interchanging the symbols a and b, and by replacing U with -U. The total LDOS will then be :-

$$n_{tot}(\varepsilon) = n_a(\varepsilon) + n_b(\varepsilon)$$

The two LDOS are given the same weight in the sum because atoms of types a and b occur in equal concentrations. We will now proceed to our third and final "special case".

2.5 INTERMEDIATE CASE: RANDOM LATTICE

2.5.1 *Introduction*

In this case we examine a purely *random* lattice, that is, where an a-type atom has the same probability of having an adjacent b-type atom as it does of having another a-type atom next to it. It can thus be seen that this situation corresponds to the "halfway mark" between the two extreme cases of the homopolar and the heteropolar lattices; as a result the coordination number m will refer to m/2 atoms of the "same" type and m/2 of the "other" type. An immediate consequence of having neighbours of different types is that a single interatomic energy parameter V is no longer sufficient. In fact we now require *three* parameters viz. V_{aa}, V_{ab} and V_{bb}: see Table 2.3 for definitions.

Parameter	Physical Description
V_{aa}	$\langle a_i\|H\|a_j\rangle$, i≠j, i.e. a-type atom interacting with (neighbouring) a-type atom
V_{ab}	$\langle a_i\|H\|b_j\rangle$ and $\langle b_i\|H\|a_j\rangle$ i.e. interaction between a-type and (neighbouring) b-type atom
V_{bb}	$\langle b_i\|H\|b_j\rangle$, i≠j, i.e. b-type atom interacting with (neighbouring) b-type atom

Table 2.3 Parameters for the random and general-case CBL.

2.5.2 *Mean Field*

As in the heteropolar case (Section 2.4.2) we will again take "cuttings" from our Bethe Lattice(BL), typical examples of which are illustrated in

Figure 2.7. Two of the equations resulting from Figure 2.7a are:-

$$(\varepsilon-U)\langle a_0|G|a_0\rangle = 1 + \frac{m}{2} V_{aa} \langle a_1|G|a_0\rangle + \frac{m}{2} V_{ab} \langle b_1|G|a_1\rangle \tag{2.33a}$$

$$(\varepsilon-U)\langle a_1|G|a_0\rangle = V_{aa} \langle a_0|G|a_0\rangle + (\frac{m}{2} - 1) V_{aa} \langle a_2|G|a_0\rangle + \frac{m}{2} V_{ab} \langle b_2|G|a_0\rangle \tag{2.33b}$$

and one of those resulting from Figure 2.7b is:-

$$(\varepsilon-U)\langle a_0|G|a_0\rangle = 1 + (\frac{m}{2} - 1) V_{aa} \langle a_1|G|a_0\rangle + \frac{m}{2} V_{ab} \langle b_1|G|a_0\rangle +$$

$$+ V_{aa} \langle a_1|G|a_0\rangle \tag{2.33c}$$

Proceeding as in Section 2.4.2 we define the following transfer matrices:-

$$T_{aa} = \frac{\langle a_2|G|a_0\rangle}{\langle a_1|G|a_0\rangle}$$

$$T_{ab} = \frac{\langle b_2|G|a_0\rangle}{\langle a_1|G|a_0\rangle}$$

} for equation (2.33b)

and:-

$$T_{aa} = \frac{\langle a_1|G|a_0\rangle}{\langle a_0|G|a_0\rangle}$$

} for equation (2.33c)

Using these definitions and the abbreviations defined by Table 2.1, we rewrite equations (2.33) as follows:-

$$\varepsilon_1 g_{a_0} = 1 + \frac{m}{2} \left[V_{aa} g_{a_1} + V_{ab} g_{b_1}\right] \tag{2.33a}$$

$$\varepsilon_1 g_{a_1} = V_{aa} g_{a_0} + \frac{m}{2} \left[V_{aa} T_{aa} + V_{ab} T_{ab}\right] g_{a_1} - V_{aa} T_{aa} g_{a_1} \tag{2.33b}$$

$$\varepsilon_1 g_{a_0} = 1 + \frac{m}{2} \left[V_{aa} g_{a_1} + V_{ab} g_{b_1}\right] + V_{aa} \left[T_{aa} g_{a_0} - g_{a_1}\right] \tag{2.33c}$$

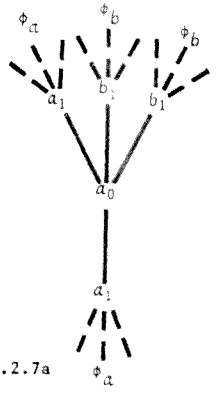

Fig.2.7a

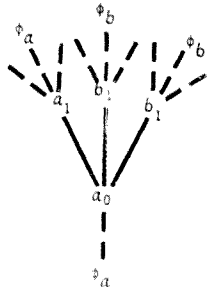

Fig.2.7b

Figures 2.7a&b Two "cuttings" from a random Bethe Lattice. Figure 2.7a: a-type atom with its four nearest neighbours; Figure 2.7b: a-type atom with three of its nearest neighbours.

We now define T_a as follows:-

$$T_a = T_{aa} = T_{ab} \tag{2.34}$$

Equation (2.34) states in effect that an a-type atom on the surface of the cluster will experience only one type of interaction (represented by T_a) with its attached BL, rather than two separate types (represented by T_{aa} and T_{ab}). That is, the interaction experienced will truly be *a mean field*. Combining equations (2.33a) and (2.33c), and using equation (2.34) leaves us with the following pair of equations:-

$$g_{a_1}/g_{a_0} = T_a \tag{2.35a}$$

$$\varepsilon_1 g_{a_1} = V_{aa} g_{a_0} + 2\left[V_{aa} + V_{ab}\right] T_a g_{a_1} - V_{aa} T_a g_{a_1} \tag{2.35b}$$

We next define a mean interaction parameter $\bar{V}_a$:-

$$\bar{V}_a = \tfrac{1}{2}\left[V_{aa} + V_{ab}\right] \tag{2.36a}$$

We note that this is a special case ($x_a = x_b = 0.5$) of:-

$$\bar{V}_a = x_a V_{aa} + x_b V_{ab} \tag{2.36b}$$

where equation (2.36b) is known as the Virtual Crystal Approximation (VCA)[2.7),2.8)]. We note that in order to have a completely random alloy we require equal concentrations of a- and b-type atoms, that is $x_a = x_b = 0.5$. Hence it is physically correct for us to state that our mean parameter of equation (2.36a) represents the VCA. Combining equations (2.35) and (2.36a) leaves us with:-

$$\varepsilon_1 T_a = V_{aa} + (m\bar{V}_a - V_{aa})T_a^2 \tag{2.37}$$

We now wish to re-write equation (2.37) in the same form as the corresponding equations for the extreme CBL cases (see equation (2.3)). We do this by extending our application of the VCA as follows:-

$$V_{aa} \approx \bar{V}_a \tag{2.38a}$$

From equation (2.36a) we see that equation (2.38a) is a good approximation provided that:-

$$V_{aa} \approx V_{ab} \tag{2.38b}$$

Now equation (2.38b) is known to be a criterion for the successful application of the VCA in general[2.8]; we are therefore in a physically consistent position provided that the condition of equation (2.38b) is met. Assuming this to be the case, we may proceed to apply the VCA provided we also incorporate one further pre-requisite of this approximation, viz.:-

$$\bar{U} = \tfrac{1}{2}\,(U_a + U_b) = 0 \tag{2.39}$$

Recalling that we have chosen $U_a = +U$ and $U_b = -U$, we see that our parameters are consistent with the requirements of equation (2.39); replacing U_a and U_b with $\bar{U}$, we are left with:-

$$\varepsilon_1 = \varepsilon_2 = \varepsilon \quad .$$

Having met all the necessary requirements we apply the VCA to equation (2.37) to obtain the following approximation:-

$$\varepsilon\, T_a = \bar{V}_a + (m-1)\,\bar{V}_a T_a^2 \tag{2.40}$$

the solution to which is:-

$$T_a = \frac{1}{2(m-1)\bar{V}_a} \left[\varepsilon \pm i\sqrt{4(m-1)\bar{V}_a^2 - \varepsilon^2} \right] \tag{2.41}$$

and so we can write down our mean field function in the usual manner, viz.:-

$$\phi_a = \bar{V}_a T_a = \frac{\varepsilon}{2(m-1)} \pm i \frac{1}{2(m-1)} \sqrt{4(m-1)\bar{V}_a^2 - \varepsilon^2} \tag{2.42a}$$

where

$$\bar{V}_a = \tfrac{1}{2} \left[V_{aa} + V_{ab} \right] \tag{2.36a}$$

By interchanging the symbols a and b we also obtain an expression for the mean field experienced by an atom of type b situated on the "surface" of the cluster:-

$$\phi_b = \bar{V}_b T_b = \frac{\varepsilon}{2(m-1)} \pm i \frac{1}{2(m-1)} \sqrt{4(m-1)\bar{V}_b^2 - \varepsilon^2} \tag{2.42b}$$

where

$$\bar{V}_b = \tfrac{1}{2} \left[V_{bb} + V_{ab} \right] .$$

2.5.3 LDOS

The cluster equations are more complex for the random alloy than for either of the two extreme cases. Because they are obtained in a very natural manner as special cases of the generalized cluster equations to be discussed in the next section, we choose not to carry through the LDOS formalism in this case.

2.6 GENERAL CASE: INTERPOLATION BETWEEN SPECIAL CASES

2.6.1 *Basic Concepts*

We are now ready to extend our LDOS expressions thus far obtained to a *general* form which will allow us to do useful calculations on metal hydride systems. We will again consider a- and b-type atoms (Section 2.4) but now we will allow them to be present in *different* amounts N_a and N_b respectively. It will be more convenient to work in terms of *concentrations* rather than the absolute numbers N_a and N_b; hence we define:-

$$\left.\begin{aligned} x_a &= N_a/(N_a + N_b) \\ x_b &= N_b/(N_a + N_b) \end{aligned}\right\} \qquad (2.43)$$

where x_a and x_b are the respective concentrations of a- and b-type atoms.

An immediate consequence of differing concentrations is a complication of our coordination parameter m. Consider for example the case $x_a > x_b$. We can build up a straightforward heteropolar lattice (Section 2.4) until our supply of b-type atoms is exhausted; we would then have the problem of incorporating the excess a-type atoms. They could be accounted for by building up an a-type homopolar lattice (Section 2.3) in addition to the heteropolar one, but in the context of an alloy this would clearly be a wrong picture physically. The only

sensible alternative then is to "squeeze" the extra atoms *into* the heteropolar lattice, which would result in a-type atoms having some a-type neighbours. Let k be the average number of these neighbours of the *same type*. We can thus say:-

$$m = k(\text{"same type"}) + (m-k)(\text{"other type"}) \qquad (2.44)$$

On the basis of equation (2.44) we can now introduce another physically-meaningful parameter λ, defined as follows:-

λ = (probability of "other type" neighbour)

- (probability of "same type" neighbour)

$$= \frac{m-k}{m} - \frac{k}{m}$$

$$\therefore \quad \lambda = \frac{m-2k}{m} \qquad (2.45)$$

Table 2.4 reveals the physical significance of equation (2.45).

k	λ	Physical Description
m	-1	All of neighbours are "same type" i.e. homopolar lattice ("segregation")
$\frac{m}{2}$	0	Half of neighbours are "same type" ("random alloy")
0	+1	No "same type" neighbours, i.e. heteropolar lattice ("perfect binary alloy")

Table 2.4 Physical significance of the parameter λ (equation (2.45)).

2.6.2 *Mean Field*

So far we have derived the mean field functions for the homopolar random and heteropolar lattices, represented by equations (2.12), (2.42a) and (2.27a) respectively:-

$$\text{Homopolar} : \phi_a = \frac{\varepsilon-U}{2(m_a-1)} \pm i\,\frac{1}{2(m_a-1)}\sqrt{4(m_a-1)V_{aa}^2 - (\varepsilon-U)^2} \qquad (2.12)$$

$$\text{Random} : \phi_a = \frac{\varepsilon}{2(m_a-1)} \pm i\,\frac{1}{2(m_a-1)}\sqrt{4(m_a-1)\bar{V}_a^2 - \varepsilon^2} \qquad (2.42a)$$

$$\text{Heteropolar:} \phi_a = \frac{\varepsilon-U}{2(m_a-1)} \pm i\,\frac{1}{2(m_a-1)}\sqrt{\frac{4(m_a-1)V_{aa}^2(\varepsilon-U)}{(\varepsilon+U)} - (\varepsilon-U)^2} \qquad (2.27a)$$

where $\bar{V}_a = \frac{1}{2}\left[V_{aa} + V_{ab}\right]$ and m_a is the coordination of an a-type atom. We now require a more general expression for ϕ_a, which will reduce to equations (2.12), (2.42a) and (2.27a) under the appropriate conditions. Recall that the parameter λ (equation (2.45); we will call it λ_a in this context) has the values -1, 0 and +1 for the cases of equations (2.12), (2.42a) and (2.27a) respectively (see Table 2.4); it would thus seem sensible to incorporate λ_a into a general formula for ϕ_a. We consider the interpolation formulae used by Falicov and Yndurain in their work on binary alloys[2.5].

Firstly, examination of equations (2.12), (2.42a) and (2.27a) reveals that we need a generalized interaction parameter $\hat{V}_a(\lambda_a)$ which will reduce to V_{aa}, $\frac{1}{2}\left[V_{aa} + V_{ab}\right]$ and V_{ab} for λ_a equal to -1, 0 and +1 respectively. A slight modification of the formula used by Falicov and Yndurain[2.5] gives:-

$$\hat{V}_a(\lambda_a) = \tfrac{1}{2}\left[(1-\lambda_a)V_{aa} + (1+\lambda_a)V_{ab}\right] \qquad (2.46)$$

which satisfies the above three conditions.

We can now write down a slightly modified form of Falicov and Yndurain's formula for ϕ_a[2,5], viz.:-

$$\phi_a(\lambda_a) = \frac{(\epsilon - |\lambda_a|U)}{2(m_a-1)} \pm i\,\frac{1}{2(m_a-1)}\sqrt{\frac{4(m_a-1)\hat{V}_a^2(\lambda_a)(\epsilon-|\lambda_a|U)}{(\epsilon+\lambda_a U)} - (\epsilon-|\lambda_a|U)^2} \qquad (2.47a)$$

This reduces to equation (2.12) for $\lambda_a = -1$, to equation (2.42a) for $\lambda_a = 0$ and to equation (2.27a) for $\lambda_a = +1$, as required. By considering equation (2.27b) and the "rules" used to obtain it from equation (2.27a) ($a \to b$, $+U \to -U$) we obtain:-

$$\phi_b(\lambda_b) = \frac{(\epsilon + |\lambda_b|U)}{2(m_b-1)} \pm i\,\frac{1}{2(m_b-1)}\sqrt{\frac{4(m_b-1)\hat{V}_b^2(\lambda_b)(\epsilon+|\lambda_b|U)}{(\epsilon-\lambda_b U)} - (\epsilon+|\lambda_b|U)^2} \qquad (2.47b)$$

where $\lambda_b = (m_b-2k_b)/m_b$, and $\hat{V}_b(\lambda_b)$ is obtained by interchanging a and b in equation (2.46) (remembering that $V_{ab} = V_{ba}$).

2.6.3 LDOS

With reference to Figure 2.8 we see that we now have a more complex cluster than in both the homopolar and heteropolar cases. This occurs because we need to distinguish between *two categories of second-nearest neighbours*, viz. those attached to a first-nearest neighbour (1st n.n.) of type a and those linked to b-type 1st n.n.s. We denote

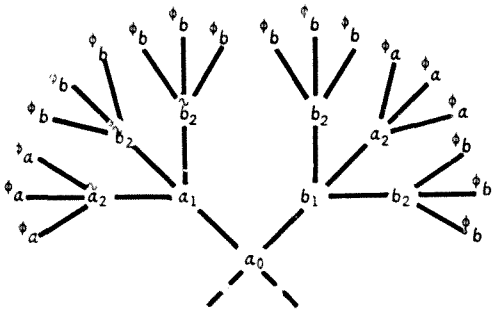

Figure 2.8 Chemically-disordered ("general-case") cluster with Bethe Lattices ϕ_a and ϕ_b attached to the dangling bonds.

atoms in the first category with superscript "~" (Figure 2.8). By again applying equations (2.2) and (2.11), and making use of our concise notation (Table 2.1), we are left with the following set of linear equations:-

$$\left.\begin{aligned}
\varepsilon_1\, g_{a_0} &= 1 + k_a V_{aa} g_{a_1} + (m_a - k_a) V_{ab} g_{b_1} \\
\varepsilon_1\, g_{a_1} &= V_{aa} g_{a_0} + (k_a - 1) V_{aa} g_{\tilde{a}_2} + (m_a - k_a) V_{ab} g_{\tilde{b}_2} \\
\varepsilon_2\, g_{b_1} &= V_{ab} g_{a_0} + (m_b - k_b - 1) V_{ab} g_{a_2} + k_b V_{bb} g_{b_2} \\
\varepsilon_1\, g_{\tilde{a}_2} &= V_{aa} g_{a_1} + (m_a - 1)\phi_a g_{\tilde{a}_2} \\
\varepsilon_2\, g_{\tilde{b}_2} &= V_{ab} g_{a_1} + (m_b - 1)\phi_b g_{\tilde{b}_2} \\
\varepsilon_1\, g_{a_2} &= V_{ab} g_{b_1} + (m_a - 1)\phi_a g_{a_2} \\
\varepsilon_2\, g_{b_2} &= V_{bb} g_{b_1} + (m_b - 1)\phi_b g_{b_2}
\end{aligned}\right\} \qquad (2.48)$$

We have seven equations in seven unknowns (the Green's function matrix elements). Solving for g_{a_0} gives:-

$$g_{a_0} = \frac{1}{\varepsilon_1 - \dfrac{k_a V_{aa}^2}{f_1} - \dfrac{(m_a - k_a) V_{ab}^2}{f_2}} \qquad (2.49)$$

where $$f_1 = \varepsilon_1 - \frac{(k_a - 1) V_{aa}^2}{\varepsilon_1 - (m_a - 1)\phi_a} - \frac{(m_a - k_a) V_{ab}^2}{\varepsilon_2 - (m_b - 1)\phi_b}$$

and $$f_2 = \varepsilon_2 - \frac{k_b V_{bb}^2}{\varepsilon_2 - (m_b - 1)\phi_b} - \frac{(m_b - k_b - 1) V_{ab}^2}{\varepsilon_1 - (m_a - 1)\phi_a}$$

Again note the continued fraction form of g_{a_0} (equation (2.49)), truncated at the third level of "nesting" by the functions ϕ_a and ϕ_b; cf equations (2.15) and (2.31) for the homopolar and heteropolar

cases respectively.

We now evaluate the LDOS for the generalized second-nearest neighbour cluster with an a-type atom at the centre, using the formula $n_a(\varepsilon) = -1/\pi \, \mathrm{Im} g_{a_0}$. The final result is:-

$$n_a(\varepsilon) = -\frac{1}{\pi} \frac{B}{A^2+B^2} \tag{2.50a}$$

where:-

$$\left.\begin{aligned} A &= \varepsilon_1 - \frac{k_a V_{aa}^2 \alpha}{\alpha^2+\beta^2} - \frac{(m_a-k_a)V_{ab}^2\gamma}{\gamma^2+\delta^2} \\ B &= \frac{k_a V_{aa}^2 \beta}{\alpha^2+\beta^2} + \frac{(m_a-k_a)V_{ab}^2\delta}{\gamma^2+\delta^2} \end{aligned}\right\} \tag{2.50b}$$

where in turn:-

$$\left.\begin{aligned} \alpha &= \varepsilon_1 - \frac{(k_a-1)V_{aa}^2 R_a}{R_a^2+I_a^2} - \frac{(m_a-k_a)V_{ab}^2 R_b}{R_b^2+I_b^2} \\ \beta &= \frac{(k_a-1)V_{aa}^2 I_a}{R_a^2+I_a^2} + \frac{(m_a-k_a)V_{ab}^2 I_b}{R_b^2+I_b^2} \\ \gamma &= \varepsilon_2 - \frac{k_b V_{bb}^2 R_b}{R_b^2+I_b^2} - \frac{(m_b-k_b-1)V_{ab}^2 R_a}{R_a^2+I_a^2} \\ \delta &= \frac{k_b V_{bb}^2 I_b}{R_b^2+I_b^2} + \frac{(m_b-k_b-1)V_{ab}^2 I_a}{R_a^2+I_a^2} \end{aligned}\right\} \tag{2.50c}$$

and:-

$$\left.\begin{aligned} R_a &= \varepsilon_1 - n_a \mathrm{Re}\phi_a \\ I_a &= n_a \mathrm{Im}\phi_a \\ R_b &= \varepsilon_2 - n_b \mathrm{Re}\phi_b \\ I_b &= n_b \mathrm{Im}\phi_b \end{aligned}\right\} \qquad (2.50d)$$

It can now be appreciated from a brief study of equations (2.50) that the formulae for the LDOS resulting from a third-nearest neighbour cluster would be impractically complicated for use in the very large number of charge and energy calculations we wish to perform (see Section 2.3.3.3).

As with the heteropolar lattice, we must also consider the case of a cluster centred on a b-type atom. The resulting LDOS ($n_b(\varepsilon)$) is obtained as before by interchanging the symbols a and b, and by replacing +U with -U. The total LDOS thus obtained is given by:-

$$n_{tot}(\varepsilon) = x_a n_a(\varepsilon) + x_b n_b(\varepsilon) \qquad (2.51)$$

where the a- and b-type LDOS ($n_a(\varepsilon)$ and $n_b(\varepsilon)$ respectively) are weighted according to the concentrations of the a- and b-type atoms (x_a and x_b respectively). Equation (2.51) provides the theoretical basis for the electronic energy calculations which will constitute the essence of this work.

2.7 SUMMARY OF CHAPTER 2

We have started with the observation that in a non-stoichiometric metal hydride the *long-range order* of a perfect crystalline system is absent and hence there is no longer any motivation to analyse the solid as a whole (cf band structure techniques). This observation, coupled with the emphasis on *local environment* in Chapter 1, has led us to break away from band structure techniques. We have started by considering the solid from the viewpoint of a *finite cluster* of atoms; however the literature reveals that this approach, using standard boundary conditions at the surface of the cluster, requires a cluster which is impractically large.

Secondly, we have commented on a quite different approach to disordered systems, viz. the *Bethe Lattice* method, in which the whole solid is represented by an infinite, branching "tree" of atoms with no long-range order. The Bethe Lattice model has the following attractive features: the *connectivity* of the solid is maintained; the *local order* of the system is retained through a constant coordination number; and the equations for the Local Density of States are analytically soluble. The main drawback of the Bethe Lattice method is that it produces rather featureless Local Densities of States and so is not very helpful.

In the present work we have employed a formalism which is essentially a *hybrid* of the above two approaches; this is the so-called *Cluster-Bethe-Lattice* (CBL) model, which consists of a *small cluster* of atoms with the surface boundary conditions being replaced by *Bethe Lattices* attached to the "dangling bonds" on the surface of the cluster. The consequent

equations for the Local Density of States (LDOS) are still analytically soluble, but now give rise to rich structure in the LDOS; the Cluster-Bethe-Lattice approach thus incorporates the best features of its constituent models.

The CBL model is formulated in terms of the *Green's functions* of the system because of the convenient methematical link between these functions and the Local Density of States. We have derived expressions for the LDOS for three physically well-defined *special cases*, viz. a *homopolar solid*, a *perfect binary alloy* and a *random alloy*, which we have synthesized into a *general* expression for the LDOS by implementing the *interpolation scheme* of Falicov and Yndurain[2,5]. This scheme is formulated in terms of a physically meaningful *order parameter*, in such a way that our expression for the LDOS reduces to the above three special cases for appropriate choices of this parameter.

In the next chapter we will evaluate suitable *energy parameters* for our CBL model, and in Section 4.2 we will write down appropriate formulae for the *order parameter* and related quantities.

APPENDIX 2.1

LDOS OF THE HOMOPOLAR "SINGLE SHELL" CLUSTER

Here we consider a Cluster-Bethe-Lattice model for a *homopolar* lattice, consisting of atoms of type a only. Specifically, we choose a cluster consisting of a central atom and only *one shell* of neighbouring atoms, that is the cluster only extends to nearest neighbours of the central atom. Hence we see that the Transfer Matrix must remove the lattice from second-nearest neighbours outwards so that, in line with equation (2.6), we obtain:-

$$T = \frac{\langle a_{N+1}|G|a_0\rangle}{\langle a_N|G|a_0\rangle} \quad , \quad N \geq 1 \qquad \text{(A2.1.1)}$$

With reference to equations (2.7a) and Table 2.1 we can then write down the following "single shell" cluster equations:-

$$\epsilon_1 \, g_{a_0} = 1 + mVg_{a_1} \qquad \text{(A2.1.2)}$$

$$\epsilon_1 \, g_{a_1} = Vg_{a_0} + n\phi g_{a_1} \qquad \text{(A2.1.3)}$$

Solving equations (A2.1.2) and (A2.1.3) for g_{a_0} gives:-

$$g_{a_0} = \frac{1}{\epsilon_1 - \frac{mV^2}{\epsilon_1 - n\phi}} \qquad \text{(A2.1.4)}$$

Comparison with equation (2.15) reveals that the mean field function ϕ truncates the continued fraction (equation(A2.1.4)) one level

sooner in the present case. We now use equation (A2.1.4) to obtain an expression for the LDOS for this cluster, viz.:-

$$n(\varepsilon) = -\frac{1}{\pi}\,\mathrm{Img}_{a_0} = -\frac{1}{\pi}\,\frac{\gamma}{\beta^2+\gamma^2} \qquad \text{(A2.1.5a)}$$

where:-

$$\left.\begin{aligned} \beta &= \varepsilon_1 - \frac{mV^2}{\alpha^2}\,(\varepsilon_1 - n\mathrm{Re}\phi) \\ \gamma &= \frac{mnV^2\,\mathrm{Im}\phi}{\alpha^2} \end{aligned}\right\} \qquad \text{(A2.1.5b)}$$

$$\left.\begin{aligned} \alpha^2 &= (\varepsilon_1 - n\mathrm{Re}\phi)^2 + (n\mathrm{Im}\phi)^2 \\ \mathrm{Re}\phi &= \frac{\varepsilon_1}{2n} \\ \mathrm{Im}\phi &= -\frac{\sqrt{\varepsilon_1^2 - 4mV^2}}{2n} \end{aligned}\right\} \qquad \text{(A2.1.5c)}$$

Note that in this case we choose the negative sign in front of Imφ so as to keep the LDOS positive.

A comparison of equations (A2.1.5) and equations (2.16) reveals a richer mathematical structure for the "double shell" cluster model; we therefore expect the latter to provide a more detailed picture of the LDOS than the "single shell" approach.

REFERENCES (CHAP. 2)

2.1) McGill T C and Klima J 1972 *Phys. Rev. B* 5 1517

2.2) Husumi K 1950 *J. Chem. Phys.* 18 682

2.3) Joannopoulos J D and Yndurain F 1974 *Phys. Rev. B* 10 5164

2.4) Yndurain F and Joannopoulos J D 1975 *Phys. Rev. B* 11 2957

2.5) Falicov L M and Yndurain F 1975 *Phys. Rev. B* 12 5664

2.6) Falicov L M and Yndurain F 1975 *J. Phys. C* 8 147

2.7) Bassani F and Brust D 1963 *Phys. Rev.* 131 1524

2.8) Ehrenreich H and Schwartz L M 1976 *The Electronic Structure of Alloys* in *Solid State Phys.* 31 149 (Ed.s: Ehrenreich H, Seitz F and Turnbull D; publ.: Academic, New York)

CHAPTER 3

PARAMETRIZATION

3.1 INTRODUCTION

In Chapter 1 we expressed the need for a non-periodic, localized model for non-stoichiometric transition metal hydrides, in particular that of palladium. Chapter 2 laid the foundation for just such a model by developing a formalism for a non-stoichiometric binary alloy with a variable order parameter λ (see equation (2.45)). In this chapter we will begin to apply this model to PdH_x by evaluating physically-sensible expressions for the three interaction parameters V_{aa}, V_{ab} and V_{bb} and for the energy-level parameter U. Section 2.3.3.1 and Table 2.2 remind us that these energy parameters are simply matrix elements of the Hamiltonian of the system. So we firstly want a simple, physically-transparent Hamiltonian which is nevertheless compatible with standard band structure parametrizations for Pd and PdH; and secondly, we require simple approximations (based on a semiempirical understanding of the electronic properties of transition metals in general) to take advantage of this compatibility.

This chapter is broken up as follows: in Section 3.2 we give thought to a suitable Hamiltonian, with particular attention paid to stripping away all but the most important terms; Section 3.3 is devoted to a review of the classic paper by Slater and Koster concerning the

parametrization of band structure calculations; this will provide sufficient information for the appreciation of Section 3.4, in which we derive an approximate expression for the palladium-palladium interaction parameter; in Section 3.5 we apply Molecular Orbital Theory and information from Section 3.3 to obtain a similar formula for the palladium-hydrogen interaction parameter; Section 3.6 considers the hydrogen-hydrogen and energy-level parameters; in Section 3.7 we choose values from a suitable BS parametrization, from which we derive a table of parameters to be used in subsequent chapters; and finally Section 3.8 contains a summary of the important features and results of this chapter.

3.2 CHOICE OF HAMILTONIAN

Palladium is a transition metal and hence its valence bands are expected to be predominantly d-type. This is confirmed by BS calculations in which we invariably find that the Fermi energy E_F falls in an energy range dominated by the d-bands[3.1]; further, we have seen already (Sections 1.2.3 and 1.2.4) that the DOS is high at E_F, which would not be the case for s- or p-type valence bands. Since the electronic properties of a metal are largely determined by the nature of its valence bands, we shall assume from the outset that the palladium-palladium interaction is purely between the d-orbitals. Thus, if we take the a-type atom of Chapter 2 to be palladium, we now have:-

$$V_{aa} = V_{PdPd} = V_{dd} \tag{3.1}$$

This equation is nevertheless only an approximation: we recall from Section 1.2.2 the experimental finding that the palladium valence bands contain 0.36 electron in the 5s orbitals; thus equation (3.1) should strictly contain a contribution of the form V_{sd}. However, due to the compatibility of BS calculations performed for both $4d^95s^1$ and $4d^{10}5s^0$ configurations of palladium (Section 1.2.3), we shall assume from here on that equation (3.1) is an adequate representation of the palladium-palladium interaction.

The so-called Tight-Binding (TB) model has proved particularly effective in describing metals with predominantly d-type valence states[3.2)p.35], and hence it seems sensible to choose a TB Hamiltonian

for our formalism. The TB approach is a particular case of the LCAO (Linear Combination of Atomic Orbitals) technique and hence we expect these two methods to be compatible; this is important because in subsequent sections we shall be applying an LCAO-based technique to obtain expressions for our interaction parameters.

Our Hamiltonian will have to include terms to account for the presence of hydrogen in the palladium lattice; these must be given the same Tight-Binding form as the pure metal terms. The b-type atoms of Chapter 2 are now taken to be hydrogen, and following equation (3.1) we can write:-

$$V_{bb} = V_{hh} \tag{3.2a}$$

$$V_{ab} = V_{ba} = V_{hd} \tag{3.2b}$$

It follows that the parameters describing the energies of the a and b states in Chapter 2 are given by:-

$$U_a = U_d \tag{3.3a}$$

$$U_b = U_h \tag{3.3b}$$

We now substitute equations (3.1)-(3.3) into the TB Hamiltonian used by Falicov and Yndurain[3.3], to obtain a Hamiltonian suitable for our purposes:-

$$H = \sum_i U_i |i><i| + \sum_{i,j} V_{ij} |i><j| \tag{3.4}$$

where:-

$|i\rangle$ is the wave function of the atom at site i;

U_i is either U_d or U_h, depending on whether there is a palladium or a hydrogen atom at site i;

the sum over i and j is restricted to nearest neighbours only;

and V_{ij} is either V_{dd}, V_{hh} or V_{hd}, depending on whether the i^{th} and j^{th} atoms are both palladium, both hydrogen, or one of each.

The rest of this chapter is concerned with finding expressions and values for the parameters V_{ij} and U_i.

3.3 THE SLATER-KOSTER INTERPOLATION SCHEME

3.3.1 Introduction

Although band structure (BS) techniques are usually highly accurate, they are nevertheless only computationally feasible at points of high symmetry in the Brillouin zone (where the secular determinant is considerably simplified, leading to degenerate states). To obtain a continuous plot of the energy bands of a crystalline solid it is therefore necessary to fit curves to the calculated points. This could be achieved with least-squares or cubic spline fits, but the polynomial coefficients would have no physical significance. In their classic paper of 1954, Slater and Koster[3.4] introduced an interpolation scheme which generates coefficients which do have physical meaning; this paper is reviewed in some detail in Appendix 1.

Section 3.3.2 is a summary of this review, and will provide the reader with an adequate working knowledge of the Slater-Koster (SK) scheme and its by-products to appreciate the rest of this chapter.

3.3.2 Outline of the Scheme

Slater and Koster start by developing an LCAO (Linear Combination of Atomic Orbitals) model for a crystalline solid. This approach assumes that the wave functions of the solid can be built up from atomic orbitals; this procedure is carried out in two main steps: firstly, a given atomic orbital $\phi_i(\underline{r}-\underline{R}_j)$, where $\underline{R}_j$ is a lattice site, is "delocalized" by summing it over a large number of sites $\underline{R}_j$;

weighting factors $e^{i\underline{k}\cdot\underline{R}_j}$ are used, where $\underline{k}$ is the crystal momentum vector. The result is a so-called Bloch sum $B_l = \sum_j e^{i\underline{k}\cdot\underline{R}_j}\phi_l(\underline{r}-\underline{R}_j)$; and secondly, a linear combination of these Bloch sums is taken, giving the complete LCAO approximation to the wave function.

The next step is to evaluate the energy matrix element $\langle B_l|H|B_{l'}\rangle$ between any two Bloch sums B_l and $B_{l'}$; this turns out to be a linear combination of a large number of complicated integrals, of the form $\langle\phi_l|H|\phi_{l'}\rangle$. The Hamiltonian H in turn contains a sum of spherically-symmetric potential wells situated on all N atoms of the system; introducing *orthogonalized* atomic orbitals $\{\psi_l\}$ (see Appendix I) we have that $\langle B_l|H|B_{l'}\rangle$ consists of a linear combination of energy integrals of the following form:-

$$E_{l,l'} = \int_V \psi_l^*(\underline{r}-\underline{R}_j)\, H\, \psi_{l'}(\underline{r}-\underline{R}_{j'})dV \qquad (3.5)$$

where H contains terms like $v(\underline{r}-\underline{R}_{j''})$, which is the potential well associated with the atom at $\underline{R}_{j''}$. Thus we see that the right-hand side of equation (3.5) is a *three-centre integral* (referring to atoms at $\underline{R}_j$, $\underline{R}_{j'}$, $\underline{R}_{j''}$), which the authors describe as being computationally intractable, both because of their complexity and number.

It is at this point that Slater and Koster introduce their ingenious parametrization scheme by simply replacing these integrals with disposable constants; in other words, we are provided with an interpolation scheme in which the coefficients represent the physically-significant integrals $\{E_{l,l'}\}$ of equation (3.5). The definition of

$E_{l,l'}$ must be extended to allow explicitly for interactions between nearest, second-nearest and third-nearest neighbours; this is done for convenience rather than for physical reasons: we require a mechanism for generating as many constants $\{E_{l,l'}\}$ as we need. Hence we write:-

$$E_{l,l'} = E_{l,l'}(n_{1j}, n_{2j}, n_{3j}) \tag{3.6}$$

where n_{1j}, n_{2j}, n_{3j} are integers such that for lattice constant "a" we have $\underset{\sim}{R}_j = n_{1j}a\hat{i} + n_{2j}a\hat{j} + n_{3j}a\hat{k}$; we recall that $\underset{\sim}{R}_j$ is the vector linking a given atom to a particular atom in its j^{th} near-neighbour shell. It follows immediately that these $\underset{\sim}{R}_j$ vectors are determined by the crystal structure of the lattice (for example fcc in the case of palladium metal). Hence the energy matrix elements may finally be expressed as:-

$$\langle B_l|H|B_{l'}\rangle = \sum_j e^{i\underset{\sim}{k}\cdot(\underset{\sim}{R}_{j'}-\underset{\sim}{R}_j)} E_{l,l'}(n_{1j}, n_{2j}, n_{3j}) \tag{3.7}$$

where the second summation which would have been present cancels with the normalization constant, and where we note that $\underset{\sim}{k}\cdot\underset{\sim}{R}_j$ can be expressed as $ak_x n_{1j} + ak_y n_{2j} + ak_z n_{3j}$. Equation (3.7) contains the essence of the Slater-Koster (SK) scheme: the energies $\langle B_l|H|B_{l'}\rangle$ are known for certain values of (k_x, k_y, k_z) from BS calculations, the $\{E_{l,l'}\}$ are the energy parameters to be evaluated, and the factors $\{e^{ia(k_x n_{1j}+k_y n_{2j}+k_z n_{3j})}\}$ ensure that the $\{E_{l,l'}\}$ will be expressed in terms of the general vector (k_x, k_y, k_z).

As mentioned above, the SK scheme allows us to *increase* the number of $\{E_{l,l'}\}$ parameters by considering more distant neighbours. But what if we are required to *reduce* the number of $E_{l,l'}$s? This question led Slater and Koster to introduce the *Two-Centre Approximation* (TCA) into their scheme; consider equation (3.5) above: for the off-diagonal case ($\underline{R}_j \neq \underline{R}_{j'}$) the integral on the right-hand side can belong to one of two classes, either $\underline{R}_j \neq \underline{R}_{j'} \neq \underline{R}_{j''}$ (three-centre integral) or $\underline{R}_j \neq \underline{R}_{j'}$, $\underline{R}_{j''} = \underline{R}_j$ or $\underline{R}_{j'}$ (two-centre integral). By orbital-overlap considerations it can be seen that three-centre integrals will be *smaller* than two-centre integrals; the underlying assumption of the TCA is that the three-centre integrals are in fact *negligible*.

The TCA thus models interatomic interactions in a way similar to that employed for diatomic molecules, with atomic-like orbitals space-quantized about the interatomic axis $\underline{R}_{j'}-\underline{R}_j$; consequently, the associated two-centre energy integrals will be directed along this axis. Slater and Koster represent these integrals by the parameters $(mn\lambda)_i$, where m,n are s,p,d states, λ is σ,π,δ and i = 1,2,3 refers to nearest, second-nearest, and third-nearest neighbours respectively. The parameters $\{E_{l,l'}\}$ can be expressed as linear combinations of the parameters $\{(mn\lambda)_i\}$ (see Table A1.1 for examples), and the appropriate substitutions made in equation (3.7). The most important feature of such a substitution is that it almost invariably reduces the number of fitting parameters, as required (see Appendix 1 for details).

Once the number of parameters equals the number of energy states which are to be fitted, equations like equation (3.7) can be solved for these energy parameters; although they will have some physical significance, we note that they are by no means unique, depending as they do on the number of states fitted as well as on the BS technique used to generate these states.

In subsequent sections we shall make use of the SK interpolation scheme, and in particular the Two-Centre Approximation, to obtain suitable interaction parameters for our model.

3.4 THE PALLADIUM-PALLADIUM INTERACTION PARAMETER (V_{dd})

3.4.1 Introduction

We are now in a position to evaluate an expression for V_{dd}, using the same approach as Lowther[3.5]; we first take up the analysis of Heine[3.2]p.57ff to obtain an approximate link between the two-centre integral (ddσ) and the width of the d bands of transition metals; and secondly, we refer back to Chapter 2 to find an expression for the width of the palladium d band in terms of our parameter V_{dd}. We are finally left with an approximate expression for V_{dd} in terms of the single two-centre integral (ddσ), which we shall choose from a suitable BS parametrization in Section 3.7.

3.4.2 Link between Two-Centre Integrals and Band Widths

Heine[3.2]p.58 and Papaconstantopoulos et al[3.1] remind us that the d bands of a transition metal cover a relatively narrow energy range, and that they overlap the broad s and p bands. The orbitals associated with the d bands have the expected TB structure, whereas those associated with the s and p bands have plane wave (PW) form (as expected of broad bands). The radial part of the Schrödinger equation for the d orbitals contains a repulsive centrifugal barrier which tends to confine d electrons within their host atoms (hence the TB concept), but they can tunnel out. Such tunnelling causes the d states to resonate with plane wave states of similar energy; an interaction of this type can be approached from the viewpoint of resonance theory, from which one may extract an approximate expression related to the width of the d bands; this is given by[3.6]:-

$$W = 2K_o\left[\int_o^s j_2(K_o r)V(r)\phi(r)r^2 dr\right]^2 \qquad (3.8)$$

where

$K_o = \sqrt{2E_o}$, E_o being the energy at resonance and hence at the centre of the resonance band;

s is the atomic radius;

$j_2(K_o r)$ is the spherical Bessel function of order 2 and represents a component of a plane wave interacting via the potential V(r) with the radial part $\phi(r)$ of the d orbital. More precisely, $\phi(r) = u(r,E_o)$, where u(r,E) is the radial wave function for any energy E.

Thus W models the interaction between TB and PW orbitals; in terms of the uncertainty principle we have that $\hbar/W$ is the time required for a d electron to escape into the PW states outside the atom. By expanding $j_2(K_o r)$ to lowest order in $K_o r$ (that is, taking $j_2(K_o r) \approx (K_o r)^2/15$) equation (3.8) becomes:-

$$W = 2K_o^5 M^2/225 \qquad (3.9a)$$

where

$$M = \left|\int_o^s V(r)\phi(r)r^4 dr\right| \qquad (3.9b)$$

Using another lowest-order expansion, the well-known expression for the radial wave function[3.6] reduces to:-

$$u(r,E) \approx \frac{E_o - E}{M} r^2 + \frac{M}{5r^3} \text{ for } r \geq s \qquad (3.10)$$

We must bear in mind that equation (3.10) refers to the d states only. By applying suitable boundary conditions to equation (3.10) we are able to find expressions for both the lowest energy (E_{min}) and highest energy (E_{max}) of the d bands; $\Delta = E_{max} - E_{min}$ can then be taken as an approximate measure of the width of the d bands of a transition metal. We eventually obtain:-

$$\Delta \simeq \tfrac{1}{2}M^2/s^5 \qquad (3.11)$$

We notice that dependence on the resonance energy E_o has been cancelled out in the derivation of equation (3.11); Δ is thus seen to depend only on atomic orbitals, the atomic potential and the atomic radius. That is, Δ is essentially an *intra-atomic* parameter; this would appear to be physically incorrect, since the band width is generally understood to be an *interatomic* effect. To resolve this paradox we consider an integral of the two-centre type (cf Section 3.3.2) between a pair of d orbitals ϕ_l and $\phi_{l'}$, located on atoms at $\underline{R}_j$ and $\underline{R}_{j'}$ respectively:-

$$(l\ l'\lambda) = \int_V \phi_l^*(\underline{r}-\underline{R}_j)v(\underline{r}-\underline{R}_{j'})\phi_{l'}(\underline{r}-\underline{R}_{j'})dV \qquad (3.12)$$

The major contribution to this integral is *not* from the region midway between $\underline{R}_j$ and $\underline{R}_{j'}$ (as would be the case for s-p bonding), the reason being that d orbitals peak very close to their parent atoms (for example at about 9% of the interatomic distance in copper). Hence the dominant contribution to the integral in equation (3.12) comes from deep inside the atom at $\underline{R}_{j'}$, where the effects of the d orbital located at $\underline{R}_j$ are hardly felt at all. We are thus left with an *interatomic* integral which nevertheless has essentially *intra-atomic* features, and the paradox is at least qualitatively resolved.

Thus a feature emphasized by this analysis is the essentially *localized* nature of transition metal d orbitals, which confirms our findings concerning the importance of near-neighbour atoms (Section 1.2.8).

With the basic physical concepts of the width Δ of the d band established, we now seek to combine equation (3.11) for Δ with the two-centre approach of equation (3.12). Because the biggest contribution to bonds between like orbitals is due to σ-overlap, we make the rough assumption that the d-d interaction can be expressed in terms of the single two-centre integral $(dd\sigma)$. Because a d orbital has at most four lobes, we can only have about four $dd\sigma$ bonds per transition metal atom. With reference to equations (3.8), (3.9a and b), and (3.12) we see that M corresponds to a two-centre integral; if we associate M with four $dd\sigma$ bonds per atom then $\Delta \propto \frac{1}{5}M^2$ consists roughly of $\frac{1}{5}(4)^2 = 8$ $(dd\sigma)$ integrals, so that:-

$$\Delta \simeq -8(dd\sigma) \tag{3.13}$$

where the minus sign is taken because $(dd\sigma)$ is expected to be negative. We now wish to test the validity of this highly intuitive derivation. Using a more rigorous approach, Heine obtains the following expression:-

$$(dd\sigma) = -6M^2/5R^5 \tag{3.14a}$$

where R is the interatomic spacing; for nearest neighbours in the fcc structure, Heine gives the relation $s \simeq 0.5526R$ so that equation (3.14a) becomes:-

$$(dd\sigma) \simeq -1.2(0.5526)^5\ M^2/s^5 \tag{3.14b}$$

Substituting equation (3.14b) into equation (3.11) gives us:-

$$\Delta = \tfrac{1}{2}t^2/s^5 = -\tfrac{1}{2}\,\frac{1}{1.2(0.5526)^5}\,(dd\sigma) \simeq -8.1(dd\sigma) \qquad (3.15)$$

leaving us with the remarkable result that equation (3.13) is accurate to about 1%, and therefore quite acceptable for our purposes.

3.4.3 *Link between our d Band Width and V_{dd}*

We wish to use one of our LDOS expressions in Chapter 2 to obtain an expression for the d band width in terms of V_{dd}. For this purpose we consider pure palladium metal, that is, the case of a *homopolar* lattice. The LDOS for such a lattice is given by equations (2.16), into which we substitute V_{dd} for V and U_d for U. We notice that the numerator η of this LDOS expression is proportional to the quantity γ, which in turn is proportional to $\mathrm{Im}\phi$, where:-

$$\mathrm{Im}\phi = \frac{1}{2(m-1)}\sqrt{4(m-1)V_{dd}^2 - (\varepsilon - U_d)^2} \qquad (3.16a)$$

Thus we have:-

$$(\text{LDOS of d-band}) \quad \propto \quad \sqrt{4(m-1)V_{dd}^2 - (\varepsilon - U_d)^2} \qquad (3.16b)$$

It follows from equation (3.16b) that the maximum energy of the d band, ε_{max}, is given by $\varepsilon_{max} = U_d - 2\sqrt{m-1}\,V_{dd}$ (assuming $V_{dd} < 0$), and that the minimum energy, ε_{min}, is given by $\varepsilon_{min} = U_d + 2\sqrt{m-1}\,V_{dd}$. Hence the band width is $\Delta = \varepsilon_{max} - \varepsilon_{min}$, giving us the result:-

$$\Delta = -4\sqrt{m-1}\ V_{dd} \tag{3.17}$$

We now combine equations (3.13) and (3.17) to give us a formula for V_{dd} in terms of the two-centre integral (ddσ). The final result is:-

$$V_{dd} = \frac{2}{\sqrt{m-1}}\ (dd\sigma) \tag{3.18}$$

We proceed now to evaluate the palladium-hydrogen interaction parameter V_{hd}.

3.5 THE PALLADIUM-HYDROGEN INTERACTION PARAMETER (V_{hd})

3.5.1 Introduction

We shall approach the evaluation of the parameter V_{hd} from the localized viewpoint of Molecular Orbital Theory (MOT), again following Lowther (1982)[3.5]; we recall the importance of local environment in the Pd/H system, and hence feel justified in using MOT. We found in Section 1.2.7 that a hydrogen atom occupies the *octahedral* interstitial site in palladium; this results in PdH_1 having the NaCl structure, that is two fcc lattices superimposed on each other. We thus see that the hydrogen and palladium sites are symmetrically identical, so that we can correctly think of a palladium atom as being in an octahedral "interstitial site" of the hydrogen lattice. This viewpoint will be convenient for the application of MOT, where it is much simpler to have a metal central atom surrounded by hydrogen ligands than vice versa. The MOT approach will require us to represent these hydrogen ligands by means of a "molecular" orbital, this being an appropriate linear combination of the hydrogen s states on the six sites surrounding the palladium atom (see Figure 3.1). The assumption is that all six octahedral sites are occupied, corresponding to PdH_1 (cf our evaluation of the parameter V_{dd}, which was done on the basis of pure Pd metal).

3.5.2 Intuitive Approach

We began with an intuitive approach to this MOT calculation; firstly, we assume that the palladium atoms has only d-type valence orbitals, in keeping with our choice of Hamiltonian in Section 3.2. There are

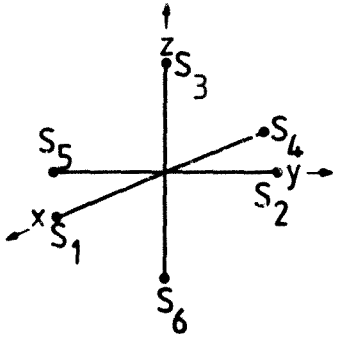

Figure 3.1 Numbering of hydrogen atoms octahedrally coordinated about a palladium atom (after Lowther[3.5] p. 900).

five d orbitals, and from Figure 3.2 we see that geometrically they fall into two distinct classes: the xy, yz, zx orbitals have *nodes* in the direction of the Cartesian axes, whereas the $3z^2-r^2$, x^2-y^2 orbitals have *lobes* in the direction of the axes. Now we see from Figure 3.1 that the hydrogen atoms are situated *on* the axes in our case of octahedral symmetry; hence we do not expect the first class of orbitals (d_{t_2}) to interact with the hydrogen s states at all, whereas the second class of orbitals (d_e) should interact with these s states, presumably forming hybrid orbitals. These observations can be proved rigorously using Group Theory, and we can thus exclude the three d_{t_2} orbitals from our discussion; further, the two d_e orbitals can be shown to be energetically degenerate (a group-theoretical consequence of their belonging to the same symmetry class), so that our picture of the d orbitals is greatly simplified.

Superimposing a d_e orbital from Figure 3.2 onto Figure 3.1 immediately reveals a directed bonding structure, such as one would expect to find in a diatomic molecule for instance; hence we immediately see the possibility of using the two-centre approximation discussed in Section 3.3.2. Ignoring the (sdπ) and (sdδ) integrals (cf our neglect of the (ddπ) and (ddδ) integrals in Section 3.4.2), we are left with the single integral (sdσ) with which we wish to model the palladium-hydrogen interaction V_{hd}.

To obtain an approximate expression for V_{hd}, we must appreciate that the simple Hamiltonian we have chosen (equation (3.4)) requires us to approximate the sum of orbitals on the palladium atom by a single wave function $|i\rangle$; because the form given to this wave function in equation (3.4) is identical to that of the hydrogen orbital, we conclude that an s-like composite d orbital is implied by this formalism. Such an approximation can be intuitively seen to be not too bad by superimposing the various d orbitals of Figure 3.2, noting

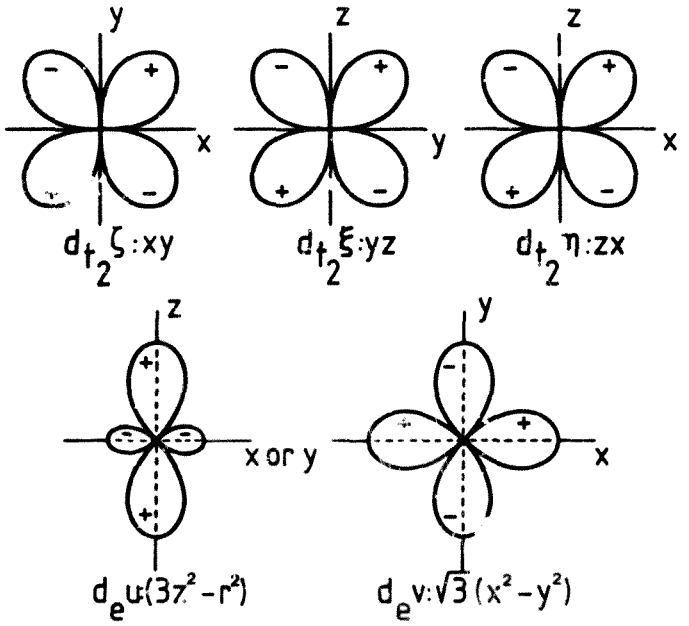

Figure 3.2 Schematic representation of the five d orbitals of a transition metal (after Watanabe[3.7]p.95).

that d_e lobes will "fill in" d_{t_2} nodes, and vice versa. We can thus express V_{hd} in terms of an s-like orbital on palladium interacting with an s-like hydrogen molecular orbital, and the detailed analysis to follow will reveal that this is sufficient for obtaining a link between V_{hd} and (sdσ), as required.

3.5.3 *Rigorous Approach*

We recall from the previous section that only the d_e orbitals of palladium interact with the adjacent hydrogen s orbitals for the case of octahedral symmetry in PdH_1. We also commented on the degeneracy of the d_e orbitals and the possibility of describing their interaction with the nearest-neighbour hydrogen orbitals in terms of the single two-centre integral (sdσ); and lastly we made some comments regarding the s-like nature of our simple Hamiltonian, which will allow us to link V_{hd} with (sdσ).

We now quantify these ideas by considering three different hydrogen molecular orbitals, octahedrally coordinated about a central palladium atom; the first two have symmetries compatible with d_e orbitals on the palladium atom, and the symmetry of the third is compatible with an s-like palladium orbital. In each case we evaluate the energy matrix element between the particular palladium and molecular orbitals, using the Slater-Koster scheme to express these in terms of two-centre integrals. The first two matrix elements will be identical, as expected of degenerate states; if we assume that these are also degenerate with the third matrix element then our expression for V_{hd} follows immediately.

The following three equations describe the above-mentioned hydrogen molecular orbitals, and are taken from work by Watanabe[3.7]:-

$$\psi_{x^2-y^2} = \tfrac{1}{2}(s_1 - s_2 + s_4 - s_5) \tag{3.19a}$$

$$\psi_{3z^2-r^2} = \frac{1}{\sqrt{12}}(-s_1 - s_2 + 2s_3 - s_4 - s_5 + 2s_6) \tag{3.19b}$$

$$\psi_s = \frac{1}{\sqrt{6}}(s_1 + s_2 + s_3 + s_4 + s_5 + s_6) \tag{3.19c}$$

where the hydrogen s orbitals s_i are as in Figure 3.1. To construct energy matrix elements using equations (3.19a-c) we need the following SK parameters, taken from Table A1.1:-

$$E_{x^2-y^2,s_i} = \tfrac{1}{2}\sqrt{3}\,(l^2-m^2)(sd\sigma) \tag{3.20a}$$

$$E_{3z^2-r^2,s_i} = \left[n^2 - \tfrac{1}{2}(l^2 + m^2)\right](sd\sigma) \tag{3.20b}$$

$$E_{s,s_i} = (ss\sigma) \tag{3.20c}$$

With reference to equations (3.19a-c), (3.20a-c) and Figure 3.1 we obtain Table 3.1:-

s_i	(l,m,n)	$E_{x^2-y^2,s_i}$	$E_{3z^2-r^2,s_i}$
s_1	(1,0,0)	$\frac{1}{2}\sqrt{3}(sd\sigma)$	$-\frac{1}{2}(sd\sigma)$
s_2	(0,1,0)	$-\frac{1}{2}\sqrt{3}(sd\sigma)$	$-\frac{1}{2}(sd\sigma)$
s_3	(0,0,1)	0	$(sd\sigma)$
s_4	(-1,0,0)	$\frac{1}{2}\sqrt{3}(sd\sigma)$	$-\frac{1}{2}(sd\sigma)$
s_5	(0,-1,0)	$-\frac{1}{2}\sqrt{3}(sd\sigma)$	$-\frac{1}{2}(sd\sigma)$
s_6	(0,0,-1)	0	$(sd\sigma)$

Table 3.1 Slater-Koster parameters for the six hydrogen s orbitals.

Let the coefficients of the s orbitals s_i in equations (3.19) be represented by the set $\{a_i(\psi_\nu)\}$, where $\nu = x^2-y^2,\ 3z^2-r^2, s$. It

$$\psi_{x^2-y^2} = \tfrac{1}{2}(s_1 - s_2 + s_4 - s_5) \tag{3.19a}$$

$$\psi_{3z^2-r^2} = \frac{1}{\sqrt{12}}(-s_1 - s_2 + 2s_3 - s_4 - s_5 + 2s_6) \tag{3.19b}$$

$$\psi_s = \frac{1}{\sqrt{6}}(s_1 + s_2 + s_3 + s_4 + s_5 + s_6) \tag{3.19c}$$

where the hydrogen s orbitals s_i are as in Figure 3.1. To construct energy matrix elements using equations (3.19a-c) we need the following SK parameters, taken from Table A1.1:-

$$E_{x^2-y^2,s_i} = \tfrac{1}{2}\sqrt{3}\,(l^2-m^2)(sd\sigma) \tag{3.20a}$$

$$E_{3z^2-r^2,s_i} = \left[n^2 - \tfrac{1}{2}(l^2+m^2)\right](sd\sigma) \tag{3.20b}$$

$$E_{s,s_i} = (ss\sigma) \tag{3.20c}$$

With reference to equations (3.19a-c), (3.20a-c) and Figure 3.1 we obtain Table 3.1:-

s_i	(l,m,n)	$E_{x^2-y^2,s_i}$	$E_{3z^2-r^2,s_i}$
s_1	(1,0,0)	$\frac{1}{2}\sqrt{3}(sd\sigma)$	$-\frac{1}{2}(sd\sigma)$
s_2	(0,1,0)	$-\frac{1}{2}\sqrt{3}(sd\sigma)$	$-\frac{1}{2}(sd\sigma)$
s_3	(0,0,1)	0	$(sd\sigma)$
s_4	(-1,0,0)	$\frac{1}{2}\sqrt{3}(sd\sigma)$	$-\frac{1}{2}(sd\sigma)$
s_5	(0,-1,0)	$-\frac{1}{2}\sqrt{3}(sd\sigma)$	$-\frac{1}{2}(sd\sigma)$
s_6	(0,0,-1)	0	$(sd\sigma)$

Table 3.1 Slater-Koster parameters for the six hydrogen s orbitals.

Let the coefficients of the s orbitals s_i in equations (3.19) be represented by the set $\{a_i(\psi_\nu)\}$, where $\nu = x^2-y^2,\ 3z^2-r^2, s$. It

then follows from the SK scheme that the energy matrix elements are given by:-

$$\langle \nu|H|\psi_\nu\rangle = \sum_{i=1}^{6} a_i(\psi_\nu)E_{\nu,s_i} \tag{3.21}$$

where $|\nu\rangle$ refers to the palladium atomic orbital and $|\psi_\nu\rangle$ to the corresponding hydrogen molecular orbital.

Using equations (3.19a and b) and Table 3.1 we find that equation (3.21) gives us:-

$$\langle x^2-y^2|H|\psi_{x^2-y^2}\rangle = \langle 2z^2-r^2|H|\psi_{3z^2-r^2}\rangle = \sqrt{3}(sd\sigma) \tag{3.22}$$

where we have the expected degeneracy of the two d_e orbitals, and by making use of equations (3.19c) and (3.20c) in equation (3.21) we obtain:-

$$\langle s|H|\psi_s\rangle = \sqrt{6}(ss\sigma) \tag{3.23a}$$

Because our Hamiltonian H is s-like (see Section 3.5.2) we expect equation (3.23a) to give us the best physical picture of the palladium-hydrogen interaction parameter V_{hd}. In deriving equation (3.23a) from equation (3.21) we have the following intermediate steps:-

$$\langle s|H|\psi_s\rangle = \sum_{i=1}^{6} a_i(\psi_s)(ss\sigma)$$

$$= \frac{1}{\sqrt{6}} \sum_{i=1}^{6} 1.(ss\sigma)$$

$$= \sqrt{6}(ss\sigma)$$

The second-last step indicates that it is quite reasonable to approximate V_{hd} by $(ss\sigma)$, so that equation (3.23a) becomes:-

$$\langle s|H|\psi_s\rangle \simeq \sqrt{6}\, V_{hd} \qquad (3.23b)$$

The final step is to assume that the matrix element of equation (3.23b) is equal to those of equation (3.22); this is physically reasonable since the s-like palladium wave function $|s\rangle$ is supposed to approximate the behaviour of the more complicated d orbitals which are present in the real metal. Hence combining equations (3.22) and (3.23b) we finally obtain:-

$$V_{hd} \simeq \frac{1}{\sqrt{2}} (sd\sigma) \qquad (3.24)$$

We next make some comments on the parameters V_{hh} and U.

3.6 THE HYDROGEN-HYDROGEN AND ENERGY-LEVEL PARAMETERS (V_{hh} AND U)

Rather than derive independent expressions for these parameters, we shall instead take them from the BS parametrization which we decide to use for evaluating V_{dd} and V_{hd} (via equations (3.18) and (3.24) respectively). We can however make certain qualitative observations regarding V_{hh} and U, and these will in fact assist us in choosing a suitable BS parametrization.

Firstly, we recall our comments of Section 1.2.8 concerning the hydrogen-hydrogen *electronic* interaction, namely that we expect it to be small (because the hydrogen-hydrogen separation in octahedral interstitial sites of the palladium lattice is roughly 4 Å, as compared to the interatomic separation of roughly 1 Å in the hydrogen molecule). Thus we wish to find a BS parametrization for which (sss) is small or zero for the hydrogen-hydrogen interaction.

Secondly, we refer to the photoelectron spectroscopy experiments performed by Schlapbach and Burger[3.8] on $PdH_{0.6}$; they find a band at about 8 eV (≈0.6 Ryd) below E_F, which they associate with hydrogen-induced states. We know that E_F is in the d bands (Section 3.2), in fact near the top of them (because of the $4d^{9.64}$ configuration); also that the d bands are roughly 5 eV wide (Sections 1.2.3 and 1.2.4). Hence we might expect the centre of gravity of these bands to be roughly 2 eV below E_F, giving a separation between the d and hydrogen-induced bands of approximately 6 eV (≈0.44 Ryd). We recall that the separation between the centres of gravity of the d and hydrogen-related bands is simply 2U (where $U = \frac{1}{2}|U_d - U_h|$). Thus we are looking for a parameter U of the order of 3 eV (≈0.22 Ryd).

Reference	Mueller et al (1970)[3.9]			Switendick (1972)[3.10]
Electronic configuration	$4d^9 5s^1$ (HFS)*	$4d^{10}5s^0$ (HFS)*	$4d^{10}5s^0$ (HF)**	$4d^9 5s^1$
$(dd\sigma)$	-0.0427	-0.0447	-0.0497	-0.0484†
U_{d_e}	0.2484	0.3062	0.3972	0.4346
U_{d_t}	0.2458	0.3064	0.3920	0.3117

Table 3.2 Slater-Koster parameters for palladium (in Ryd)

*Hartree-Fock-Slater

**Hartree-Fock

Reference	Faulkner (1976)[3.11]	Switendick (1972)[3.10]	Papaconstantopoulos et al (1978b)[3.1]
$(dd\sigma)$	494	-0.0430†	-0.0401†
$(sd\sigma)$	0.1200	0.1141	0.0005
$(ss\sigma)$	0.0	-0.0234	0.0208
U_{d_e}	1.3700	0.4557	0.3538
U_{d_t}	1.3700	0.3661	0.3883
U_h	1.00	0.7482	1.0839

Table 3.3 Slater-Koster parameters for palladium hydride (in Ryd)

†Taking $(dd\sigma) = \frac{1}{4}(3E^{110}_{xy,xy} - E^{110}_{z^2,z^2})$

3.7 EVALUATION OF PARAMETERS

We again follow Lowther[3.5] in our choice of Slater-Koster (SK) parameters; Tables 3.2 and 3.3 are taken from his Tables 1 and 2.

We see immediately from Table 3.3 that Faulkner's parametrization satisfies the semi-quantitative requirements of Section 3.6; firstly, the hydrogen-hydrogen interaction parameter (ssσ) is zero; secondly, the centroid of the hydrogen band, U_h, is lower in energy than that of the d bands; and thirdly, we have $U = \frac{1}{2}|U_d - U_h| = \frac{1}{2}|1.37-1.00|$ Ryd = 0.185 Ryd (cf our rough prediction of U = 0.22 Ryd). Hence we will use Faulkner's values as the basis of our parameter sets. We notice that his values imply degeneracy of the d_e and d_t states; though we would not expect to find this degeneracy in the real system, neither do we expect the large splitting of states implied by Switendick's parameters (Table 3.3). The calculations of Papaconstantopoulos et al (Table 3.3) indicate only a small separation between d_e and d_t states (roughly 0.035 Ryd, less than a tenth of Faulkner's hydrogen-palladium band separation of 2U = 0.37 Ryd). Furthermore, Mueller's results for palladium (Table 3.2) show a negligible difference between the parameters U_{d_e} and U_{d_t} for the pure metal. Hence we shall make the assumption $U_d = U_{d_e} = U_{d_t}$.

We recall from Section 3.4 that we need the integral (ddσ) for the case of pure palladium metal, and from Section 3.5 that (sdσ) is needed for the stoichiometric hydride. Thus Faulkner's value for (ddσ) in Table 3.3 is not strictly appropriate; however, its small deviation from the values for pure palladium metal (Table 3.2) suggests that

we can use Faulkner's results for all our parameters, thus retaining a certain consistency and simplicity in our approach.

Because palladium metal has the fcc structure, the coordination of an atom in the Pd lattice is given by m = 12. Hence, using Table 3.3 and equation (3.18), we obtain an approximate numerical value for our palladium-palladium interaction parameter, viz:-

$$V_{dd} \simeq -0.0298 \text{ Ryd} \tag{3.25}$$

Similarly we obtain from equation (3.24) our palladium-hydrogen interaction parameter, viz:-

$$V_{hd} \simeq -0.08485 \text{ Ryd} \tag{3.26}$$

where the minus sign has been introduced on the physically-intuitive basis of an attractive palladium-hydrogen interaction. Table 3.4 contains what shall henceforth be referred to as "parameter set (a.1)" or "prm-set (a.1)":-

Parameter	Value (Ryd)
V_{dd}	-0.0298
V_{hd}	-0.08485
V_{hh}	0.0
$U_d = +U$	+0.185
$U_h = -U$	-0.185

Table 3.4 Parameter set (a.1).

Set	V_{hd}	Subset	V_{hh}
a	V	a.1	0.0
		a.2	+V/10.0
		a.3	-V/10.0
b	$\sqrt{2}$ V	b.1	0.0
		b.2	+V/10.0
		b.3	-V/10.0
c	V/$\sqrt{2}$	c.1	0.0
		c.2	+V/10.0
		c.3	-V/10.0
V = -0.08485 Ryd			

Table 3.5 Parameter sets used for present calculations. The choice of the factor $\sqrt{2}$ follows from equation (3.24). The non-zero V_{hh} values have been chosen arbitrarily. V_{dd} = -0.0298 Ryd and U = 0.185 Ryd are used in all cases.

In the following chapters we shall keep V_{dd} and U constant, as in Table 3.4; we are hence left with only two parameters to vary, viz. those associated with the palladium-hydrogen interaction (V_{hd}) and the hydrogen-hydrogen interaction (V_{hh}). Because of the form of equation (3.24), we arbitrarily choose to vary V_{hd} by the factor $\sqrt{2}$; and because V_{hh} is small, we arbitrarily let it take on the values $-V_{hd}/10$, 0.0, $+V_{hd}/10$, where V_{hd} is only allowed the value given it in parameter set (a.1) (Table 3.4). We now use these arbitrary choices to generate the rest of the parameter sets to be employed in the present work; the sets chosen are displayed in Table 3.5.

We emphasize the fact that we are dealing with an underlying model with only two variable interaction parameters; in fact, since we shall focus most of our attention on the case $V_{hh} = 0.0$ (implied by Faulkner), we are essentially left with an electronic model with only one interaction parameter, viz. V_{hd}.

3.8 SUMMARY OF CHAPTER 3

In this chapter we have:-

- chosen a simple Tight-Binding (TB) Hamiltonian which is compatible with both the localized nature of the Pd/H system (with particular reference to the d orbitals) and with the Slater-Koster (SK) interpolation scheme;

- reviewed the key features of the SK scheme, with a particular emphasis on the physically transparent and highly useful two-centre approximation;

- combined TB and band width arguments with the SK two-centre approximation to obtain an expression for the palladium-palladium interaction parameter V_{dd} (equation (3.18));

- applied Molecular Orbital Theory and the two-centre approximation to derive a formula for the palladium-hydrogen interaction parameter V_{hd} (equation (3.24));

- applied intuitive considerations of the hydrogen molecule and used the photoelectron spectroscopy experiments of Schlapbach and Burger[3.8] to provide semi-quantitative guidelines for choosing the hydrogen-hydrogen interaction parameter V_{hh} and the hydrogen-band-palladium-band separation 2U respectively;

- tabulated the SK parametrizations of various BS calculations in terms of two-centre integrals, and found Faulkner's values[3.11] to be most consistent with both experiment and qualitative considerations;

- substituted Faulkner's parameters into equations (3.18) and (3.24) to generate our parameter set (a.1) (Table 3.4), and hence, by sensible though arbitrary changes, tabulated a number of other parameter sets to be used in subsequent chapters (Table 3.5);

- noted that we are essentially left with a single-parameter electronic model, the parameter being V_{hd}.

We are now in a position to make a detailed application of our CBL formalism (Chapter 2) to the LDOS of PdH_x.

REFERENCES (CHAP. 3)

3.1) Papaconstantopoulos D A, Klein B M, Faulkner J S and Boyer L L 1978b *Phys. Rev. B* 18 2784

3.2) Heine V 1980 *Electronic Structure from the Point of View of the Local Atomic Environment* in *Solid State Phys.* 35 1 (Ed.s: Ehrenreich H, Seitz F and Turnbull D; publ.: Academic Press)

3.3) Falicov L M and Yndurain F 1975 *Phys. Rev. B* 12 5664

3.4) Slater J C and Koster G F 1954 *Phys. Rev.* 94 1498

3.5) Lowther J E 1982 *J. Phys. F : Met. Phys.* 12 895

3.6) Hubbard J 1967 *Proc. Phys. Soc., London* 92 921

3.7) Watanabe H 1966 *Operator Methods In Ligand Field Theory* (Prentice-Hall, Inc.)

3.8) Schlapbach L and Burger J P 1982 *J. Physique* 43 L273

3.9) Mueller F M, Freeman J, Dimmock J O and Furdyna A M 1970 *Phys. Rev. B* 1 4617

3.10) Switendick A C 1971 *Ber. Bunsenges. Phys. Chem.* 76 535

3.11) Faulkner J S 1976 *Phys. Rev. B* 13 2391

CHAPTER 4

ONE-PHASE MODEL

4.1 INTRODUCTION

In this chapter we apply our formalism for the LDOS of a disordered binary system (Chapter 2) to PdH_x, making use of the parameters obtained in Chapter 3. We provide plots of LDOS versus energy for various hydrogen concentrations and make semi-qualitative observations and comparisons to provide insight into the useful features of our CBL model. These LDOS plots have the Fermi energies (E_F) marked on them, and we proceed to show how E_F is calculated. Once E_F is known we are able to evaluate the total and constituent charges of the system as functions of x, and plots of both E_F and charge versus x provide further insight into our model. We then proceed to evaluate the total electronic energy (E^{el}_{tot}), noting that it has no physical significance as an absolute number because the parameter U results in our LDOS having an arbitrary zero of energy. Hence in implementing our E^{el}_{tot} calculations we will always work with the following *relative* quantity:-

$$\Delta E^{el}(x) = E^{el}_{tot}(x) - E^{el}_{tot}(0)$$

This is the change in electronic energy on formation of PdH_x, which *does* have physical significance, being an important term in our expression for the heat of formation (ΔH) of PdH_x. Because ΔH is known as a function of x from experiment, we have investigated this quantity using our theory; we find that our ΔH values are in remarkably

good agreement with experiment over the range $0.5 \leq x < 1$, but that they disagree for $0 < x \leq 0.5$. Part of the reason for this disagreement is clear from numerical considerations; we also comment that although $E_{tot}^{el}(x)$ is of the order of 1.5 Ryd the quantity ΔH is very small by comparison (~ -0.02 Ryd), so that the calculation of ΔH is highly sensitive to cancellation effects (a problem common to such calculations: see for example Section 1.2.7). However the magnitude of the discrepancies for low x indicates that there might also be problems in the physics for this range of x values. We obtain an important clue from a somewhat unexpected source viz. the thermodynamics of the system. We recall from Section 1.2.4 that for $x \geq 0.6$ PdH_x consists of only one phase (the β-phase), and consequently we infer that our present model provides a good description of the high concentration, *one-phase* hydride, though it fails for lower x. Hence we choose retrospectively to designate the title "One-Phase Model" to the present formalism, bearing in mind that we shall extend this to obtain a "Two-Phase Model" in the next chapter.

The contents of the present chapter are as follows:-

- Section 4.2 deals with our parametrization of the PdH_x system from the viewpoint of *correlation* (cf *electronic* parametrization of Chapter 3); we find that our coordination and order parameters can all be expressed in terms of the single parameter x, giving rise to a "quasi-local" approach to the Pd/H system;

- Section 4.3 provides us with expressions for the LDOS of PdH_x in terms of the formalism of Chapter 2 and in terms of the parametrizations of Chapter 3 and Section 4.2. These are

followed by plots of LDOS versus energy for different x values and parameter sets, with accompanying comments on important features;

- Section 4.4 furnishes us with equations for the evaluation of the *Fermi energy* and *charges* of the system; plots of these quantities versus x follow, and some comments and comparisons are made;

- In Section 4.5 we firstly provide expressions for the numerical evaluation of $E_{tot}^{el}(x)$, along with suitable plots; we implement our knowledge of $E_{tot}^{el}(x)$ by next deriving an expression for the *heat of formation* ΔH, which we proceed to plot as a function of x for a variety of parameter sets. We then compare our curves with experimental results;

- And finally in Section 4.6 we summarize the important findings of this chapter.

4.2 COORDINATION AND CORRELATION PARAMETERS

4.2.1 *"Quasi-Local" Approach*

We recall from Section 1.2.7 that it is generally accepted that hydrogen atoms occupy the octahedral interstitial sites of the fcc palladium lattice. Because there is only one octahedral interstitial site per palladium atom, we have that the probability of such a site being occupied in PdH_1 is unity; hence the *average* site occupation probability for PdH_x is simply given by x. For computational simplicity we shall use this *average* occupation probability when considering the *local* environment, so that we are left with a "quasi-local" rather than strictly local model.

4.2.2 *Coordination Parameters*

We now consider the parameters m and k, where m is the coordination of a given atom and k is the number of neighbours of the same type as the central atom (Section 2.6.1). The parameter m is strictly the number of nearest neighbours only (Section 2.6.1); this concept works in Chapter 2 because there we consider a *substitutional* alloy, which allows us the possibility of neighbouring atoms of *both* kinds. However, PdH_x is an *interstitial* alloy, which has near-neighbour shells of alternating atomic type; for example, in PdH_1 a palladium atom has six nearest-neighbour hydrogens, twelve second-nearest neighbour palladiums and so on. Hence we adapt the original substitutional formalism by defining our interstitial m value as the number of nearest-*and* second-nearest neighbour atoms; it follows that k in this interstitial scheme is simply the number of second-nearest neighbours.

As in Chapter 3 we let palladium be the a-type and hydrogen the b-type atom. We recall that PdH_1 has the NaCℓ structure and hence both sublattices have identical m values, viz. 6+12 = 18. For the case of PdH_x, however, we recall our comments on site-occupation in Section 4.2.1 and hence we write:-

$$m_a = m_d = 6x(\text{hydrogens}) + 12(\text{palladiums}) \tag{4.1a}$$

$$k_a = k_d = 12(\text{palladiums}) \tag{4.1b}$$

$$m_b = m_h = 6(\text{palladiums}) + 12x(\text{hydrogens}) \tag{4.2a}$$

$$k_b = k_h = 12x(\text{hydrogens}) \tag{4.2b}$$

4.2.3 Order Parameters

With reference to equation (2.45), we can now generate the two order parameters:-

$$\lambda_d = \frac{m_d - 2k_d}{m_d} = \frac{6x-12}{6x+12} \tag{4.3a}$$

$$\lambda_h = \frac{m_h - 2k_h}{m_h} = \frac{6-12x}{6+12x} \tag{4.3b}$$

We recall that λ was introduced in Section 2.6.1 as part of the Falicov-Yndurain interpolation scheme and that its three special cases of -1, 0, +1 have important physical significance from the viewpoint of correlation and local environment (see Table 2.4).

4.2.4 *Summary of Section 4.2*

We see from equations (4.1)-(4.3) that all the coordination and correlation parameters depend solely on the *average* occupation probability x, emphasizing both the "quasi-local" nature and the physical transparency of our model.

4.3 LDOS OF PDH_X

4.3.1 Detailed Expressions

The final product of Chapter 2 was the following general expression for the total LDOS of a substitutional binary alloy (equation (2.51)):-

$$n_{tot}(\varepsilon) = x_a n_a(\varepsilon) + x_b n_b(\varepsilon) \qquad (4.4a)$$

where $n_a(\varepsilon)$ and $n_b(\varepsilon)$ are the LDOS of a- and b-type atoms respectively, and x_a and x_b are the respective concentrations of the two atomic species.

We must now adapt equation (4.4a) for the case of an *interstitial* alloy, where we only have *one* variable concentration. Hence, taking a and b to refer to palladium and hydrogen respectively, and defining $x_b = x$, we have:-

$$n_{tot}(x,\varepsilon) = n_{Pd}(x,\varepsilon) + x\, n_h(x,\varepsilon) \qquad (4.4b)$$

Furthermore we recall from Chapter 3 that our Tight-Binding Hamiltonian models the behaviour of palladium using only its ten 4d electrons, four of which (the d_e electrons) are affected by the presence of hydrogen, and the other six of which (the d_t electrons) are unperturbed by hydrogen. In other words, the palladium d_t electrons are not perturbed to a first approximation by the hydrogen electron at all; hence in their case we take x always to be zero in equations (4.1)-(4.3), no matter what the concentration of hydrogen actually is. Consequently we need to split $n_{Pd}(x,\varepsilon)$ into two contributions, viz. $n_{d_e}(x,\varepsilon)$ and $n_{d_t}(\varepsilon)$, and we thus have:-

$$n_{tot}(x,\varepsilon) = 4n_{d_e}(x,\varepsilon) + 6n_{d_t}(\varepsilon) + xn_h(x,\varepsilon) \tag{4.5}$$

where $n_{d_t}(\varepsilon) = n_{d_e}(0,\varepsilon)$

Finally we require the explicit forms of $n_{d_e}(x,\varepsilon)$ and $n_h(x,\varepsilon)$. These are obtained by substituting equations (4.1) and (4.2) into equation (2.49), to give us the following expressions:-

$$n_{d_e}(x,\varepsilon) = -\frac{1}{\pi}\,\mathrm{Im}\left[(\varepsilon-U) - \frac{12V_{dd}^2}{f_1} - \frac{6xV_{hd}^2}{f_2}\right]^{-1} \tag{4.6a}$$

where:-

$$f_1 = (\varepsilon-U) - \frac{11V_{dd}^2}{(\varepsilon-U)-(11+6x)\phi_d} - \frac{6xV_{hd}^2}{(\varepsilon+U)-(5+12x)\phi_h} \tag{4.6b}$$

$$f_2 = (\varepsilon+U) - \frac{12xV_{hh}^2}{(\varepsilon+U)-(5+12x)\phi_h} - \frac{5V_{hd}^2}{(\varepsilon-U)-(11+6x)\phi_d} \tag{4.6c}$$

$$n_h(x,\varepsilon) = -\frac{1}{\pi}\,\mathrm{Im}\left[(\varepsilon+U) - \frac{12xV_{hh}^2}{f_3} - \frac{6V_{hd}^2}{f_4}\right]^{-1} \tag{4.7a}$$

where:-

$$f_3 = (\varepsilon+U) - \frac{(12x-1)V_{hh}^2}{(\varepsilon+U)-(5+12x)\phi_h} - \frac{6V_{hd}^2}{(\varepsilon-U)-(11+6x)\phi_d} \tag{4.7b}$$

$$f_4 = (\varepsilon-U) - \frac{12V_{dd}^2}{(\varepsilon-U)-(11+6x)\phi_d} - \frac{(6x-1)V_{hd}^2}{(\varepsilon+U)-(5+12x)\phi_h} \tag{4.7c}$$

ϕ_d and ϕ_h in equations (4.6) and (4.7) are obtained by substituting equations (4.1)-(4.3) into equations (2.47), that is:-

$$\phi_d(x) = \frac{1}{22+12x}\left\{(\varepsilon-|\lambda_d|U) - i\left[\frac{(44+24x)\tilde{V}_d^2(\lambda_d)(\varepsilon-|\lambda_d|U)}{(\varepsilon+\lambda_d U)} - (\varepsilon-|\lambda_d|U)^2\right]^{\frac{1}{2}}\right\} \tag{4.8a}$$

where:-

$$\tilde{V}_d = \tfrac{1}{2}\left[(1-\lambda_d)V_{dd} + (1+\lambda_d)V_{hh}\right] \quad \text{(from equation (2.46))} \tag{4.8b}$$

$$\lambda_d = \frac{6x-12}{6x+12} \qquad \text{(from equation (4.3a))} \tag{4.8c}$$

$$\phi_h(x) = \frac{1}{10+24x}\left\{(\varepsilon+|\lambda_h|U) - i\left[\frac{(20+48x)\tilde{V}_h^2(\lambda_h)(\varepsilon+|\lambda_h|U)}{(\varepsilon-\lambda_h U)} - (\varepsilon+|\lambda_h|U)^2\right]^{\frac{1}{2}}\right\} \tag{4.9a}$$

where:-

$$\tilde{V}_h = \tfrac{1}{2}\left[(1-\lambda_h)V_{hh} + (1+\lambda_h)V_{hd}\right] \quad \text{(from equation 2.46))} \tag{4.9b}$$

$$\lambda_h = \frac{6-12x}{6+12x} \qquad \text{(from equation 4.3b))} \tag{4.9c}$$

We have chosen to write these LDOS expressions in the form of equation (2.49) for the sake of clarity. In our computer programmes they are of course written as in equation (2.50).

4.3.2 *Results and Discussion*

In Figure 4.1 we display the simplest LDOS curves that we can generate, viz. those for pure palladium metal. This corresponds to the case $x = 0$, for which equation (4.5) is:-

$$n_{tot}(0,\varepsilon) = 10\, n_{d_e}(0,\varepsilon) \tag{4.10}$$

It can be seen from equations (4.6) that $n_{d_e}(0,\varepsilon)$ does not depend on V_{hd} or on V_{hh} (as expected for the pure metal) and hence it does not vary with the choice of parameter set (Table 3.5). The full curve in Figure 4.1 is a plot of equation (4.10), whereas the broken curve represents the quantity $6n_{d_t}(\varepsilon)$ which remains constant for all x values and for all parameter sets.

We note that both these bands are centred on $\varepsilon = +U = 0.185$ Ryd and that they have the width $\Delta = -4\sqrt{11}\, V_{dd} = 0.40$ Ryd (see equations (3.17) and (3.25)), as expected. In addition we note the smoothness of the bands, that is, the lack of structure (cf DOS for palladium metal obtained using BS calculations, for example Faulkner[4.1] and Papaconstantopoulos et al[4.2]). Our $n_{d_e}(0,\varepsilon)$ has a shape clearly reminiscent of that of the d band in the RBM, as can be seen by comparing Figure 4.1 with Figure 4.2 (after Wicke and Brodowsky[4.3] p.76).

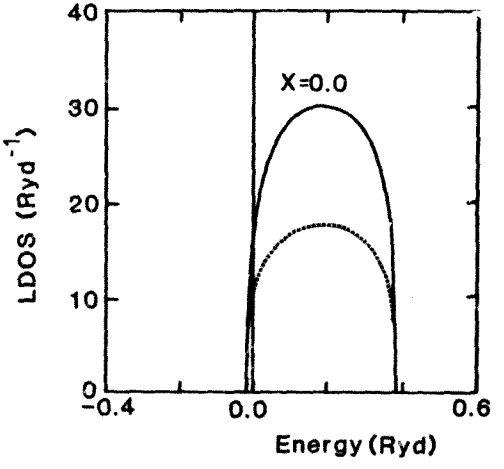

Figure 4.1 Local Density of States for pure Pd. Full curve: total LDOS; broken curve: LDOS for d_t states.

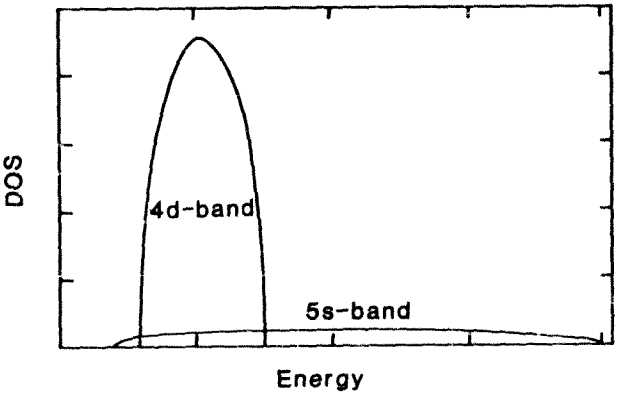

Figure 4.2 Density of States for PdH_x according to Rigid Band Model (after Wicke and Brodowsky[4.3)p.76]).

We recall from Section 1.2.2 that the RBM is of only limited applicability, and in Section 1.3 we implied that our model would provide a more realistic band structure than that of the RBM. A cursory examination of equations (4.6) and (4.7) reveals a strong x-dependence in both our palladium and hydrogen bands; that is, we expect not only the Fermi energy (E_F) to change with addition of hydrogen to the palladium lattice but also the shapes of the bands themselves, in agreement with more sophisticated BS techniques[4.3),4.2]. Our model is therefore expected to be more realistic than the RBM, though Figure 4.1 shows that we do retain some of the appealing simplicity of the RBM.

In Figure 4.3 we display $n_{tot}(x,\epsilon)$ for the three cases x = 0.0, 0.6, 1.0, using our prm.set (a.1). We at once notice fundamental departures from the RBM (Figure 4.2) in two main features: firstly, the considerable *change of shape of the d bands*, as expected; and secondly, the *emergence of another band* in the vicinity of $\epsilon = -U$. This new band and the shoulder on the high-energy side of the d band are both products of our hydrogen LDOS, that is $n_h(x,\epsilon)$; this point is clearly brought out by Figure 3 of the work of Lowther[4.4]. The appearance of this low-energy hydrogen-induced band in our model is in agreement with one of the findings of Chapter 1, viz. the consistent appearance of a *low-lying hydrogen-related band* in BS calculations on the Pd/H system. Our model furthermore agrees with the *experimental photoelectron results* of Schlapbach and Burger[4.5] for $PdH_{0.6}$: they obtain hydrogen-related emission at about 0.59 Ryd below E_F while in our LDOS we see that for x = 0.6 the hydrogen-induced band peaks at approximately 0.58 Ryd below E_F. In

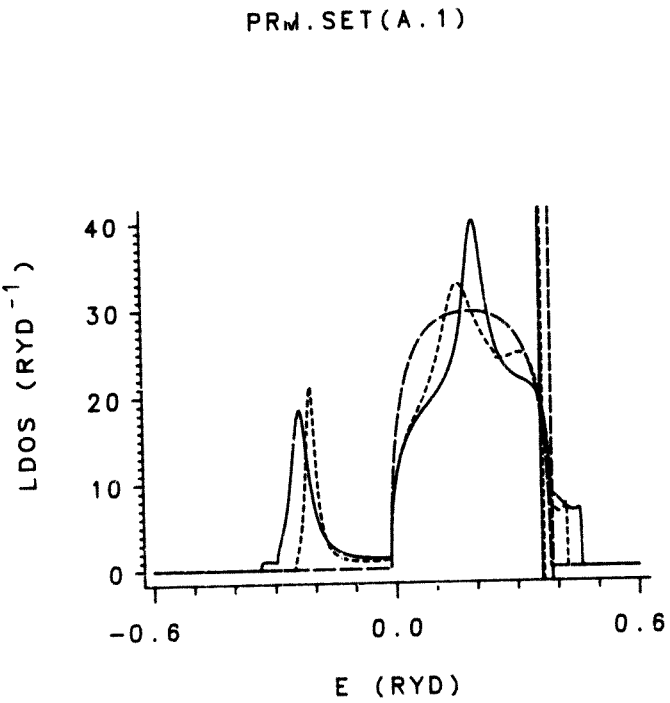

Figure 4.3 Local Densities of States for PdH_x using parameter set (a.1). Coarsely broken curve: x = 0.0; finely broken curve: x = 0.6; full curve: x = 1.0; vertical lines: Fermi energies.

addition, they obtain a slight increase in emission at roughly 0.22 Ryd below E_F, which is exactly the same position at which we find a peak in our $PdH_{0.6}$ d band.

The high-energy low-LDOS shoulders appearing in Figure 4.3 remind us somewhat of the low-DOS 5s band emerging from the high-DOS 4d band in the RBM (Figure 4.2). We notice in particular that the shoulder extends upwards in energy as x increases, reminiscent of the manner in which E_F rises higher in the 5s band of the RBM with increasing x This behaviour provides a second point of similarity with the RBM.

We recollect from Section 1.2.6 that a strictly localized state is represented by a delta function in a DOS plot (for example the DOS of an isolated hydrogen atom in its ground state consists of a delta function at an energy of -1 Ryd). We further recall from Section 1.2.6 that the hydrogen-related *energy level* found below the d bands for low x *broadens* into a *band* for higher values of x. On the basis of these two observations we expect a narrow, highly peaked hydrogen-related band in a solid to *broaden* as the interactions between the hydrogen and its surroundings are *increased*. The physical credibility of our LDOS functions must now be tested in terms of this physically-fundamental broadening phenomenon. We do this by replotting Figure 4.3 for different parameter sets, viz. set (b.1) (greater V_{hd}; Figure 4.4) and set (b.2) (nonzero V_{hh}; Figure 4.5). In both cases the *broadening* and diminished intensity of the hydrogen band is immediately obvious, and the d band also lessens in intensity. Thus Figures 4.4 and 4.5 confirm yet again the physical validity of our model.

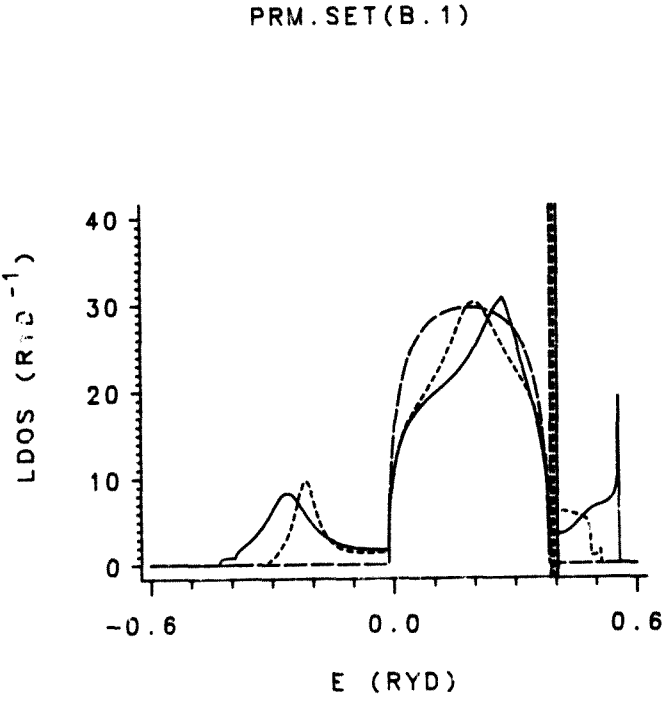

Figure 4.4 Local Densities of States for PdH_x using parameter set (b.1). Coarsely broken curve: x = 0.0; finely broken curve: x = 0.6; full curve: x = 1.0; vertical lines: Fermi energies.

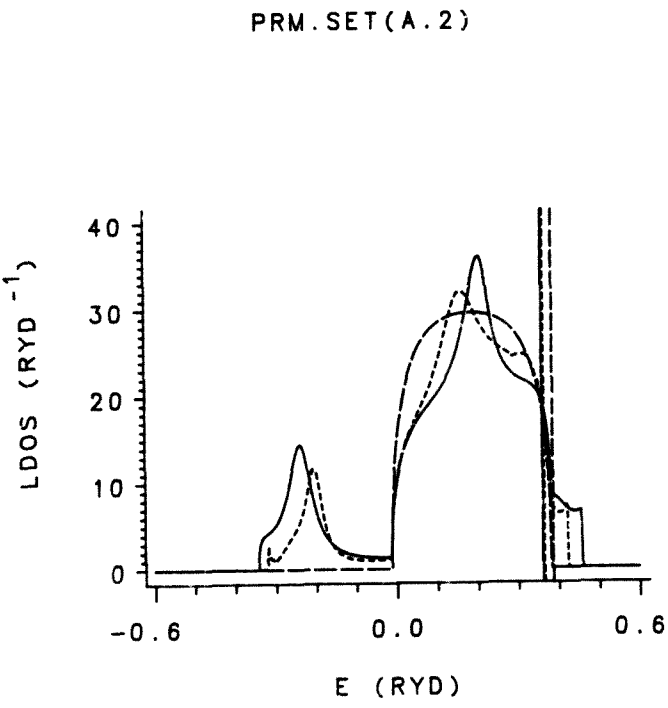

Figure 4.5 Local Densities of States for PdH_x using parameter set (a.2). Coarsely broken curve: x = 0.0; finely broken curve: x = 0.6; full curve: x = 1.0; vertical lines: Fermi energies.

We further point out the physically qualitative expectation that hydrogen-related bands should become narrower as the value of x decreases; this is because in the low x case a given hydrogen interstitial is further separated from other hydrogen atoms, as well as its *mean* separation from the palladium atoms being greater. We recall from Section 1.2.6 that band structure results confirm this expectation.

By referring back to Figures 4.3 - 4.5 and in particular by looking ahead to Figures 5.1 and 5.2 we can see that our model *satisfies* this criterion as well. To obtain an insight into the mechanics of this effective x-dependence of our interaction parameters, the reader is referred to equations (4.6) - (4.9) in which it can be seen that the coefficients of these parameters are usually simple functions of x. Another clearly-discernible feature in Figures 4.3 - 4.5 is the movement of both the hydrogen- and d-band peaks away from the origin as x increases; this results in a broadening of the peak separation by several percent in going from $PdH_{0.6}$ to $PdH_{1.0}$. This behaviour is a direct consequence of our application of the Virtual Crystal Approximation in Chapter 2, which required us to take U = 0 for the case of a completely random alloy. Hence we see that the interpolation formulae for the mean field functions (equations (4.8a) and (4.9a)) have a factor λ or $|\lambda|$ in front of the "peak separation" parameter U, giving rise to an *effective* peak separation which varies with x.

4.3.3 *Summary of Section 4.3*

In this section we have derived expressions for the LDOS of PdH_x which have the following appealing features:-

- they have closed, analytical form;
- they deal equally naturally with the stoichiometric ($x=1$) and non-stoichiometric ($x<1$) hydrides;
- they retain some of the simplicity and clarity of the RBM;
- and they are in good agreement with both experimental findings and computationally-intensive BS calculations.

4.4 FERMI ENERGY AND CHARGE

4.4.1 Introduction

In this section we provide expressions for the evaluation of the Fermi energy (E_F) of the Pd/H system, using the model developed in Chapter 2 and Sections 4.1 - 4.3. We note from the start that the numerical values of our E_F are only meaningful relative to our "centre-of-states" parameter U. Once we have E_F as a function of x for a given parameter set, we are able to evaluate the corresponding charges of palladium and hydrogen atoms, and consequently of the PdH_x "unit". The advantage of using the *Local* Density of States is that it is physically meaningful to speak in terms of a single PdH_x unit, consisting of a single, localized palladium atom and the fraction x of a hydrogen atom associated with it. Although we will not be using the concept of charge in the rest of our work, we nevertheless examine it briefly because it provides another physically-meaningful criterion for testing our formalism.

Evaluation of E_F and the charge require us to integrate our LDOS expressions; because this is done numerically, we will from here on be carrying a non-physical thread in our argument, which we will not always be able to separate from the central physical themes. The reader might therefore enquire as to the possibility of analytical integration, a topic which we discuss in Appendix 4.1.

In Section 4.4.2 we evaluate and comment on E_F; then in Section 4.4.3 we use E_F to calculate the various charges associated with a single PdH_x "unit", and we summarize our findings in Section 4.4.4.

4.4.2 *Evaluation of the Fermi Energy*

4.4.2.1 Method

Our LDOS is defined as the number of electronic states between energies ε and $\varepsilon + d\varepsilon$, so that integrating over all ε gives us the total number of electronic states. In our PdH_x unit we have ten palladium 4d states and 2x hydrogen 1s states. We therefore expect to find:-

$$\int_{-\infty}^{+\infty} n_{tot}(x,\varepsilon)d\varepsilon = 10 + 2x \qquad (4.11)$$

At the absolute zero of temperature ($T = 0K$), the Fermi energy (E_F) is the energy of the highest occupied state of the system, with all the states below E_F also being occupied (a consequence of Fermi-Dirac statistics: see Appendix 4.2). Thus if we integrate the LDOS over all energies up to E_F we obtain the total number of occupied states for $T = 0K$ (in Appendix 4.2 we show that the calculation at absolute zero is adequate for our purposes). In our case we have 10 *occupied* palladium states and x *occupied* hydrogen states per PdH_x unit, and we thus expect the following equation to hold:-

$$\int_{-\infty}^{E_F} n_{tot}(x,\varepsilon)d\varepsilon = 10 + x \qquad (4.12)$$

Combining equations (4.11) and (4.12) gives us:-

$$\frac{1}{10+2x}\int_{-\infty}^{+\infty} n_{tot}(x,\varepsilon)d\varepsilon = \frac{1}{10+x}\int_{-\infty}^{E_F} n_{tot}(x,\varepsilon)d\varepsilon \qquad (4.13a)$$

or:-

$$\int_{-\infty}^{E_F} n_{tot}(x,\varepsilon)d\varepsilon = \frac{10+x}{10+2x}\int_{-\infty}^{+\infty} n_{tot}(x,\varepsilon)d\varepsilon \qquad (4.13b)$$

It is clear from our LDOS plots (for example Figure 4.4) that we can replace the limits of integration $-\infty$ and $+\infty$ by numbers of the order -0.6 Ryd and +0.6 Ryd respectively. We are then able to evaluate the right-hand side of equation (4.13b) numerically, for a given value of the parameter x, and hence determine E_F numerically by means of a bisection method (see Appendix 2 for details).

We comment that equations (4.11) and (4.12) give us the result that both sides of equation (4.13a) are unity; because we are integrating numerically we do not however expect this to be the case for our calculated numbers. We thus do not use equation (4.13a) (and hence equation (4.13b)) on the assumption that equations (4.11) and (4.12) hold numerically, but instead on the assumption that they contain the same percentage error. This is a reasonable approximation when one considers the similarity of equations (4.11) and (4.12).

4.4.2.2 Results and Discussion

We recall from Section 4.3.2 that our LDOS for the case x = 0.0 do not depend on the parameter set used; hence E_F (x = 0.0) will be the same for all our parameter sets. With reference to equation (4.13b) we can see that E_F (x = 0.0) is evaluated simply by finding the point at which the upper edge of our d band cuts the energy axis, that is by finding the larger root of $n_{tot}(0,\varepsilon) = 0$. The solution is:-

$$E_F(\text{Pd metal}) = 0.3859 \text{ Ryd} \qquad (4.14)$$

In Figure 4.6 we show plots of E_F vs x for prm.sets (a.1) and (b.1). The most striking feature in both cases is that E_F is seen to *decrease* over certain ranges of concentration in contrast to the *monotonic increase* with x which is a fundamental feature of the RBM. This highlights the fact that

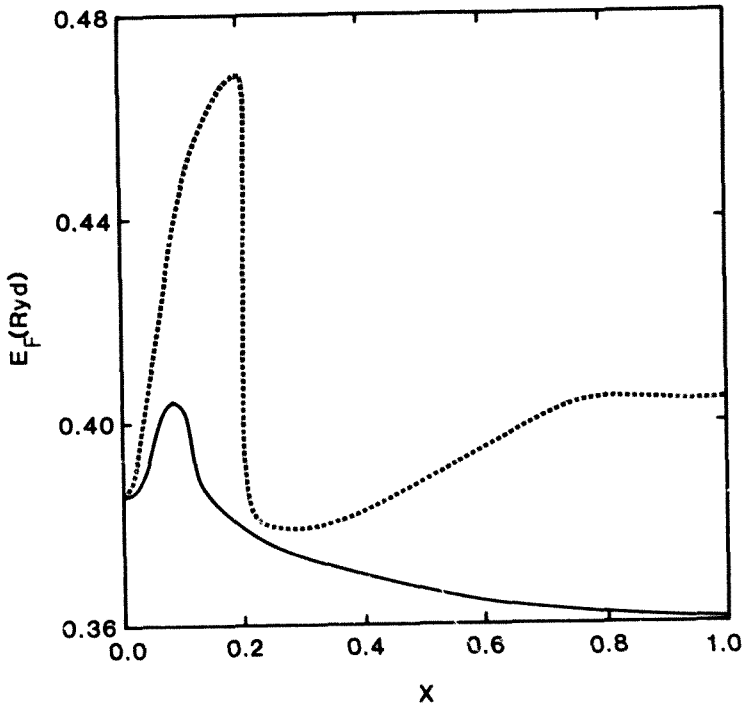

Figure 4.6 Fermi energy vs x. Full curve : parameter set (a.1); broken curve: parameter set (b.1).

our model does not have rigid bands, which makes possible this decrease of E_F with x. However, the BS calculations of Gelatt et al[4.6], Faulkner[4.1] and Papaconstantopoulos et al[4.2] all show a slight overall increase of E_F with x, in agreement with the RBM; see Table 4.1 for rough values.

Source	$[E_F(PdH) - E_F(Pd)]$ (Ryd)
present work, prm.set (a.1)	-0.03
Gelatt et al[4.6]	+0.02
Faulkner[4.1]	+0.04
Papaconstantopoulos et al[4.2]	+0.06

Table 4.1 Difference in the Fermi energy of palladium and its stoichiometric hydride, according to various sources.

Although the trend of our E_F values for prm.set (a.1) is different to that found in BS calculations, we notice that the values in Table 4.1 are only a few percent of the overall width of the PdH_x band structure (about 0.8 Ryd in our case), and so we do not expect this discrepancy to be significant. We note that our calculated values of E_F for prm.sets (a.2) and (a.3) would be barely distinguishable from the values for prm.set (a.1) on the energy scale of Figure 4.6. In a similar manner our values of E_F calculated for prm.sets (b.2) and (b.3) would almost coincide with the curve for prm.set (b.1) if plotted on Figure 4.6. Hence we see that our Fermi energy is insensitive to changes in V_{hh} over the range of V_{hh} values we have employed, although it is clear from Figure 4.6 that it has strong V_{hd} dependence.

We will now make use of our values for E_F to evaluate the charge on each atomic species and hence the total charge of the average PdH_x unit.

4.4.3 Calculation of Charge

4.4.3.1 Method

We recall from equation (4.12) that the total number of occupied electronic states per PdH_x unit is obtained by integrating $n_{tot}(x,\varepsilon)$ up to the Fermi energy E_F, and that this number is expected to be 10+x for a given x. This integral therefore represents a number of electrons, and multiplying it by the electronic charge $e = 1.602 \times 10^{-19}C$ consequently gives us the electronic charge of the PdH_x valence electrons in Coulombs. For convenience we choose e=1, so that we may then write:-

$$q_{tot}(x) = q_d(x) + q_h(x) \tag{4.15a}$$

where

$$q_d(x) = \int_{-\infty}^{E_F} [6n_{d_t}(\varepsilon) + 4n_{d_e}(x,\varepsilon)]d\varepsilon \tag{4.15b}$$

and

$$q_h(x) = \int_{-\infty}^{E_F} 2xn_h(x,\varepsilon)d\varepsilon \tag{4.15c}$$

4.4.3.2 Results and Discussion

In Figure 4.7 we show plots $q_{tot}(x)$ vs x for prm.sets (a.1) and (b.1). In both cases we have that $q_{tot}(0) = 9.999$, that is almost exactly the expected value of 10.0; this accuracy is a direct consequence

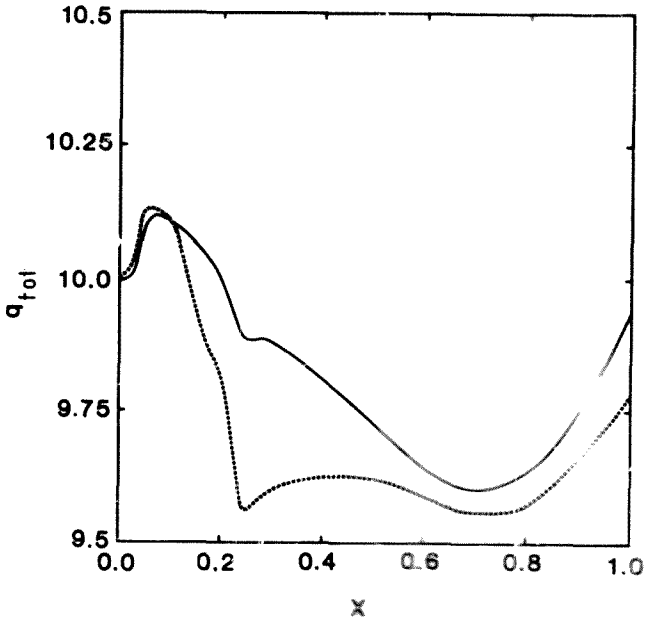

Figure 4.7 Total charge vs x. Full curve: parameter set (a.1); broken curve: parameter set (b.1).

of the smooth, featureless LDOS we have for the case x = 0.0 (Figure 4.1). However, we see that the accuracy begins to drop off with increasing x; we quantify this in Table 4.2.

x	10+x	Calculated Charge		Percentage difference	
		Prm.set (a.1)	Prm.set (b.1)	Prm.set (a.1)	Prm.set (b.1)
0.0	10.0	10.0	10.0	0.0	0.0
0.2	10.2	10.0	9.85	2.0	3.4
0.4	10.4	9.84	9.62	5.4	7.5
0.6	10.6	9.72	9.59	8.3	9.5
0.8	10.8	9.70	9.57	10.2	11.4
1.0	11.0	9.95	9.78	9.5	11.1

Table 4.2 Charge deviations for prm.sets (a.1) and (b.1).

It can be seen from Table 4.2 that the loss of accuracy is not linear in x, the worst error being in the region of x = 0.8. These errors are almost certainly purely numerical in nature; that is, they do not reflect a weakness in our physics, but rather reveal the numerical difficulties associated with integration of a highly-peaked function. More specifically, we take note of two competing error effects involved in integrating the LDOS, viz. one due to the diminishing smoothness of the d band and another due to the sharpness of the lower hydrogen-induced band. The first effect *increases* with x whereas the second *decreases* with x, and Table 4.2 reveals that the combined effect is worst in the high x region,

that is, the *d-band* error term dominates in *charge* calculations. It will be seen in the following section that for *energy* calculations the *hydrogen-band* error contribution dominates. We take up the theme of numerics in a more quantitative manner in Appendix 2.

In Figures 4.8 and 4.9 we show respectively the plots of $q_d(x)$ vs x and $q_h(x)$ vs x which correspond to the $q_{tot}(x)$ values plotted in Figure 4.7. In Figures 4.10 and 4.11 we again show $q_d(x)$ and $q_h(x)$ for prm.set (a.1), as well as their "scaled-up" values $F(x)q_d(x)$ and $F(x)q_h(x)$, where F(x) is simply a scaling factor given by:-

$$F(x) = (10+x)/q_{tot}(x) \qquad (4.16)$$

From equations (4.15a) and (4.16) we see that the sum $[F(x)q_d(x) + F(x)q_h(x)]$ equals the physically-anticipated charge value of (10+x). Hence the "scaled-up" curves are essentially physical corrections to our numerically-evaluated charges.

We see from Figures 4.8 and 4.10 that the palladium atom in the PdH_x unit loses charge with increasing x, even in the scaled-up case. This effect is most transparent for the stoichiometric hydride (x=1); we display the various scaled charges for the case x=1 in Table 4.3.

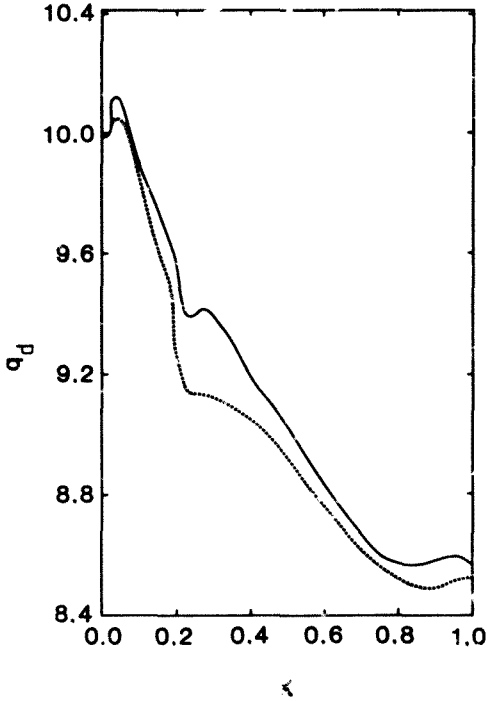

Figure 4.8 Palladium charge vs x. Full curve: parameter set (a.1); broken curve: parameter set (b.1).

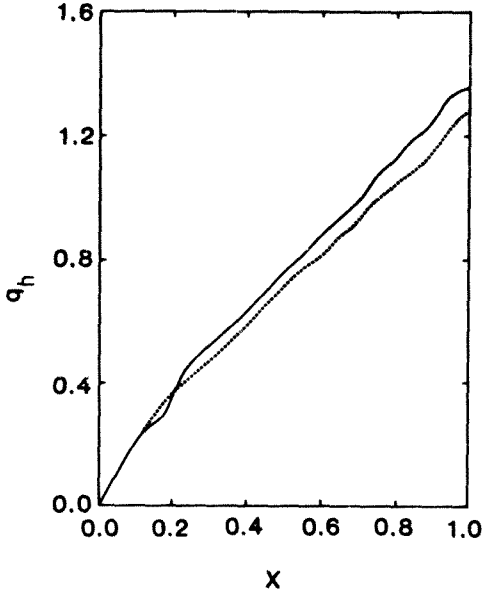

Figure 4.9 Hydrogen charge vs x. Full curve: parameter set (a.1); broken curve: parameter set (b.1).

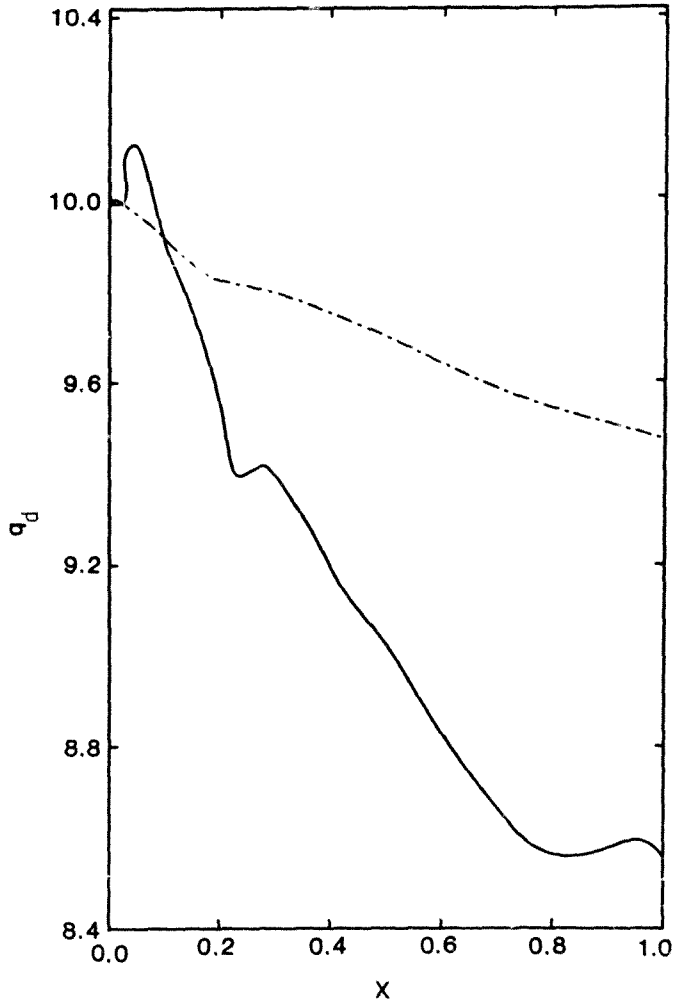

Figure 4.10 Palladium charge vs x for parameter set (a.1). Full curve: unscaled; chained curve: scaled.

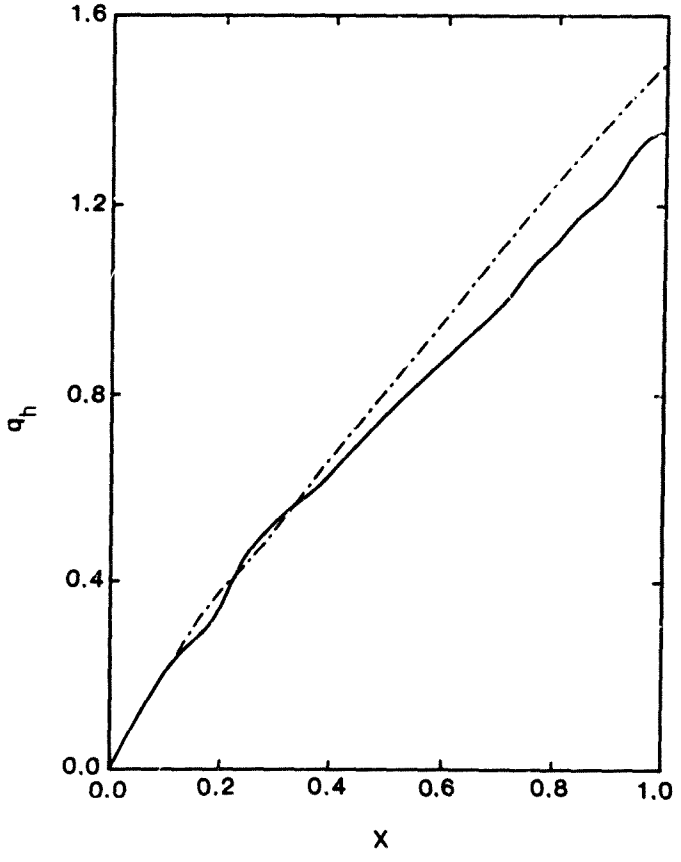

Figure 4.11 Hydrogen charge vs x for parameter set (a.1). Full curve: unscaled; chained curve: scaled.

Parameter Set	$q_d(1)$	$q_h(1)$	$q_{tot}(1)$
a.1	9.484	1.516	11.000
b.1	9.573	1.427	11.000

Table 4.3 Charges for PdH_1, scaled by the correction factor F (equation (4.16)).

We note from Table 4.3 that the increase in V_{hd} of approximately 40% in going from prm-set (a.1) to set (b.1) causes only a 1% change in the charge distribution of the stoichiometric hydride, with the larger V_{hd} value (prm-set (b.1)) giving the larger palladium charge.

Consequently our formalism results in charge transfers which are more akin to those of the so-called *ionic model* than to the proton model discussed in Section 1.2.2. The ionic model for transition metal hydrides is based on the assumption that hydrogen exists in the metal lattice in the form of the negative ion H^-; although this model is diametrically opposed to the proton model there is nevertheless some evidence in its favour[4,7]; we also recall that the proton model is itself of only limited applicability (Section 1.2.2).

4.4.4 *Summary of Section 4.4*

In this section we have developed and applied suitable equations for the numerical evaluation of the Fermi energy of PdH_x; we have also provided and applied expressions for the numerical determination of the constituent and total charges of this system, noting that these expressions depend on the values of E_F. We find that our Fermi energies sometimes decrease with x, as opposed to REM and BS calculations which show a consistent increase of E_F with x. However the change in the Fermi energy is in all cases seen to be only a few percent of the total width of the DOS, and hence we do not see this deviation as being of any great significance in the context of integration of the DOS.

Our charge calculations are highly accurate for the case of pure palladium, though they develop inaccuracies of several percent for higher x; this apparent loss of charge is understood to be a numerical effect and not a reflection on the underlying physics. We have applied a scaling correction to our charge values and found that our formalism favours an *anionic* rather than a protonic view of the Pd/H system.

We will not attempt to use scaling factors in the energy calculations which follow; our knowledge of the inaccuracies in our charge values (Table 4.2) is therefore helpful because these deviations give us a rough indication of the percentage errors we are likely to make in evaluating the total electronic energy. Appendix 2 deals with the issue of numerical errors in a more quantitative manner.

4.5 TOTAL ELECTRONIC ENERGY AND HEAT OF FORMATION

4.5.1 *Introduction*

The evaluation of the total electronic energy ($E_{tot}^{e\ell}$) of PdH_x, using our LDOS expressions, is of central importance because the results are necessary for the calculation of the heat of formation which follows. The evaluation of $E_{tot}^{e\ell}$ is along similar lines to the charge calculations of Section 4.4 because we use previously-calculated values of E_F and numerical integration of a continued fraction expression.

4.5.2 *Total Electronic Energy*

The total electronic energy (at the absolute zero of temperature, see Appendix 4.2) is determined by means of the following expressions:-

$$E_{tot}^{e\ell}(x) = E_d^{e\ell}(x) + E_h^{e\ell}(x) \tag{4.17a}$$

where

$$E_d^{e\ell}(x) = \int_{-\infty}^{E_F} \left[6n_{d_t}(\varepsilon) + 4n_{d_e}(x,\varepsilon)\right]\varepsilon d\varepsilon \tag{4.17b}$$

and

$$E_h^{e\ell}(x) = \int_{-\infty}^{E_F} 2xn_h(x,\varepsilon)\varepsilon d\varepsilon \tag{4.17c}$$

cf equations (4.15) for the various charge contributions. In Figure 4.12 we display curves of $E_{tot}^{e\ell}(x)$ vs x for prm.sets (a.1), (b.1) and (a.2). In all three cases we have $E_{tot}^{e\ell}(0) = E_d^{e\ell}(0) = 1.8505$ Ryd and $E_h^{e\ell}(0) = 0.0$; Table 4.4 contains various energies calculated for the stoichiometric hydride.

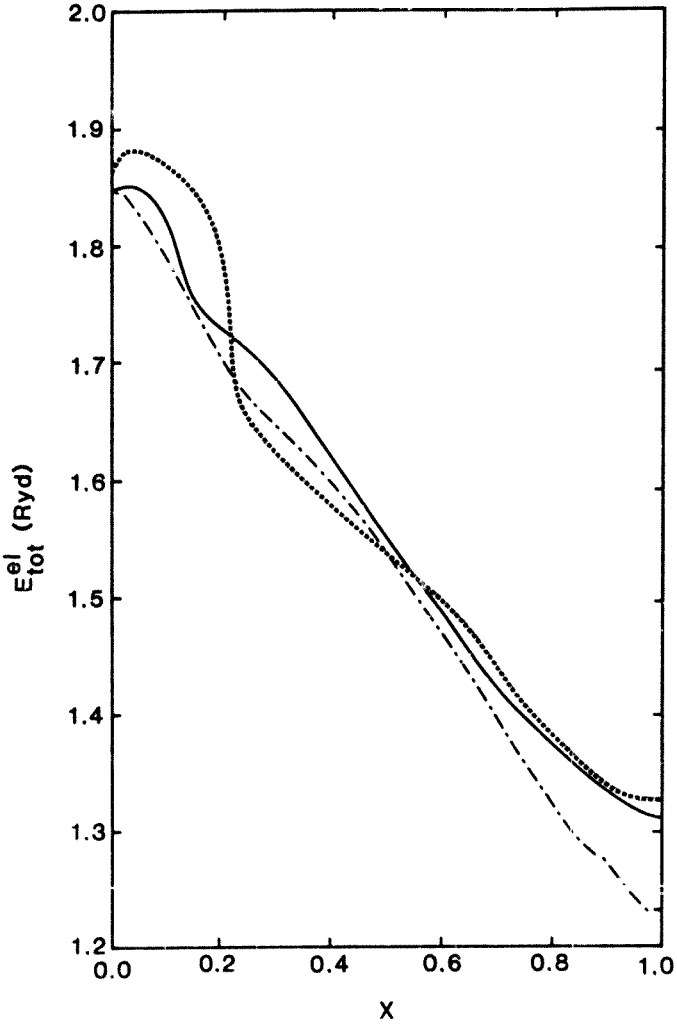

Figure 4.12 Total electronic energy vs x. Full curve: parameter set (a.1); broken curve: parameter set (b.1); chained curve: parameter set (a.2).

Parameter Set	$E_d^{e\ell}(1)$ (Ryd)	$E_h^{e\ell}(1)$ (Ryd)	$E_{tot}^{e\ell}(1)$ (Ryd)	$[E_{tot}^{e\ell}(1)-E_{tot}^{e\ell}(0)]$ (Ryd)
a.1	1.5452	-0.2370	1.3082	-0.5423
b.1	1.5870	-0.2592	1.3278	-0.5227
a.2	1.5024	-0.2757	1.2268	-0.6238

Table 4.4 Electronic energies and energy changes for PdH_1, using $E_{tot}^{e\ell}(0) = 1.8505$ Ryd.

We note that for all three parameter sets $E_{tot}^{e\ell}$ *decreases* with x; this decrease is essentially monotonic (and in fact approximately linear up to $x \approx 0.5$ if the curves are suitably smoothed). Table 4.4 reveals that the electronic energies drop by roughly 30% in going from pure Pd to PdH_1. We recall that our $E_{tot}^{e\ell}$ values have no significance as *absolute* numbers because they are evaluated in terms of the parameter U, which gives an *arbitrary* zero of energy for our LDOS; hence we will work in terms of the *difference* in energy between palladium and a given hydride, viz. $E_{tot}^{e\ell}(x) - E_{tot}^{e\ell}(0)$, which *does* have physical significance and which we will implement in the next section.

4.5.3 Heat of Formation

4.5.3.1 Formalism and Calculations

The heat of formation (ΔH) is the total energy difference between the metal hydride on the one hand and the pure metal lattice and hydrogen molecules from which it is formed on the other. Thus for *stoichiometric*

palladium hydride we have:-

$$\Delta H = E(PdH_1) - E(Pd) - \tfrac{1}{2}E(H_2) \qquad (4.18a)$$

where $E(PdH_1)$ is the *total* energy of PdH_1.

Following Shull and Smith[4.8] we identify $E(H_2)$ as the *ionization energy* of the hydrogen molecule, that is the energy required to separate the molecule into its constituent protons and electrons; the value of this constant[4.6] is $E(H_2) = -2.266$ Ryd. Generalizing equation (4.18a) to allow for the *substoichiometric hydride* PdH_x leads us to the following expression:-

$$\Delta H(x) = \Delta E(x) - \tfrac{1}{2}xE(H_2) \qquad (4.18b)$$

where

$$\Delta E(x) = E(PdH_x) - E(Pd) \qquad (4.18c)$$

The presence of hydrogen atoms in the palladium lattice causes strains to be set up and hence we expect an *elastic* contribution to ΔE in addition to the electronic component ΔE^{elec}. Gelatt et al (1975)[4.9] estimate an elastic energy of roughly -0.01 Ryd for PdH_1, while the analyses of Wagner and Horner[4.10] and Harada[4.11] indicate that the elastic contribution varies *linearly* with hydrogen concentration; we can thus write:-

$$\Delta E^{elas} = cx$$

where

$$c \approx -0.01 \text{ Ryd}$$

We note further that Gelatt et al (1978)[4.6] record a *decrease* of roughly 0.04 Ryd in the average energy of the d bands in going from Pd to PdH_1. Assuming that the d-band shift for concentration x is given by $\delta(x)$, the *corrected* total electronic energy can be approximated to as follows[4.12]:-

$$\left[E^{e\ell}_{tot}(x)\right]_{corrected} \approx \int_{-\infty}^{E_F} n_{tot}(x,\varepsilon)(\varepsilon-\delta(x))d\varepsilon$$

$$= \int_{-\infty}^{E_F} n_{tot}(x,\varepsilon)\varepsilon d\varepsilon - \delta(x)\int_{-\infty}^{E_F} n_{tot}(x,\varepsilon)d\varepsilon$$

$$= E^{e\ell}_{tot}(x) - \delta(x)(10+x) \qquad (4.19)$$

We see from this equation that the correction term is $(10+x)\delta(x)$. Now $\delta(x)$ must be zero at x=0 and must increase with x; the simplest function that satisfies these conditions is $\delta(x) = x\Delta$, where Δ is a constant. Thus our correction term becomes simply $(10+x)x\Delta$, and collecting together the various contributions to the heat of formation we finally obtain[4.12]:-

$$\Delta H(x) = E^{e\ell}_{tot}(x) - E^{e\ell}_{tot}(0) - (10+x)x\Delta - \tfrac{1}{2}xE(H_2) + cx \qquad (4.20)$$

where

$E^{e\ell}_{tot}(x)$ is given by equations (4.17)

$E^{e\ell}_{tot}(0) \approx 1.8505$ Ryd

$E(H_2) \approx -2.266$ Ryd

Δ and c are unknown parameters.

We expect $\Delta \approx 0.04$ Ryd from Gelatt et al (1978)[4.6] and $c \approx -0.01$ Ryd from Gelatt et al (1975)[4.9]. Following the procedure of our first paper[4.12], we evaluate the parameters Δ and c by fitting them to experimental results. Sholl and Smith[4.8] quote the experimental value of ΔH, determined by Gillespie and Hall[4.13] for low hydrogen concentration ($x < 0.02$), as being -0.0096 Ryd. If we make the crude approximation that the empirical ΔH function is symmetric around $x = 0.5$ (the results of Kuji et al[4.14] and Harada[4.11] lend some credence to such an assumption, especially if we take the average of their values), then we have that ΔH is also -0.0096 Ryd very close to the stoichiometric case. Hence we make the following approximation: $\Delta H(x=1) \approx -0.0096$ Ryd. Sholl and Smith use Gillespie and Hall's ΔH value to obtain the corresponding change in *electronic energy*, viz. $\Delta E^{exp} = -1.123$ Ryd. ΔE^{exp} is equal to our $\Delta E^{e\ell}(1)$(corrected according to equation 4. 9) so that by applying our approximation $\Delta H(x=1) \approx \Delta H(\text{low } x)$ we can write:-

$$\Delta E^{e\ell}(1) = E^{e\ell}_{tot}(1) - E^{e\ell}_{tot}(0) - 11\Delta = -1.123 \text{ Ryd}$$

and hence:-

$$\Delta = \left[E^{e\ell}_{tot}(1) - E^{e\ell}_{tot}(0) + 1.123\right]/11 \text{ Ryd} \qquad (4.21)$$

Table 4.5 contains values of Δ used with four of our parameter sets.

Parameter Set	$E_{tot}^{e\ell}(1)$ (Ryd)	Δ (Ryd)
a.1	1.3082	0.0528
b.1	1.3278	0.0546
a.2	1.2268	0.0454
a.3	1.3130	0.0532

Table 4.5 Values of $E_{tot}^{e\ell}(1)$ and the band-shift coefficient Δ for different parameter sets.

We see from this table that our values of Δ are consistent with the shift of approximately 0.04 Ryd recorded by Gelatt et al[4.6]. To evaluate the parameter c we note that for the case of stoichiometric palladium hydride equation (4.20) can be rewritten in the following form:-

$$\Delta H(1) = \Delta E^{e\ell}(1) - \tfrac{1}{2}E(H_2) + c$$

where $\Delta E^{e\ell}(1) = \Delta E^{exp} = -1.123$ Ryd

Hence we obtain $c = -0.0196$ Ryd for *all* parameter sets. We now substitute our values of Δ and c into equation (4.20) and in Figure 4.13 we plot ΔH as a function of x for the four parameter sets of Table 4.5. A comparison between our calculated values and the experimental results of Harada[4.11] is shown in Figure 4.14. We note that our ΔH expression refers to one mole of hydrogen *atoms*, and hence we have halved Harada's original results which referred to one mole of hydrogen *molecules*. In

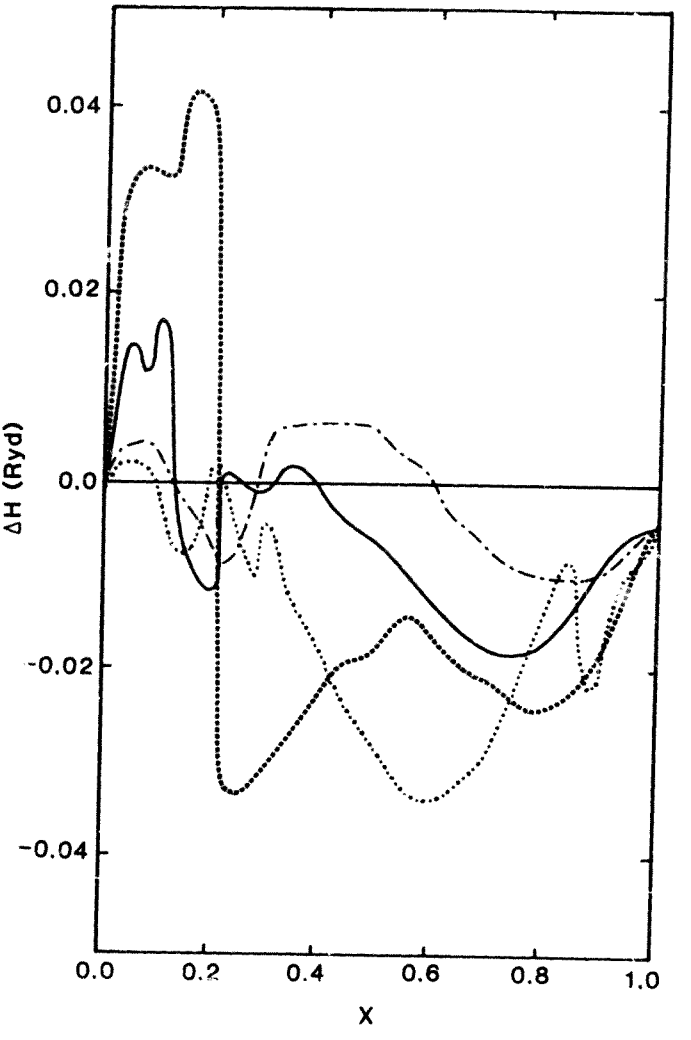

Figure 4.13 Calculated heats of formation vs x using different parameter sets: full curve, set (a.1); broken curve: set (b.1); chained curve: set (a.2); dotted curve: set (a.3).

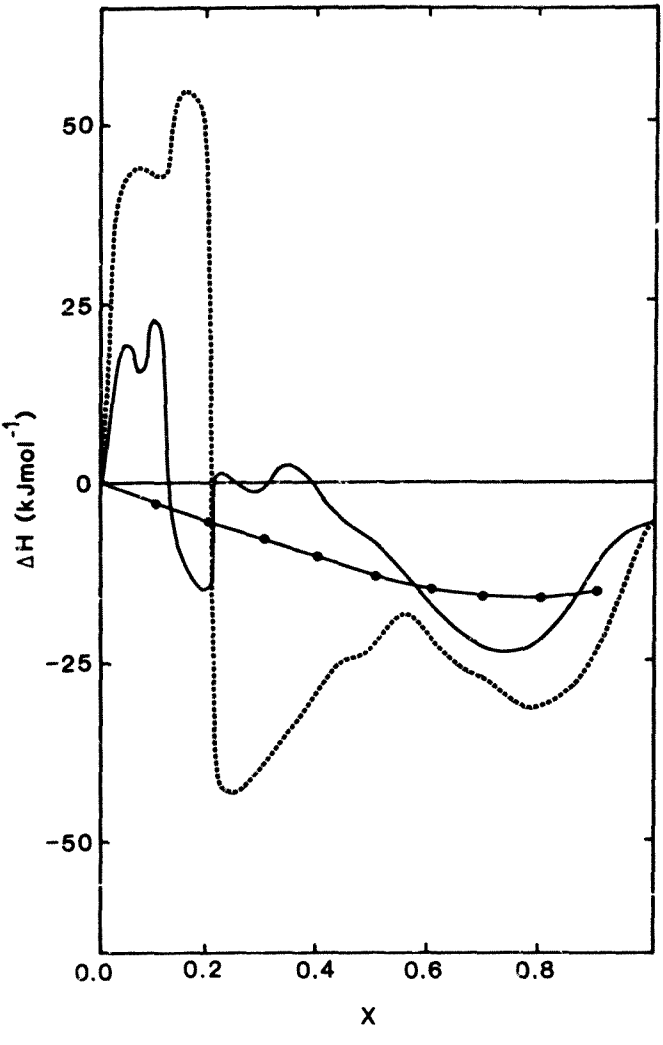

Figure 4.14 Comparison of calculated heats of formation (full curve, parameter set (a.1); broken curve, parameter set (b.1)) with the experimental results of Harada[4.11] (full curve with full circles).

addition we have shifted the origin of Harada's curve so as to compare it with our calculations which are based on the definition $\Delta H(0) = 0$ (see equation (4.20)).

4.5.3.2 Discussion

Figure 4.13 reveals the following trends in our ΔH curves:-

- firstly, they are largely negative, implying a *stable* hydride (in agreement with experiment: see Figure 4.14);

- secondly, our ΔH values are typically a *factor of fifty* smaller than our total electronic energy values (compare Figures 4.12 and 4.13), implying that we have significant and subtle *cancellation effects* in equation (4.20). We recall that Sholl and Smith (Section 1.2.7) found similar effects in their theoretical model;

- thirdly, we have the physically-sensible finding that the *larger* choice of $|V_{hd}|$, for $V_{hd} < 0$ (prm.set (b.1)), gives a *lower* ΔH curve and hence a *more stable hydride* than does the smaller $|V_{hd}|$ value ($V_{hd} < 0$) of prm. set (a.1) (recalling that both sets (a.1) and (b.1) have $V_{hh} = 0.0$);

- fourthly, we observe that a *small, negative* V_{hh} makes the hydride *less* stable (prm.set (a.2)) while the corresponding positive quantity (prm.set (a.3)) results in a *more* stable hydride; this finding is consistent with the *blocking model* to be discussed in Chapter 6;

- and fifthly, considerable numerical instability is apparent, particularly for $x \leq 0.5$. Examination of equation (4.20) reveals that these fluctuations can only be due to instabilities in our calculation of $E_{tot}^{e\ell}(x)$. With reference to the discussion of errors in Section 4.4.3.2, we see that the dominant error term in the case of $E_{tot}^{e\ell}$ must be that due to the sharpness of the low x hydrogen bands.

Moving on to Figure 4.14, we see that the two parameter sets having zero V_{hh} are in quite good agreement with the experimental results of Harada[4.11] for $x \geq 0.5$; in fact Harada's curve is "sandwiched" between our two curves for most values of x. We recall from Section 4.2 that our model is built on the underlying physical assumption of an averaged but nevertheless *random* distribution of hydrogen atoms throughout the palladium lattice, and hence the fair agreement with experiment which we find for $x \geq 0.5$ implies that our physical picture is correct for larger x. The disagreement with experiment at lower x is no doubt partly due to the numerical instability reflected in the large fluctuations in our ΔH values for the $x < 0.5$ regime. However, even taking this into account, the very marked disagreement with experiment at lower values of x makes us suspicious of the underlying physical validity of our present model in this concentration range.

An important clue to the shortcomings of our model is the well-established multiphase nature of PdH_x which was emphasized in Chapter 1; the various phases have been described in some detail from

a macroscopic, thermodynamic viewpoint (especially via pressure-concentration isotherms), but a thorough microscopic, electronic model for the phases does not exist. Our results suggest that the high-concentration β-phase ($x \gtrsim 0.6$) can be associated with a *random* distribution of hydrogen throughout the lattice, whereas other phases may not share this random nature. We take up this theme in the next chapter, where we adapt our present model to allow for the *two-phase* nature of PdH_x.

4.5.4 *Summary of Section 4.5*

E_{tot}^{el} is found to decrease with x in an essentially monotonic fashion, and in fact almost linearly up to $x \approx 0.5$; it plays an important role in our formula for ΔH, being the only x-dependent contribution to ΔH from our model. Although certain rough approximations are made in evaluating the band-shift and elastic contributions to ΔH, and although most of the terms in our ΔH expression are individually over an order of magnitude larger than empirical values for ΔH, we nevertheless obtain a remarkable agreement with experiment for $x \gtrsim 0.5$.

4.6 SUMMARY OF CHAPTER 4

In this chapter we have firstly modelled the correlation-related aspects of PdH_x within a "quasi-local", interstitial-alloy formalism which requires the hydrogen concentration x as its only parameter. On the basis of this formalism detailed expressions for the Local Densities of States of PdH_x and its constituent atoms have been formulated; these have several appealing features, including a closed, analytical form and direct applicability to non-stoichiometric hydrides, as well as producing bands which are in good agreement with both experimental results and band structure calculations.

The total LDOS are then integrated numerically to find the Fermi energy and hence the various charge and electronic energy contributions as functions of x. Although the charge calculations are highly accurate for the case of pure palladium metal, the numerical integrations start generating errors for $x > 0$ which are manifested as spurious charge losses. The percentage error is not monotonic in x but maximizes at $x \approx 0.8$; this is because there are two competing error effects viz. that due to the sharp peaks in the hydrogen band for low x, and that due to the development of peaks in the d band at high x. The second effect is dominant in the charge calculations whereas the first dominates the electronic energy computations.

Having made allowances for an elastic energy contribution and shifts in the d band as a function of hydrogen concentration, we have finally formulated an expression for the heat of formation of non-stoichiometric

palladium hydride and plotted this as a function of x for several parameter sets. Our values are in fairly good agreement with experiment in the region $x \gtrsim 0.5$, especially for those parameter sets with no interaction between hydrogen atoms. Although the lack of agreement for $x \lesssim 0.5$ is partly numerical in origin it is significant enough for us to doubt the physical validity of our model in its present form for lower values of x. Our suspicion is substantiated by the fact that our results agree with experiment in the high x, β phase region ($x \gtrsim 0.6$), though not in the regions of lower x. We recall that our model is based on the assumption of a *random* distribution of hydrogen in the palladium lattice, and hence an implication of our results is that the PdH_x β-phase is essentially random in nature, whereas the other phases may not be disordered to the same extent. In the following chapter we modify our present formalism so that we can explore the physics of the low x regime.

APPENDIX 4.1

INTEGRATION OF LDOS

We attempted to integrate the general LDOS expression of equations (2.50) analytically, using the simplifying assumptions $|\lambda_d| = \lambda_d$ and $|\lambda_h| = \lambda_h$ (it can be seen from equations (4.3a) and (4.3b) that the first assumption is true for all allowed x, that is $0 \leq x \leq 1$, whereas the second only holds for $x \geq 0.5$). To do this we first re-expressed the LDOS in terms of a rational function (as opposed to the original continued fraction format). The result is:-

$$\text{LDOS} = \frac{f(x,\varepsilon)}{g(x,\varepsilon)} \qquad \text{(A4.1.1)}$$

where $f(x,\varepsilon)$ is a function of $O(V^2\varepsilon^7)$

and $g(x,\varepsilon)$ is a function of $O(\varepsilon^{10})$.

We note that V mentioned in connection with $f(x,\varepsilon)$ is one of V_{dd}, V_{hd}, V_{hh}.

Without presenting details, we can make the following general comments regarding the functions $f(x,\varepsilon)$ and $g(x,\varepsilon)$:-

- although they are of finite order in ε, they are not polynomials;
- specifically, the terms of these functions consist of products of non-negative, integral powers of ε and irreducible quadratics in ε;
- the coefficients of these terms are rational functions of x.

Because of the high powers of ε as well as the presence of irreducible quadratics in ε it can be appreciated that analytic integration of

equation (A4.1.1) is out of the question, even in this simplified case of $|\lambda_d| = \lambda_d$ and $|\lambda_h| = \lambda_h$. We are thus obliged to turn to numerical quadrature techniques. It will be appreciated from plots of the LDOS (for example Figure 4.3) that we are dealing with a sharply-peaked integrand, and hence we suspect that application of a simple technique such as Simpson's rule will probably be inadequate or inefficient for our purposes. We take this matter up in more detail in Appendix 2.

APPENDIX 4.2

FERMI-DIRAC STATISTICS FOR PdH_x

The Fermi-Dirac distribution function for electrons and other fermions is given by:-

$$f(\varepsilon,E_F,T) = \frac{1}{e^{(\varepsilon-E_F)/kT} + 1} \qquad (A4.2.1)$$

where T is the absolute temperature.

We see that:-

$$\lim_{T\to 0^+} f(\varepsilon,E_F,T) = \begin{cases} 1 \text{ for } \varepsilon < E_F \\ 0 \text{ for } \varepsilon > E_F \end{cases} \qquad (A4.2.2)$$

For the general case $T \geq 0$ the number ν of *occupied* states per PdH_x unit is given by:-

$$\nu(T) = \int_{-\infty}^{+\infty} n_{tot}(x,\varepsilon) f(\varepsilon,E_F,T) d\varepsilon \qquad (A4.2.3)$$

If we now substitute equations (A4.2.2) into equation (A4.2.3) we obtain:-

$$\nu(0) = \int_{-\infty}^{E_F} n_{tot}(x,\varepsilon) d\varepsilon \qquad (A4.2.4)$$

In Sections (4.4.2) and (4.4.3) we have used the approximation $\nu(T) \approx \nu(0)$, and we have made a similar assumption in Section (4.5.2). The validity of this approximation can be appreciated at an intuitive level by examining Table A4.2.1 in which we compare values of $f(\varepsilon,E_F,T)$ for T = 0K and T = 300K.

$\varepsilon - E_F$ (Ryd)	$f(\varepsilon,E_F,T)$	
	T = 0K	T = 300K
-0.02	1.000	1.000
-0.01	1.000	0.995
-0.001	1.000	0.629
0.0	0.500	0.500
0.001	0.000	0.371
0.01	0.000	0.005
0.02	0.000	0.000

Table A4.2.1 Values of $f(\varepsilon,E_F,T)$, according to equation (A4.2.1).

We firstly note from this table that $f(\varepsilon,E_F,300K)$ would only affect equation (A4.2.4) over the range $-0.01 \text{ Ryd} \leq \varepsilon - E_F \leq +0.01$ Ryd, this being only 2.5% of the total LDOS energy distribution of about 0.8 Pyd; and secondly we see that for a given energy ε in the above range, $f(\varepsilon,E_F,300K)$ would cause a slight *decrease* in $\nu(0)$ to the *left* of E_F and a slight *increase* to the *right* of E_F, resulting in a cancellation effect.

In conclusion then we can say that the error introduced by making the approximation $v(T) \approx v(0)$ is negligible, and hence we implicitly use this and similar approximations in calculating our Fermi energies, charges and total electronic energies.

The approximation $E_F \approx \mu$ can also be justified qualitatively by considering the relationship between these two quantities obtained from the free electron model, viz.[4.15]:-

$$\mu = E_F\left[1 - \frac{\pi^2}{12}\left(\frac{T}{T_F}\right)^2 - \frac{\pi^4}{80}\left(\frac{T}{T_F}\right)^4\right] \text{ for } T \ll T_F \qquad \text{(A4.2.5)}$$

where T_F is the Fermi temperature of the metal.

Equation (A4.2.5) reveals that μ and E_F are in fact identical at T = 0K. We recall from Section 1.2.2 that silver metal and stoichiometric palladium hydride have certain electronic features in common, and from Section 1.2.5 that the behaviour of the non-stoichiometric hydride is essentially metallic at E_F. Approximating the Fermi temperature of PdH_x to that of silver metal ($T_F = 6.38 \times 10^4$ K[4.16]), we readily obtain $\mu = 1.000E_F$ at 300K by using equation (A4.2.5). Hence we conclude that the approximation $\mu \approx E_F$ is valid.

REFERENCES (CHAP. 4)

4.1) Faulkner J S 1976 *Phys. Rev. B* 13 2391

4.2) Papaconstantopoulos D A, Klein B M, Faulkner J S and Boyer L L 1978b *Phys. Rev. B* 18 2784

4.3) Wicke E and Brodowsky H 1978 *Hydrogen in Palladium and Palladium Alloys* in *Topics in Appl. Phys.* 29 73 (Ed.s: Alefeld G and Völkl J; publ.: Springer-Verlag)

4.4) Lowther J E 1982 *J. Phys.F: Met. Phys.* 12 895

4.5) Schlapbach L and Burger J P 1982 *J. Physique* 43 L273

4.6) Gelatt C D, Ehrenreich H and Weiss J A 1978 *Phys. Rev. B* 17 1940

4.7) Mackay K M 1966 *Hydrogen Compounds of the Metallic Elements* 46 (E. and F.N. Spon Ltd, London)

4.8) Sholl . and Smith P V 1977 *J. Phys. F: Met. Phys.* 7 789

4.9) Gelatt C D, Weiss J A and Ehrenreich H 1975 *Solid State Commun.* 17 663

4.10) Wagner H and Horner H 1974 *Adv. Phys.* 23 587

4.11) Harada S 1983 *J. Phys.F: Met. Phys.* 13 607

4.12) Anagnostaras P D and Lowther J E 1984 *J. Phys. F: Met. Phys.* 14 1445

REFERENCES (CHAP. 4) continued

4.13) Gillespie L J and Hall F P 1926 *J. Am. Chem. Soc.* 48 1207

4.14) Kuji T, Oates W A, Bowerman B S and Flanagan T B 1983 *J. Phys. F: Met. Phys.* 13 1785

4.15) Münster A 1974 *Statistical Thermodynamics* Vol II 49 (publ.s: Springer-Verlag and Academic Press)

4.16) Ashcroft N W and Mermin N D 1976 *Solid State Physics* 38 (publ.: Holt-Saunders International Editions)

CHAPTER 5

TWO-PHASE MODEL

5.1 INTRODUCTION

Our two-phase model incorporates the same fundamental Cluster-Bethe-Lattice (CBL) formalism as its one-phase counterpart (Chapter 4) except that it makes fuller use of the rich structural possibilities of the CBL approach. Specifically, we construct Local Densities of States (LDOS) which consist of *linear combinations* of single-phase LDOS of the type developed in the previous chapter. In keeping with the specifically *two-phase* nature of the hydride and so as not to obscure the essential features of our LDOS, we consider linear combinations consisting of only two terms weighted in a physically sensible manner.

We then evaluate Fermi energies, charges, total electronic energies and heats of formation in the same manner as in Chapter 4, except that we now implement our more sophisticated LDOS formalism as well as an energy minimization technique; the consequence of this approach is a marked improvement in our ΔH curves. In addition we introduce a simple segregation parameter which gives us insights into phase transition phenomena of the hydride.

This chapter consists of the following sections:-

- Section 5.2, in which we introduce and develop our two-phase formalism for the LDOS, substitute it into the various charge

CHAPTER 5

TWO-PHASE MODEL

5.1 INTRODUCTION

Our two-phase model incorporates the same fundamental Cluster-Bethe-Lattice (CBL) formalism as its one-phase counterpart (Chapter 4) except that it makes fuller use of the rich structural possibilities of the CBL approach. Specifically, we construct Local Densities of States (LDOS) which consist of *linear combinations* of single-phase LDOS of the type developed in the previous chapter. In keeping with the specifically *two-phase* nature of the hydride and so as not to obscure the essential features of our LDOS, we consider linear combinations consisting of only two terms weighted in a physically sensible manner.

We then evaluate Fermi energies, charges, total electronic energies and heats of formation in the same manner as in Chapter 4, except that we now implement our more sophisticated LDOS formalism as well as an energy minimization technique; the consequence of this approach is a marked improvement in our ΔH curves. In addition we introduce a simple segregation parameter which gives us insights into phase transition phenomena of the hydride.

This chapter consists of the following sections:-

- Section 5.2, in which we introduce and develop our two-phase formalism for the LDOS, substitute it into the various charge

and energy-related expressions developed in Chapter 4, and define and explain the purpose of the segregation parameter;

- Section 5.3 which is essentially a comparison of the results obtained using the one- and two-phase models;

- Section 5.4 in which we examine the segregation parameter and other features of the two-phase model for all our parameter sets;

- and Section 5.5 which summarizes some important findings of this chapter.

5.2 TWO-PHASE THEORY

5.2.1 *LDOS*

We follow the approach outlined in our second paper[5.1], that is we assume that for a given value of x there are *two* phases present in the hydride, with fractional hydrogen concentrations of p and q respectively. We further assume that the phase of concentration p constitutes a fraction α of the total hydride, so that the other phase is present in a fractional amount (1-α). This can be expressed in terms of a chemical reaction equation as follows:-

$$PdH_x = \alpha PdH_p + (1-\alpha)PdH_q \qquad (5.1)$$

Comparison of coefficients reveals that the palladium contribution drops out of this equation, which is physically correct because we have an *unvarying* Pd sublattice (our model only takes the expansion of the Pd lattice into account via the empirical parameter c in the expression for ΔH: see equation (4.20)). Hence by comparing coefficients of the hydrogen atoms in equation (5.1) we are left with the following equation:-

$$x = \alpha p + (1-\alpha)q \qquad \text{or} \qquad q = (x-\alpha p)/(1-\alpha) \qquad (5.2)$$

Recalling that $0 \leq x \leq 1$ for PdH_x, we assume that the two constituent phases are subject to the same restrictions, viz. $0 \leq p \leq 1$ and $0 \leq q \leq 1$. With reference to equation (5.2) this second inequality becomes:-

$$0 \leq (x - \alpha p)/(1-\alpha) \leq 1$$

which in turn gives rise to the following set of inequalities:-

$$\left.\begin{array}{l} 0 < \alpha < 1 \\ p \geq 0 \text{ and } p \geq (x + \alpha - 1)/\alpha \\ p \leq 1 \text{ and } p \leq x/\alpha \end{array}\right\} \qquad (5.3)$$

For given values of x and α we then generate values of p subject to equations (5.3) and hence we evaluate the parameter $q = (x-\alpha p)/(1-\alpha)$ (equation (5.2)).

We see that q depends solely on x, α and p and hence that we have only introduced *two* extra independent parameters into our two-phase formalism. Taking the two phases to be independent of each other we evaluate the total LDOS for each one according to equation (4.5), viz:-

$$\left.\begin{array}{l} n_{tot}^{(p)}(p,\varepsilon) = 4n_{d_e}(p,\varepsilon) + 6n_{d_t}(\varepsilon) + pn_h(p,\varepsilon) \\ \text{and} \\ n_{tot}^{(q)}(q,\varepsilon) = 4n_{d_e}(q,\varepsilon) + 6n_{d_t}(\varepsilon) + qn_h(q,\varepsilon) \end{array}\right\} \qquad (5.4)$$

and hence we evaluate the total LDOS for the *two-phase model* according to the following equation:-

$$n_{tot}^{(2)}(x,\varepsilon) = \alpha n_{tot}^{(p)}(p,\varepsilon) + (1-\alpha)n_{tot}^{(q)}(q,\varepsilon) \qquad (5.5)$$

We can now implement our two-phase expression for the LDOS by applying it to the various charge- and energy-related expressions developed in Chapter 4.

5.2.2 *Energies, Charges and Heat of Formation*

The *two-phase Fermi energies* are now calculated by solving the following equation for $E_F^{(2)}$:-

$$\int_{-\infty}^{E_F^{(2)}} n_{tot}^{(2)}(x,\varepsilon)d\varepsilon = \frac{10+x}{10+2x}\int_{-\infty}^{+\infty} n_{tot}^{(2)}(x,\varepsilon)d\varepsilon \qquad (5.6)$$

which corresponds exactly to equation (4.13b) for the one-phase model, except that the total LDOS is now given by equation (5.5) instead of equation (4.5). Hence we obtain the *two-phase charges* by analogy with equations (4.15):-

$$q_{tot}^{(2)}(x) = q_d^{(2)}(x) + q_h^{(2)}(x) \qquad (5.7a)$$

where

$$q_d^{(2)}(x) = \int_{-\infty}^{E_F^{(2)}} \left[6n_{d_t}(\varepsilon) - 4\{\alpha n_{d_e}(p,\varepsilon) + (1-\alpha)n_{d_e}(q,\varepsilon)\}\right]d\varepsilon \qquad (5.7b)$$

and

$$q_h^{(2)}(x) = \int_{-\infty}^{E_F^{(2)}} 2x\{\alpha n_{h_t}(p,\varepsilon) + (1-\alpha)n_{h_t}(q,\varepsilon)\}d\varepsilon \qquad (5.7c)$$

Similarly, by analogy with equations (4.17) we obtain the *electronic energies* for the two-phase model:-

$$E_{tot}^{el(2)}(x) = E_d^{el(2)}(x) + E_h^{el(2)}(x) \qquad (5.8a)$$

where

$$E_d^{el(2)}(x) = \int_{-\infty}^{E_F^{(2)}} \left[6n_{d_t}(\varepsilon) + 4\{\alpha n_{d_e}(p,\varepsilon) + (1-\alpha)n_{d_e}(q,\varepsilon)\}\right]\varepsilon d\varepsilon \tag{5.8b}$$

and

$$E_h^{el(2)}(x) = \int_{-\infty}^{E_F^{(2)}} 2x\{\alpha n_h(p,\varepsilon) + (1-\alpha)n_h(q,\varepsilon)\}\varepsilon d\varepsilon \tag{5.8c}$$

Finally we can write down an expression for the *heat of formation* $\Delta H^{(2)}$ of the two-phase hydride by adapting equation (4.20) to the following form:-

$$\Delta H^{(2)}(x) = E_{tot}^{el(2)}(x) - E_{tot}^{el(2)}(0) - (10+x)x\Delta^{(2)} - \tfrac{1}{2}xE(H_2) + c^{(2)}x \tag{5.9a}$$

where $E(H_2) = -2.266$ Ryd.

We see from Appendix 5.1 that $n_{tot}^{(2)}(0,\varepsilon) = n_{tot}(0,\varepsilon)$ and $n_{tot}^{(2)}(1,\varepsilon) = n_{tot}(1,\varepsilon)$, from which follow $E_{tot}^{el(2)}(0) = E_{tot}^{el}(0)$ and $E_{tot}^{el(2)}(1) = E_{tot}^{el}(1)$ respectively, and substituting these energy equations into equation (4.21) gives us $\Delta^{(2)} = \Delta$. We also recall from Section 4.5.3 that the elastic energy parameter c depends solely on fixed empirical data and so is constant, leading to $c^{(2)} = c$. Equation (5.9a) can thus be rewritten as follows:-

$$\Delta H^{(2)}(x) = E_{tot}^{el(2)}(x) - E_{tot}^{el}(0) - (10+x)x\Delta - \tfrac{1}{2}xE(H_2) + cx \tag{5.9b}$$

It is thus clear that our two-phase expression for the heat of formation differs from its one-phase counterpart *solely* in the total electronic energy term.

Equation (5.9b) can be rewritten as follows:-

$$\Delta H^{(2)}(x,\alpha,p,q) = E_{tot}^{el(2)}(x,\alpha,p,q) + F(x) \qquad (5.10a)$$

where

$$F(x) = -E_{tot}^{el}(0) - (10+x)x\Delta - \tfrac{1}{2}xE(H_2) + cx \qquad (5.10b)$$

We choose the parameters (α,p,q) which *minimize* $\Delta H^{(2)}$ for a particular x value, this being the physically correct selection criterion at the absolute zero of temperature. In our case this minimization is carried out numerically by evaluating $E_{tot}^{el(2)}$ for a large number of (α,p,q) values, x being kept constant during the procedure; it is clear from equations (5.10) that minimization of $E_{tot}^{el(2)}$ for a fixed x also minimizes $\Delta H^{(2)}$ at that x value.

5.2.3 *Segregation Parameter*

Once we have found the parameters (α,p,q) which minimize ΔH for a given value of x, we can evaluate our *segregation parameter* (r) which we define as follows:-

$$r = \min(p,q)/\max(p,q) \qquad (5.11)$$

where $\min(p,q)$ is the smaller of p and q and $\max(p,q)$ is the larger of the two.

It can be seen from this equation that r=1 implies p=q, which in turn indicates a *one-phase* system (x = p = q in equation (5.1)). Recalling the experimental finding that PdH_x is a single-phase hydride for $x \geq 0.6$ (refer to Figure 6.1), we expect to find $r = 1$ for $x \geq 0.6$; this gives us one criterion for evaluating the relative physical correctness of our various parameter sets.

5.2.4 *Summary of Section 5.2*

In this section we have firstly laid the foundation for our two-phase model by expressing it in terms of a chemical reaction equation, on which we have imposed physically-sensible boundary conditions. Secondly, we have implemented this formalism by deriving two-phase expressions for the LDOS in terms of our new two-phase parameters and the one-phase LDOS equations. Thirdly, the formulae for the Fermi energy, charges, total electronic energy and heat of formation follow immediately by substituting the two-phase LDOS expressions into the appropriate one-phase charge and energy formulae. And lastly, two of the new parameters have been used to define a segregation parameter which will help us detect phase transitions in the hydride.

5.3 COMPARISON OF ONE- AND TWO-PHASE RESULTS

5.3.1 LDOS

Figures 5.1 and 5.2 provide a comprehensive comparison between our one- and two-phase LDOS (equations (4.5) and (5.5) respectively), with Figures 5.1 being plotted using prm.set (a.1) and Figures 5.2 making use of prm.set (a.2); the parameters (α,p,q) employed for the two-phase results are those which minimize $\Delta H^{(2)}$ for a given x. We take note of the following features:-

- the two-phase LDOS are *generally richer in structure* than their one-phase counterparts, and usually have d-band peaks centred at *higher* energies than the corresponding single-phase peaks;

- the *high-energy shoulders* discussed in Section 4.3 are also present in the two-phase LDOS, including at lower values of x where they do not appear in the one-phase model. However, the two-phase shoulders are of *lower* intensity than those of the one-phase formalism for intermediate values of x;

- the most dramatic differences are observed in the *hydrogen-related peaks* below the d band. We see that in general the two-phase LDOS have noticeably *less* structure than those of the single-phase model for low x, whereas for intermediate values of x the two-phase structure is distinctly richer. If we compare Figures 5.1 and 5.2 we observe that these hydrogen-related peaks both *broaden* and *diminish in intensity* very considerably in going from prm.set (a.1) to prm.set (a.2). Now the only difference between these two

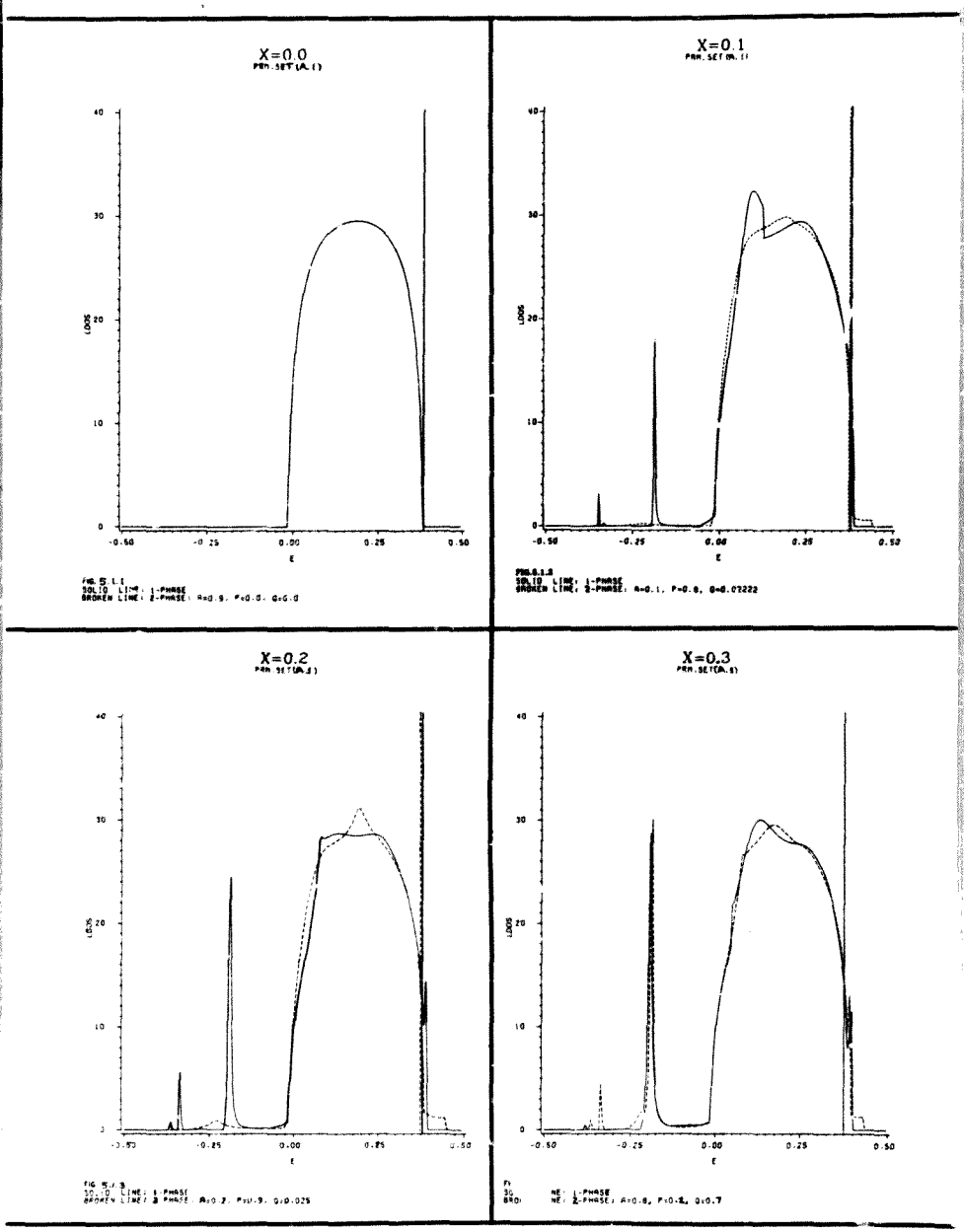

Figures 5.1.1-5.1.4 Total LDOS for prm.set (a.1), x = 0.0-0.3. Full curves: 1-phase model; broken curves: 2-phase model; vertical lines: E_Fs.

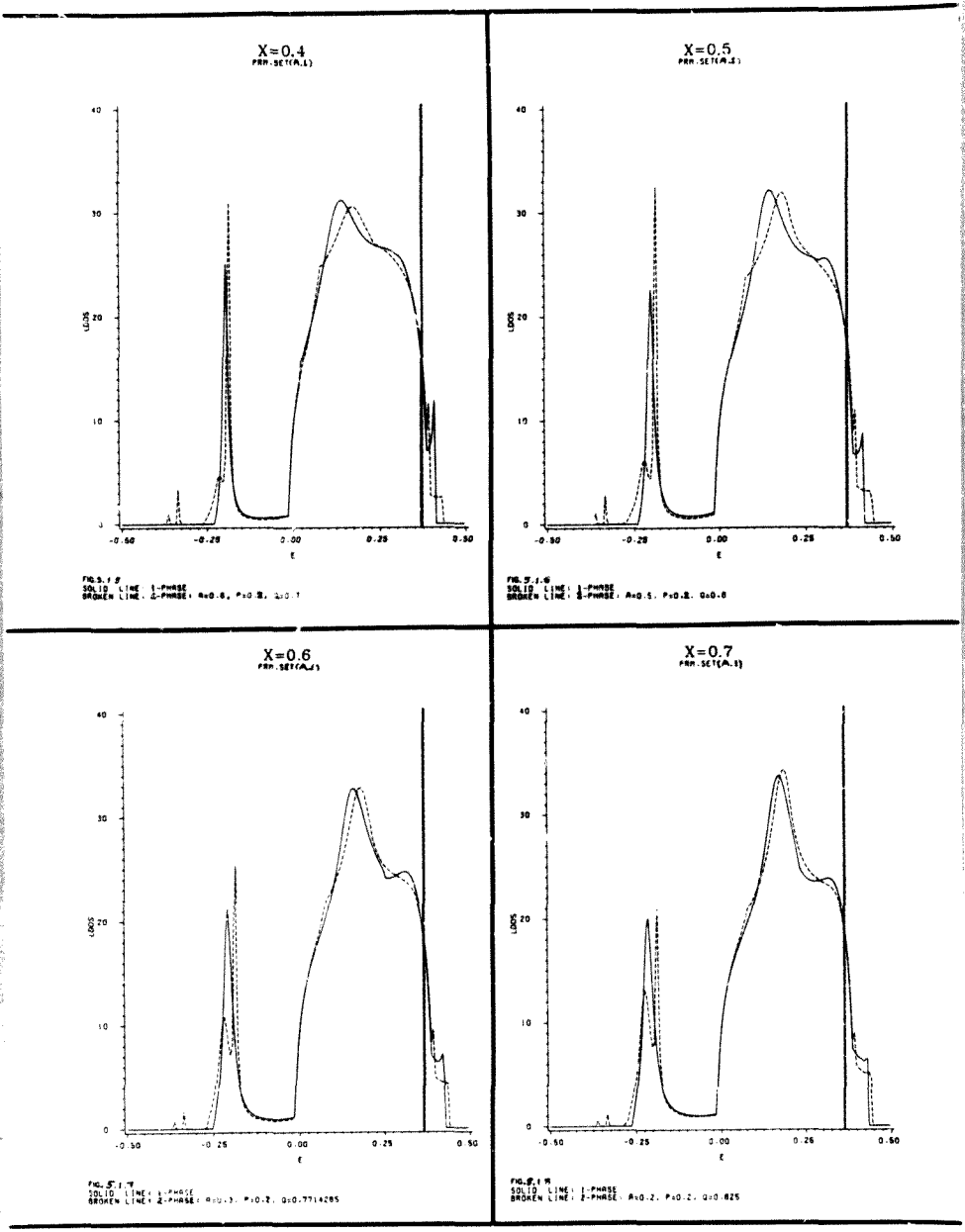

Figures 5.1.5-5.1.8 Total LDOS for prm.set (a.1), x = 0.4-0.7. Full curves: 1-phase model; broken curves: 2-phase model; vertical lines: E_Fs.

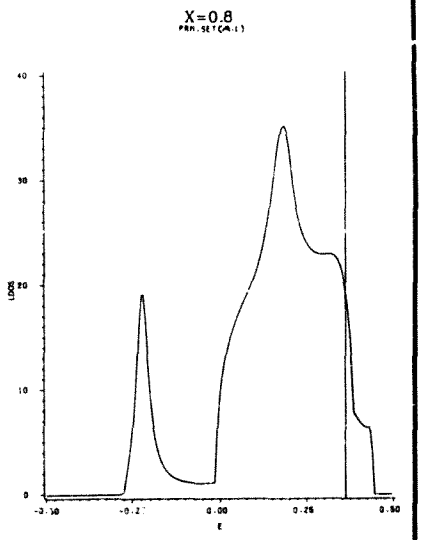

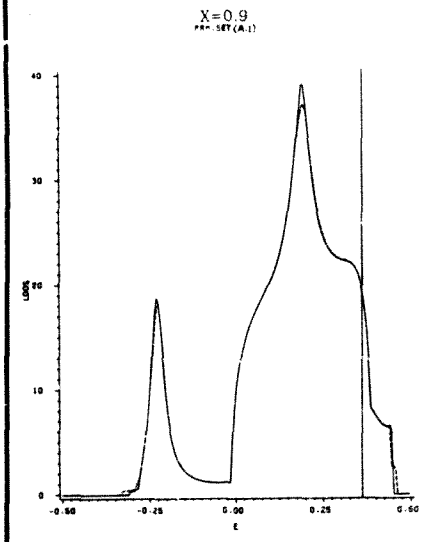

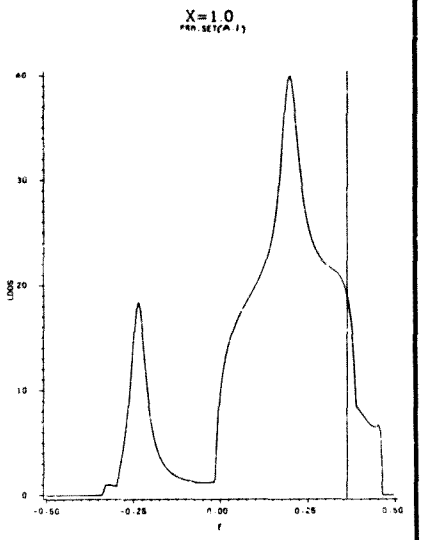

Figures 5.1.9-5.1.11 Total LDOS for prm.set (a.1), x = 0.8-1.0. Full curves: 1-phase model; broken curves: 2-phase model; vertical lines: E_Fs.

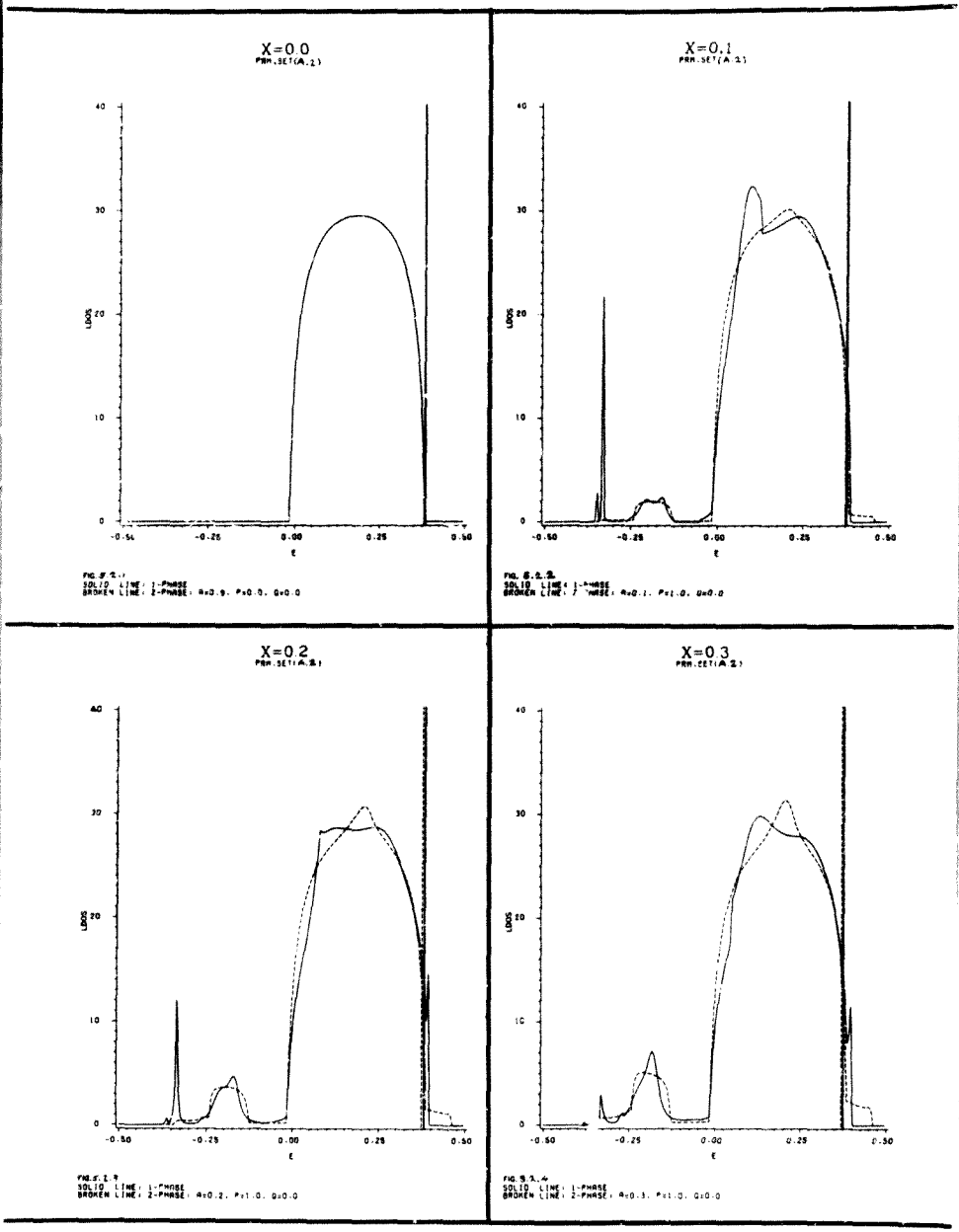

Figures 5.2.1-5.2.4 Total LDOS for prm.set (a.2), x = 0.0-0.3. Full curves: 1-phase model; broken curves: 2-phase model; vertical lines: E_Fs.

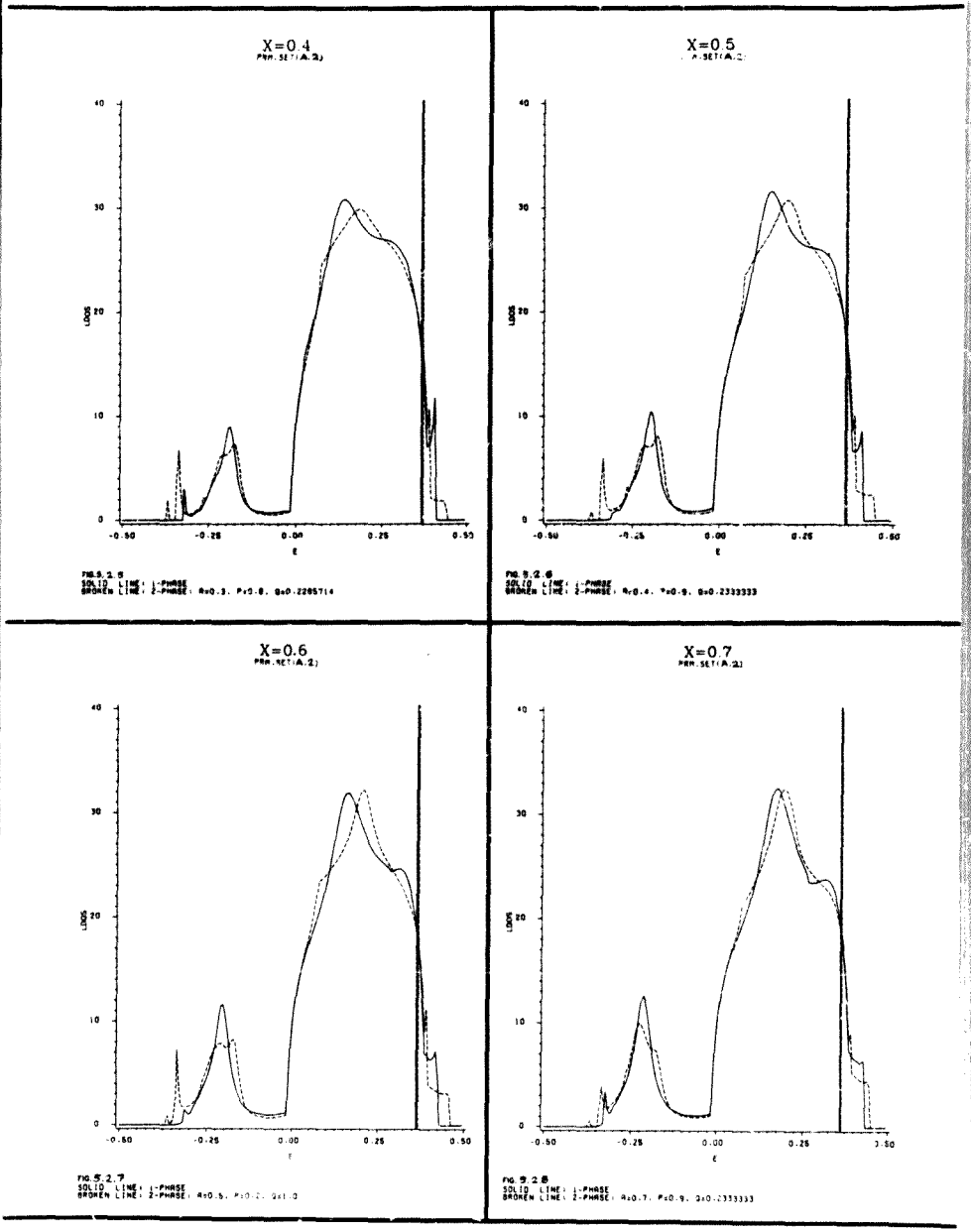

Figures 5.2.5-5.2.8 Total LDOS for prm.set (a.2), x = 0.4-0.7. Full curves: 1-phase model; broken curves: 2-phase model; vertical lines: E_Fs.

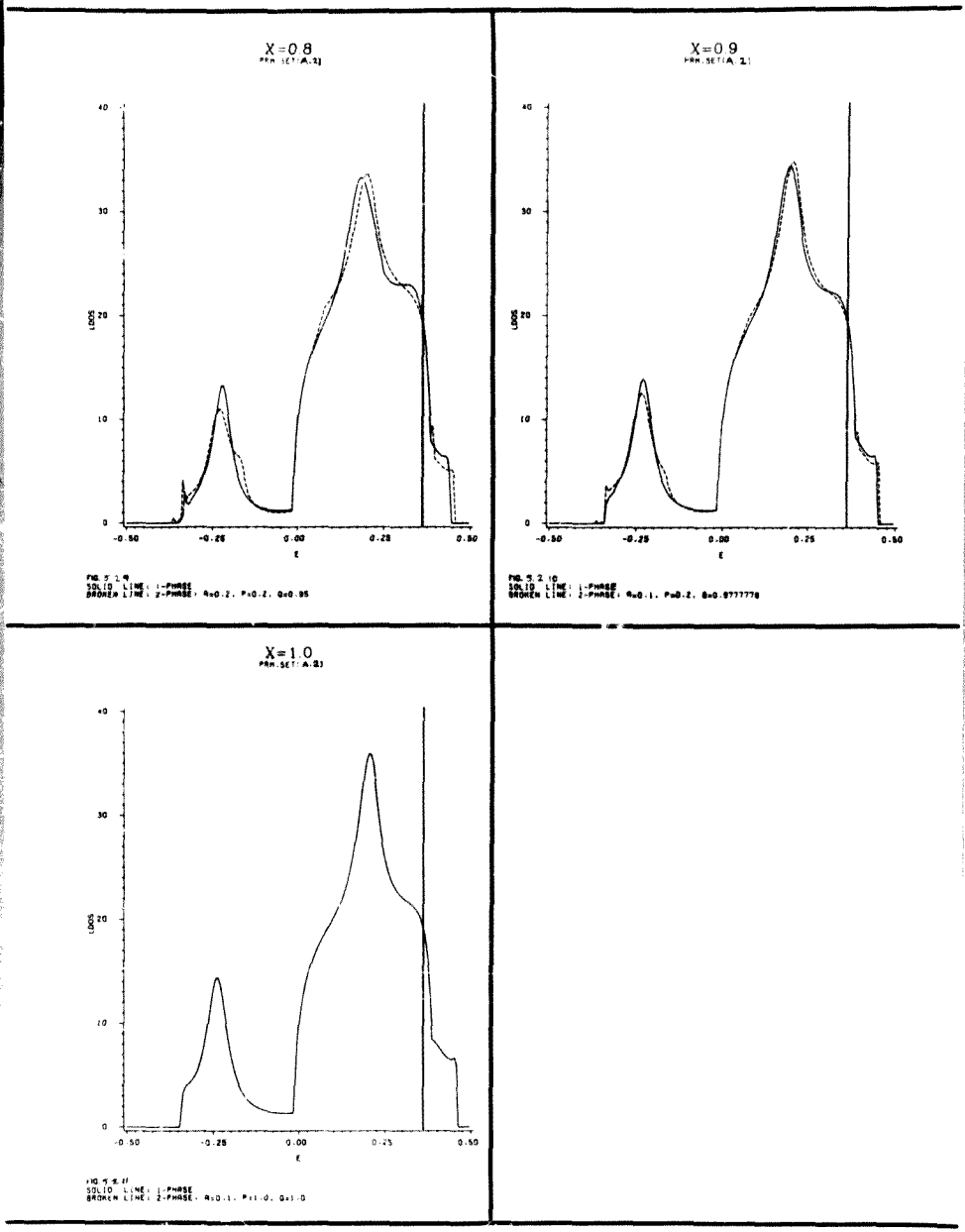

Figures 5.2.9-5.2.11 Total LDOS for prm.set (a.2), x = 0.8-1.0. Full curves: 1-phase model; broken curves: 2-phase model; vertical lines: E_Fs.

parameter sets is that the former has $V_{hh} = 0.0$ whereas the latter has $V_{hh} = +V_{hd}/10.0 = -0.0084$ Ryd, and hence we see that a relatively small change in V_{hh} has a considerable effect on the low-lying hydrogen-related peaks;

- and finally, we observe that for $x > 0.7$ the dramatic differences between the one- and two-phase LDOS found for low and intermediate x have all but disappeared. This feature is particularly encouraging since it shows that our two models become almost indistinguishable in the high-concentration β-phase regime, which is precisely what we wish to see. Specifically, we observe from the footnotes of Figures 5.1 and 5.2 that in this high-concentration region the p and q values of the two-phase model are mostly similar in size to their associated x value, so that for $x > 0.7$, our two-phase model is seen to converge on one of its special cases, viz. the one-phase model.

Having observed the important differences between our one- and two-phase models, we now proceed to find out what effects these differences have on our charge and energy formalisms.

5.3.2 *Energies, Charges and Heat of Formation*

In this section we compare one- and two-phase results[5.1] for prm.set (a.1). We display the *Fermi energies* as a function of x in Figure 5.3, plotted according to equations (4.13b) and (5.6); we note that the two-phase values are lower than the single-phase curve up to $x \approx 0.25$ and slightly higher for $0.3 \leq x \leq 0.8$; on the scale of Figure 5.3 the results for the

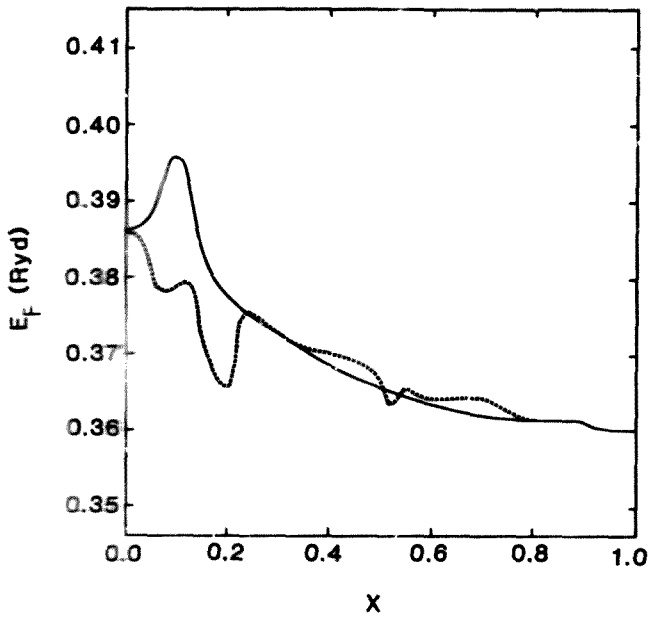

Figure 5.3 Fermi energy vs x for parameter set (a.1). Full curve: one-phase model; broken curve, two-phase model.

two models coincide for $x \geq 0.8$, as is to be expected from the findings of the previous section. Figures 5.4 to 5.6 show plots of the various *charges* versus x, obtained via equations (4.15) and (5.7); we find that the two-phase values are very similar to their one-phase counterparts, the main difference being that they exhibit greater oscillation than do the one-phase charges. This behaviour is due to an increase in numerical instability, which in turn is a consequence of the richer structure in the LDOS of the two-phase formalism.

A comparison between the *total electronic energies* appears in Figure 5.7, for which we have used equations (4.17) and (5.8); the following features are apparent: firstly, the two-phase energies are always less than or equal to the one-phase values, in accordance with our minimization procedure; secondly, the two-phase curve exhibits greater instability than the one-phase curve in the region $0.2 \leq x \leq 0.6$, again because of numerical considerations; and thirdly, the curves for the two models coincide on the scale of this particular figure for most of $x \geq 0.8$.

In Figure 5.8 we display plots of our one- and two-phase heats of formation versus x, together with Harada's experimental values[5.2]. These three curves agree substantially for $x \geq 0.7$, whereas for most $x \leq 0.7$ the one- and two-phase plots encompass the experimental curve. Our *two-phase* model for the heat of formation ($\Delta H^{(2)}$) is seen to be superior to the corresponding one-phase model (ΔH) for the following reasons: firstly, $\Delta H^{(2)}$ is noticeably closer in *shape* to the experimental curve than ΔH; and secondly, $\Delta H^{(2)}$ remains *negative* for almost all x values, again in better agreement with the entirely *exothermic* experimental curve.

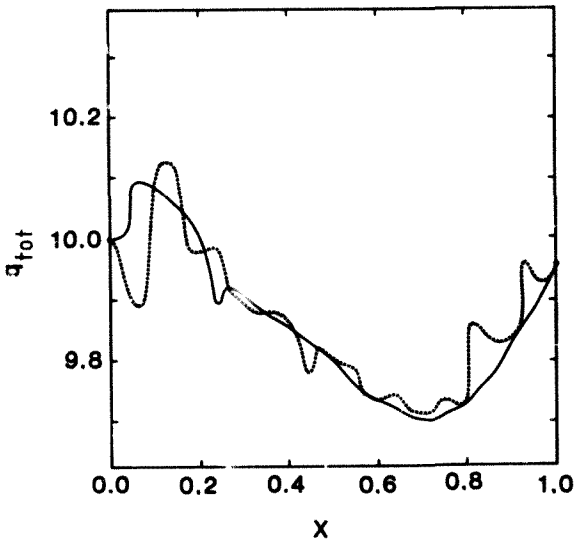

Figure 5.4 Total charge vs x for parameter set (a.1). Full curve: one-phase model; broken curve: two-phase model.

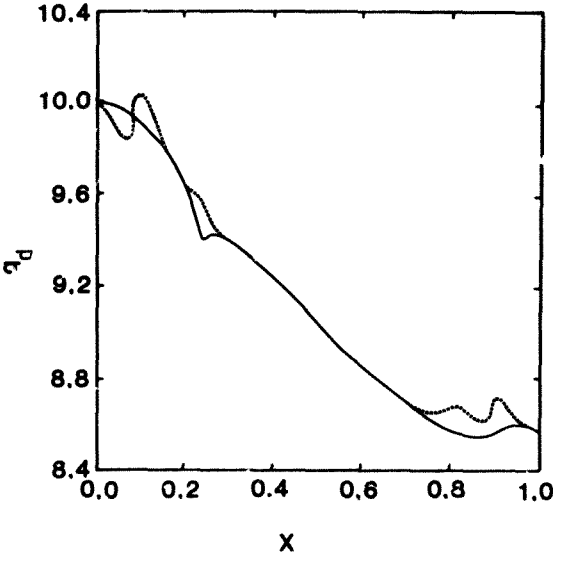

Figure 5.5 Palladium charge vs x for parameter set (a.1). Full curve: one-phase model; broken curve: two-phase model.

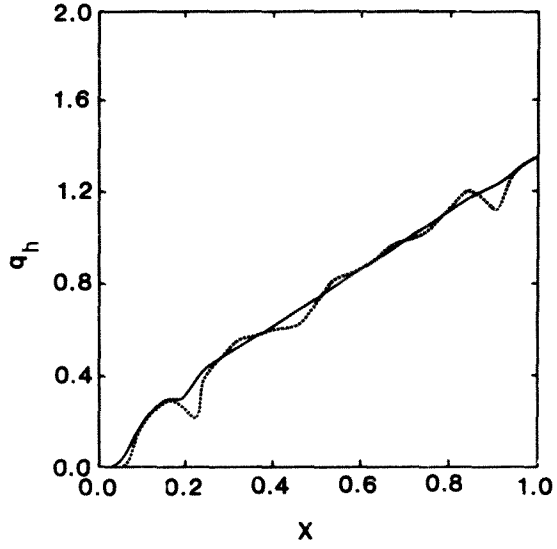

Figure 5.6 Hydrogen charge vs x for parameter set (a.1). Full curve: one-phase model; broken curve: two-phase model.

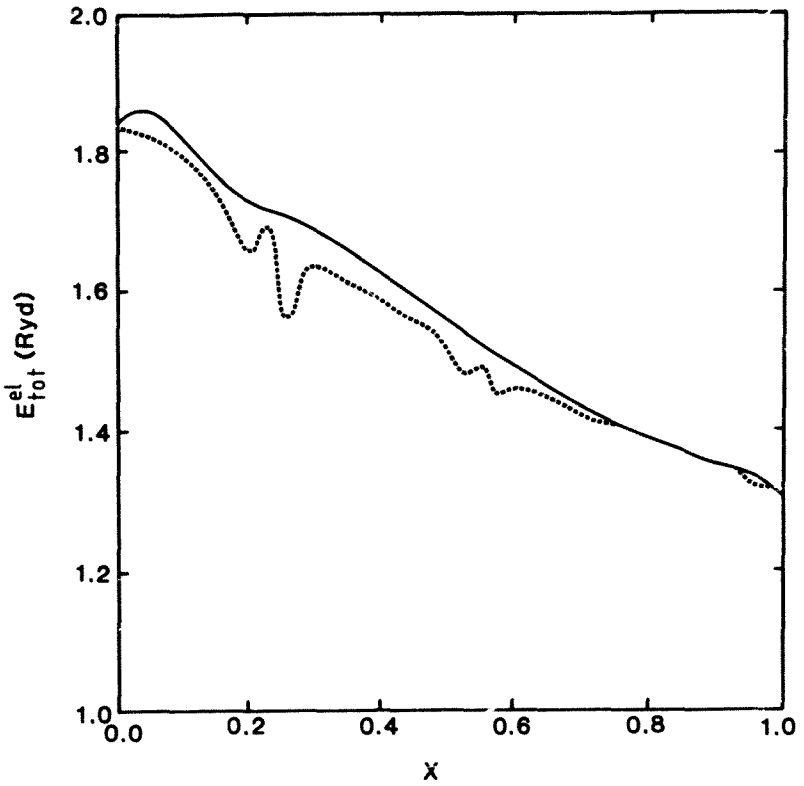

Figure 5.7 Total electronic energy vs x for parameter set (a.1). Full curve: one-phase model; broken curve: two-phase model.

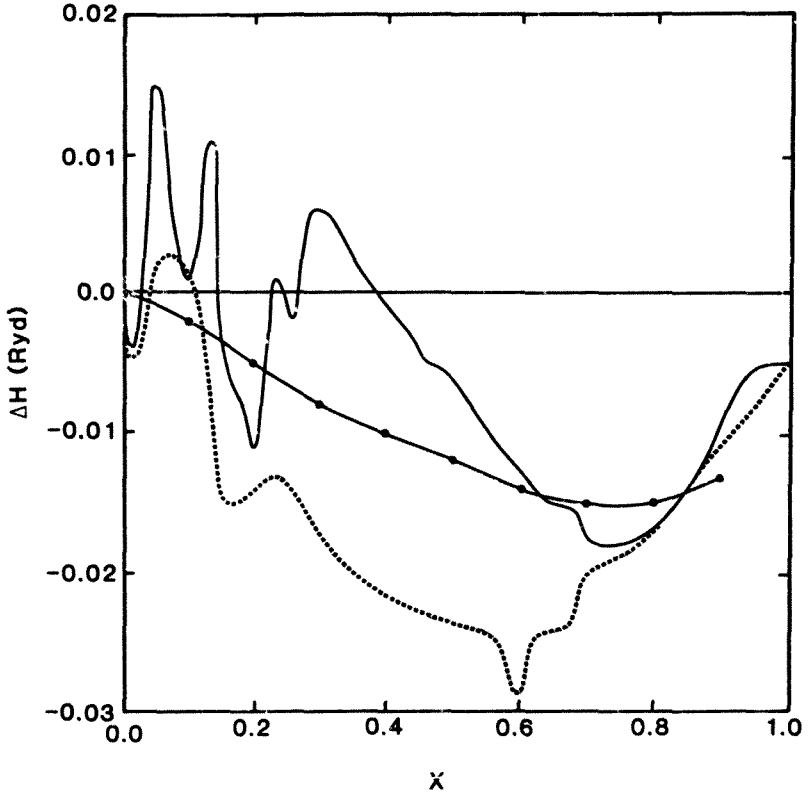

Figure 5.8 Comparison of heats of formation for parameter set (a.1) (full curve: one-phase model; broken curve: two-phase model) with the experimental results of Harada[5.2] (full curve with full circles).

In particular we observe that the region where the two-phase model for the heat of formation improves the most markedly on its one-phase counterpart coincides to a large extent with the experimentally well-established *two-phase region*, viz. $0.01 \leq x \leq 0.6$ at room temperature[5.3] (cf Figure 6.1). The good agreement between the two models for higher x values is seen to coincide with the experimentally-established *single-phase* nature of the hydride for $x \geq 0.6$ (see Figure 6.1). These improvements to the heat of formation indicate that our two-phase model has some physical validity, leading us to infer that in the two-phase region the *microscopic structure* of PdH_x is a *non-homogeneous* distribution of hydrogen, consisting of segregated forms of each phase.

We recall from equations (4.20) and (5.10) that our one- and two-phase heat of formation expressions differ only in their total electronic energy terms, which we have already compared in Figure 5.7. The total electronic energy is in turn a function of the Fermi energy E_F (Figure 5.3). However, a comparison of Figures 5.3 and 5.7 reveals that the differences in total energies between the two models correlate only slightly to the positions of the respective Fermi energies. We must therefore attribute the differences between the heats of formation largely to other features of the band structure, for example the shift in the position of the hybridized d_e-band peak, which Figures 5.1 and 5.2 reveal to be higher in energy for the two-phase LDOS.

5.3.3 *Summary of Section 5.3*

We have compared results for our one- and two-phase models and found that they are substantially the same for $x \geq 0.8$ and in close agreement for $x \geq 0.7$; this is in keeping with the experimentally-established fact that PdH_x is indeed a single-phase hydride for $x \geq 0.6$. The noticeable differences between our models for $x \leq 0.7$ manifest themselves specifically in the heats of formation, which we are employing as the experimentally-verifiable test of these models; a distinct deepening and also a smoothing of the ΔH curve occurs in moving from our single-phase to our two-phase formalism (see Figure 5.8). We are left with a two-phase curve which exhibits a smoothness and exothermic nature in keeping with experiment, though we notice from Figure 5.8 that the magnitudes of the experimental data are "sandwiched" between our one- and two-phase results for prm.set (a.1).

Having established the superiority of the two-phase formalism, we now proceed to implement it in further detail.

5.4 DETAILED APPLICATION OF TWO-PHASE MODEL

5.4.1 *Introduction*

This section is based on the results and discussion incorporated in our third paper[5.4], and serves to establish our two-phase concepts by calculating the segregation parameters, related LDOS and heats of formation for all nine parameter sets given in Table 3.5 and repeated in Table 5.1. Instead of thinking in terms of nine separate parameter sets we prefer rather to consider three groups of three sets, where only the first set in each group is in keeping with our original choice of hydrogen-hydrogen interaction parameter (Section 3.7). In effect we are considering only *three* key parameter sets (a.1, b.1, c.1), each one complemented by two arbitrarily-perturbed sets (a.2 and a.3, b.2 and b.3, c.2 and c.3 respectively). The three key sets differ only in their choice of hydrogen-palladium interaction strength V_{hd}; set a.1 incorporates the V_{hd} value derived in Section 3.7, while V_{hd} for sets b.1 and c.1 are respectively bigger and smaller by the arbitrary factor $\sqrt{2}$ chosen for convenience in accordance with equation (3.24). Our results for each physical quantity are presented in the form of three adjacent figures, referring to parameter sets a, parameter sets b and parameter sets c respectively.

Set	V_{hd}	Subset	V_{hh}
a	V	a.1	0.0
		a.2	+V/10.0
		a.3	-V/10.0
b	$\sqrt{2}$V	b.1	0.0
		b.2	+V/10.0
		b.3	-V/10.0
c	V, $\sqrt{2}$	c.1	0.0
		c.2	+V/10.0
		c.3	-V/10.0
V = - 0.08485 Ryd			

Table 5.1 Parameter sets used for present calculations. The choice of the factor $\sqrt{2}$ follows from equation (3.24). The non-zero V_{hh} values have been chosen arbitrarily. V_{dd} = -0.0298 Ryd and U = 0.185 Ryd are used in all cases.

5.4.2 *Segregation Parameter Results*

Curves of r versus x, plotted according to equation (5.11), appear in Figures 5.9a-5.9c. We see immediately that we do indeed have the desired behaviour of r for higher values of x, viz. $r \to 1$ at some "critical" x value (x_{crit}) and $r \approx 1$ for $x > x_{crit}$. The abruptness of the upswing in r and the maintenance of large r values for $x > x_{crit}$ indicate that the two-phase formalism is qualitatively successful in modelling the transition of the hydride into the β-phase at higher concentrations of hydrogen. The only parameter set which gives a *quantitatively* accurate transition concentration is set (a.3) for which $x_{crit} \approx 0.57$ (cf the experimentally-predicted value of $x_{crit} \approx 0.6$: see Figure 6.1); for the other sets we have $0.73 \leq x_{crit} \leq 0.94$, though the upper limit is probably pessimistically large due to oscillations caused by numerical instabilities in the calculations with sets c (this instability is apparent from our results for the heats of formation below).

We now proceed to evaluate the LDOS for the various parameter sets at $x = x_{crit}$.

5.4.3 *LDOS Results*

In Figures 5.10a-5.10c we display plots of the two-phase total LDOS, each curve evaluated for $x = x_{crit}$ and for parameters (α,p,q) which minimize $\Delta H^{(2)}$ at x_{crit}. The value of $x = x_{crit}$ was chosen to give us insight into the *electronic behaviour* of the hydride at its high-concentration *phase boundary*, bearing in mind the physical importance of such boundaries.

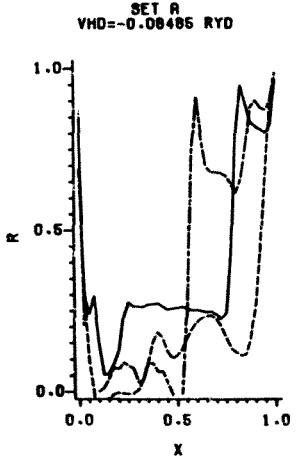

Fig.5.9a

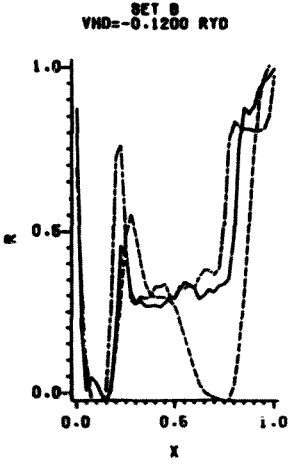

Fig.5.9b

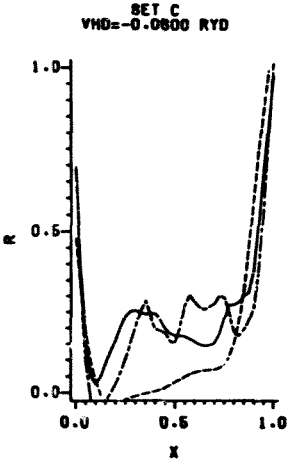

Fig.5.9c

Figures 5.9 a-c Segregation parameters vs x for parameter sets (a.i), (b.i) and (c.i) respectively. Full curves: i = 1 (V_{hh} = 0.0 Ryd); broken curves: i = 2 (V_{hh} =-0.00849 Ryd); chained curves: i = 3 (V_{hh} = +0.00849 Ryd).

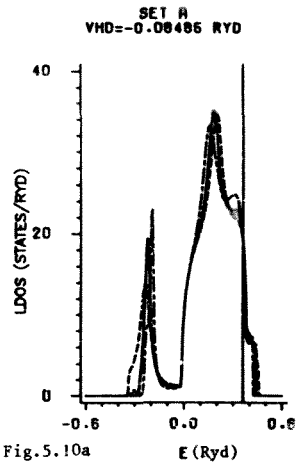

Fig.5.10a

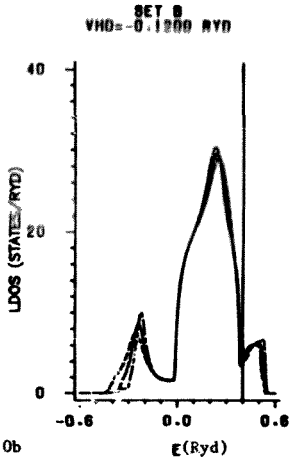

Fig.5.10b

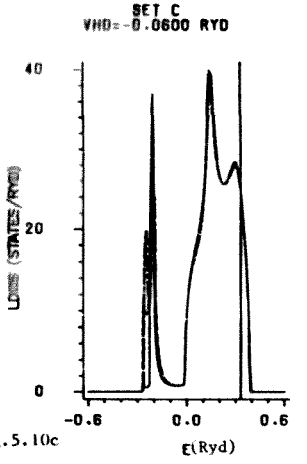

Fig.5.10c

Figures 5.10 a-c Total Local Densities of States vs energy (evaluated at the critical concentrations) for parameter sets (a.i), (b.i) and (c.i) respectively. Full curves: i = 1 (V_{hh} = 0.0 Ryd); broken curves: i = 2 (V_{hh} = -0.00849 Ryd); chained curves: i = 3 (V_{hh} = +0.00849 Ryd); vertical lines: Fermi energies.

In comparing Figures 5.10a-c we must bear in mind that the corresponding curves differ for *two* reasons, viz. the respective values of x_{crit} and V_{hd} employed; we must therefore be careful to distinguish between these two effects. We firstly confine our attention to the case $V_{hh} = 0.0$ in each of Figures 5.10a-c; for these plots the x_{crit} values are roughly 0.78, 0.81 and 0.92 respectively. The first two x_{crit} values are sufficiently close for us not to expect any significant effects in the LDOS due to their difference (compare with the same range of x values in Figures 5.1). We can thus safely state that the broadening and diminished intensity of the hydrogen peak in going from Figure 5.10a to 5.10b is due to the increased magnitude of V_{hd}, in accordance with our findings of Section 4.3.2. Furthermore we observe that the hydrogen and perturbed palladium states are particularly *sharply peaked* in the case of Figure 5.10c; this sharpness of the hydrogen band is particularly surprising because of the high x value employed for this plot ($x_{crit} \simeq 0.92$), recalling that we have previously associated high x values with *broad* hydrogen bands (see Figures 5.1). The effect can only be due to the small magnitude of V_{hd} used; this is physically sensible because we expect the hydrogen band to "condense" into a localized state when the interaction between the interstitial hydrogen and its various neighbours becomes sufficiently small. We also notice the expected sharpening of the d-band peaks with *decreasing* magnitude of V_{hd}, a feature which in conjunction with the hydrogen band 'peakiness" just discussed gives rise to *numerical instabilities* in the integration of the LDOS of Figure 5.10c.

We now examine the effect of "switching on" the interaction V_{hh}. It is seen that for a given value of V_{hd} the hydrogen bonding peak is broadened,

diminished in intensity and lowered in energy when V_{hh} is made negative, while the opposite effects occur for positive V_{hh}, suggesting that the hydride should be most stable for the case $V_{hh} < 0.0$. However we have already seen in Section 4.5.3 and will see again below that this is *not* the case; hence we deduce that the *upward* shift of the hybridized d-band peak observed for the case $V_{hh} < 0.0$ causes an increase in the total electronic energy which offsets the energy reduction due to the downward shift of the hydrogen states. The d-band peak is in the range (2.5±0.5)eV below E_F for all parameter sets employed, so that we again have the agreement with the experimental results of Schlapbach and Burger[5.5] found in Section 4.3.2 (we recall that these workers found a slight *increase* in the d-band DOS of $PdH_{0.6}$ at 3 eV below E_F). Furthermore our lower, hydrogen-related peak is centred between 7.6 and 9.0 eV below E_F, again consistent with Schlapbach and Burger's result of approximately 8 eV[5.5].

The Fermi energy is seen to fall in a region where the LDOS is changing rapidly, particularly for parameter sets a and c, and we notice that the LDOS at the Fermi energy drops with increasing V_{hd}. We observe the expected shoulder in the LDOS above E_F for sets a, which partially resolves into a peak for sets b but which is absent for sets c.

Having gained some insight into the electronic structure of PdH_x for the various parameter sets, we are now in a position to appreciate more fully the corresponding heats of formation.

5.4.4 Heat of Formation Results

We have again plotted $\Delta H^{(2)}$ versus x according to equations (5.10) and the results appear in Figures 5.11a to 5.11c, where we also show the experimental curves of Harada[5.2] and Kuji et al[5.3]. We observe that sets c.1 and c.3 give rise to curves which oscillate considerably, this being indicative of instabilities in the numerical quadrature procedure employed. However, the remarkably smooth curve obtained for parameter set c.2 suggests that this instability might not be purely numerical in nature, possibly reflecting the reaction of the model to physically-unacceptable parameter sets. If this is the case then the distinct smoothing out of the curves for larger magnitudes of V_{hd} would indicate that the parameter sets with the larger V_{hd} values are physically more correct.

We observe that for the energetically and numerically more stable parameter sets a and b the positive V_{hh} value makes the hydride energetically more stable whereas the negative V_{hh} value has the opposite effect; some of the electronic features contributing to this behaviour were discussed in Section 5.4.3. It can be seen that our plots of $\Delta H^{(2)}$ versus x are in qualitative agreement with experiment, both as far as shape and exothermal properties are concerned. However our $\Delta H^{(2)}$ minima are two to three times larger in magnitude than the experimental ones. Because our LDOS are consistent with experimental photoelectron results[5.5] and with the essential features of detailed band structure calculations[5.6],[5.7],[5.8] it would appear that the electronic contributions to $\Delta H^{(2)}$ from our formalism are not seriously at fault, but rather our modelling of the band-shift and elastic terms; we note

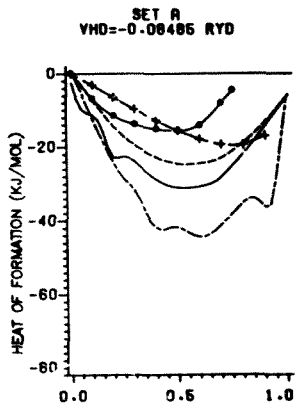

Fig.5.11a

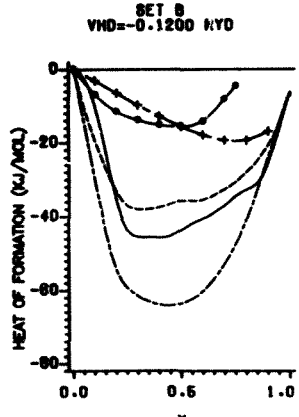

Fig.5.11b

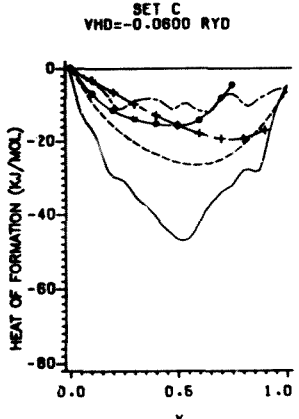

Fig.5.11c

Figures 5.11 a-c Calculated heats of formation vs x for parameter sets (a.i), (b.i) and (c.i) respectively, together with experimental results. Full curves: i = 1 (V_{hh} = 0.0 Ryd); broken curves: i = 2 (V_{hh} = -0.00849 Ryd); chained curves: i = 3 (V_{hh} = + 0.00849 Ryd); full curves with full circles: experimental results of Kuji et al[5.3]; chained curves with (+) symbols: experimental results of Harada[5.2].

that difficulties in accomodating the elastic energy have been experienced by other workers[5.9].

5.4.5 *Summary of Section 5.4*

In this section we have applied our two-phase formalism in some depth, making use of all our parameter sets. We have firstly evaluated the segregation parameter r as a function of x and in all cases have found a sharply-defined "critical" hydrogen concentration (x_{crit}) at which r increases very rapidly to values close to unity; x_{crit} is in the range $0.57 \leq x \leq 0.94$, and we have $r \approx 1$ for $x > x_{crit}$. In terms of our definition of r this means that our model gives rise to a phase transition at x_{crit}, with a single phase being present for $x > x_{crit}$. This is in good qualitative agreement with the experimentally-established phase transition at $x \approx 0.6$, with only the β-phase being present for $x > 0.6$.

In order to obtain insight into the electronic properties of the hydride at the phase transition we have also plotted the LDOS for each parameter set at $x = x_{crit}$, finding inter alia that these LDOS become narrower and more sharply-peaked for smaller magnitudes of V_{hd}. We have finally given plots of the heats of formation for the various parameter sets, finding that a weak metal-hydrogen interaction (small absolute value of V_{hd}) results in a shallow and oscillating curve for the heat of formation, whereas larger absolute values of V_{hd} give rise to smoother, more exothermic curves. The oscillatory behaviour for small magnitudes of V_{hd} is a direct consequence of the narrow, sharply-peaked bands found in the LDOS for such V_{hd} values.

that difficulties in accomodating the elastic energy have been experienced by other workers[5.9].

5.4.5 *Summar of Section 5.4*

In this section we have applied our two-phase formalism in some depth, making use of all our parameter sets. We have firstly evaluated the segregation parameter r as a function of x and in all cases have found a sharply-defined "critical" hydrogen concentration (x_{crit}) at which r increases very rapidly to values close to unity; x_{crit} is in the range $0.57 \leq x \leq 0.94$, and we have $r \approx 1$ for $x > x_{crit}$. In terms of our definition of r this means that our model gives rise to a phase transition at x_{crit}, with a single phase being present for $x > x_{crit}$. This is in good qualitative agreement with the experimentally-established phase transition at $x \approx 0.6$, with only the β-phase being present for $x > 0.6$.

In order to obtain insight into the electronic properties of the hydride at the phase transition we have also plotted the LDOS for each parameter set at $x = x_{crit}$, finding inter alia that these LDOS become narrower and more sharply-peaked for smaller magnitudes of V_{hd}. We have finally given plots of the heats of formation for the various parameter sets, finding that a weak metal-hydrogen interaction (small absolute value of V_{hd}) results in a shallow and oscillating curve for the heat of formation, whereas larger absolute values of V_{hd} give rise to smoother, more exothermic curves. The oscillatory behaviour for small magnitudes of V_{hd} is a direct consequence of the narrow, sharply-peaked bands found in the LDOS for such V_{hd} values.

5.5 SUMMARY OF CHAPTER 5

In this chapter we have introduced and demonstrated the superiority of a model which accommodates the two-phase characteristics of PdH_x. This two-phase model is based on the assumption that the hydride consists of two segregated, non-interacting phases, each with the essentially random nature of the one-phase model developed in Chapter 4. The more sophisticated two-phase formalism requires that we implement a numerical energy-minimization technique which results in a more computationally-intensive method for evaluating the correct electronic energies of the system; we nevertheless consider the marked improvement in our heats of formation to be ample justification for implementing the two-phase approach.

A further benefit of this improved formalism is that it allows us to evaluate a suitable segregation parameter, which successfully predicts the higher-concentration phase transition in PdH_x.

These successes in describing aspects of the phase behaviour of the hydride encourage us to apply our two-phase model to the *thermodynamics* of the system, even if only in a semi-qualitative manner.

5.5 SUMMARY OF CHAPTER 5

In this chapter we have introduced and demonstrated the superiority of a model which accommodates the two-phase characteristics of PdH_x. This two-phase model is based on the assumption that the hydride consists of two segregated, non-interacting phases, each with the essentially random nature of the one-phase model developed in Chapter 4. The more sophisticated two-phase formalism requires that we implement a numerical energy-minimization technique which results in a more computationally-intensive method for evaluating the correct electronic energies of the system; we nevertheless consider the marked improvement in our heats of formation to be ample justification for implementing the two-phase approach.

A further benefit of this improved formalism is that it allows us to evaluate a suitable segregation parameter, which successfully predicts the higher-concentration phase transition in PdH_x.

These successes in describing aspects of the phase behaviour of the hydride encourage us to apply our two-phase model to the *thermodynamics* of the system, even if only in a semi-qualitative manner.

APPENDIX 5.1

EQUIVALENCE OF ONE- AND TWO-PHASE MODELS FOR X = 0 AND 1

We recall equations (5.2) and (5.3a) respectively:-

$$x = \alpha p + (1-\alpha)q \tag{A5.1.1}$$

$$0 < \alpha < 1 \tag{A5.1.2}$$

Solving equation (A5.1.1) for α and applying equation (A5.1.2) we obtain:-

$$0 < \frac{x-q}{p-q} < 1 \tag{A5.1.3}$$

Assuming $p > q$, it firstly follows from equation (A5.1.3) that:-

$$x - q < p - q$$

$$\therefore \quad x < p \tag{A5.1.4}$$

and secondly that:-

$$x - q > 0$$

$$\therefore \quad x > q \tag{A5.1.5}$$

Equations (A5.1.4) and (A5.1.5) together give us $q < x < p$, or more fully:-

$$0 \leq q < x < p \leq 1 \tag{A5.1.6}$$

For the case $x \to 0$ equation (A5.1.6) gives $q \to 0$, which when substituted into equation (A5.1.1) results in $p \to 0$ (recalling that $a > 0$). Hence we have $p \to q \to x \to 0$, proving that the two-phase model reduces to the one-phase model as $x \to 0$.

For the case $x \to 1$ we obtain $p \to 1$ from equation (A5.1.6) which we also substitute into equation (A5.1.1) to obtain the result $q \to 1$. So we are left with $p \to q \to x \to 1$, which proves that the two models are also equivalent as $x \to 1$.

Similar arguments can be used for the case $p < q$.

REFERENCES (CHAP. 5)

5.1) Anagnostaras P D and Lowther J E 1985 *J. Phys. F: Met. Phys.* 15 55

5.2) Harada S 1983 *J. Phys. F: Met. Phys.* 13 607

5.3) Kuji T, Oates W A, Bowerman B S and Flanagan T B 1983 *J. Phys. F: Met. Phys.* 13 1785

5.4) Anagnostaras P D and Lowther J E to be published in *J. Less-Common Met.*

5.5) Schlapbach L and Burger J P 1982 *J. Physique* 43 L273

5.6) Switendick A C 1972 *Ber. Bunsenges. Phys. Chem.* 76 535

5.7) Faulkner J S 1976 *Phys. Rev. B* 13 2391

5.8) Papaconstantopoulos D A, Klein B M, Faulkner J S and Boyer L L 1978b *Phys. Rev. B* 18 2784

5.9) Oates W A 1982 *J. Less-Common Met.* 88 411

CHAPTER 6

THERMODYNAMIC CONSIDERATIONS

6.1 INTRODUCTION

Most of the thermodynamic models for PdH_x are expressed in terms of a semiempirical *partial pressure equation* (Section 1.2.8) so as to facilitate direct comparison with experimentally-known pressure-composition isotherms. This equation is characterized by a *correction term* (the so-called *excess chemical potential*) for modelling the *non-ideal behaviour* of the system, and we wish to determine how effective our one- and two-phase formalisms are in describing this non-ideal contribution. To do this we divide the excess chemical potential into its enthalpic and entropic contributions, for each of which we develop one- and two-phase models; we then incorporate these terms in the underlying partial pressure equation, thereby obtaining our own one- and two-phase expressions for the partial pressure. We are then able to compare both our formalisms with experimental isotherms in order to ascertain which is more applicable to the palladium-hydrogen system.

In Section 6.2 the semiempirical partial pressure equation is derived and discussed, with an emphasis on the enthalpic and entropic parts of the correction term; in Sections 6.3 and 6.4 we develop suitable models for the enthalpic and entropic contributions respectively to the correction term; in Section 6.5 we generate pressure-composition isotherms using both our partial pressure equations, enabling us to compare our models with experiment and with each other; and finally the important findings of this chapter are summarized in Section 6.6.

6.2 SEMIEMPIRICAL MODELS

6.2.1 *Underlying Formalism*

The following is a fundamental thermodynamic equation for a metal hydride in equilibrium with an atmosphere of molecular hydrogen[6.1)p.75]:-

$$\mu_H = \tfrac{1}{2}\,\mu_{H_2} \tag{6.1}$$

where μ_H and μ_{H_2} are the *partial Gibbs free energies* of atomic hydrogen dissolved in the lattice and molecular hydrogen gas in the surrounding atmosphere respectively.

For the case of an *ideal solution* (that is very low concentration) Sieverts' Law[6.1)p.75] holds for the dissolved hydrogen gas, giving rise to the following approximation for $x << 1$:-

$$\mu_H \simeq \mu_H^{\circ} + RT\ell n\,\frac{x}{b-x} \tag{6.2}$$

where μ_H° is the *standard chemical potential* of hydrogen in the lattice (that is the chemical potential at *infinite dilution* of hydrogen), R is the universal gas constant (Boltzmann's constant k_B multiplied by Avogadro's number N_A), T is the absolute temperature of the system and b is a site-availability parameter (see Appendix 6.1).

Assuming that the molecular hydrogen can be modelled by an *ideal gas* formalism , we then also have a simple expression for μ_{H_2}, viz.:-

$$\mu_{H_2} = \mu_{H_2}^{\circ} + RT\ell n(p_{H_2}/atm) \tag{6.3}$$

where $\mu^{o}_{H_2}$ is the chemical potential for the hypothetical case of infinitely-dilute molecular hydrogen, and p_{H_2} is the partial pressure of the molecular hydrogen gas in atmospheres; both these are experimentally-accessible quantities.

Because we are interested in *all* concentrations $0 < x < 1$ and not merely the ideal case $x << 1$, we must add an x-dependent correction term (the excess chemical potential, μ^{E}_{H}) to the right-hand side of equation (6.2), giving rise to the following more general equation:-

$$\mu_H = \mu^{o}_{H} + RT\ell n \frac{x}{b-x} + \mu^{E}_{H} \qquad (6.4)$$

Substituting equations (6.3) and (6.4) into equation (6.1) gives us the following partial pressure equation, commonly used in the application of *semiempirical formalisms*[6.2]:-

$$\ell n(p_{H_2}/atm)^{\frac{1}{2}} = \frac{\Delta\mu^{o}_{H}}{RT} + \frac{\mu^{E}_{H}}{RT} + \ell n \frac{x}{b-x} \qquad (6.5)$$

where $\Delta\mu^{o}_{H} = \mu^{o}_{H} - \frac{1}{2}\mu^{o}_{H_2}$.

Kuji et al[6.3] express the excess chemical potential in the following manner:-

$$\mu^{E}_{H} = H^{E}_{H} - TS^{E}_{H} \qquad (6.6)$$

where H^{E}_{H} and S^{E}_{H} are the *partial excess enthalpy and entropy* respectively. Now the term $\ell n\, x/(b-x)$ in equation (6.5) is *also entropic* in nature (Appendix 6.1) and hence equation (6.5) contains *two* entropic contributions.

Substituting equation (6.6) into equation (6.5) gives us:-

$$\ln(p_{H_2}/\text{atm})^{\frac{1}{2}} = \frac{\Delta\mu_H^\circ}{RT} + \frac{H_H^E}{RT} - \left[\frac{S_H^E}{R} - \ln\frac{x}{b-x}\right] \qquad (6.7)$$

where the entropic terms are grouped together in square brackets. The left-hand side of equation (6.7) is known from experimentally-determined pressure-composition isotherms (for example Figure 6.1) and so the success of a given semiempirical formalism is determined by the accuracy with which the right-hand side of equation (6.7) reproduces the experimental trends.

In modelling the right-hand side of equation (6.7) we make use of the $\Delta\mu_H^\circ$ values provided by Kuji et al[6.3]; the specific values used are displayed in Table 5.1 (see Section 6.5). In the following two sections we derive expressions for H_H^E/RT and for the *combined* entropic contribution viz. $\left[S_H^E/R - \ln x/(b-x)\right]$, employing both our one- and two-phase models.

6.2.2 *Summary of Section 6.2*

In this section we have applied standard thermodynamic equations to the PdH_x system in equilibrium with an environment of molecular hydrogen. The equation describing the partial Gibbs free energy of hydrogen in PdH_x strictly applies only to *low* hydrogen concentrations; hence a *correction term*, referred to as the *excess chemical potential*, is added to make this equation physically acceptable at higher values of x. The correct modelling of this non-ideal correction term is the key challenge to electronic and other formalisms applied to these simple underlying thermodynamic equations. For convenience we have followed the usual procedure of combining the equations into a single equilibrium equation

Substituting equation (6.6) into equation (6.5) gives us:-

$$\ell n(p_{H_2}/atm)^{\frac{1}{2}} = \frac{\Delta\mu_H^\circ}{RT} + \frac{H_H^E}{RT} - \left[\frac{S_H^E}{R} - \ell n\,\frac{x}{b-x}\right] \qquad (6.7)$$

where the entropic terms are grouped together in square brackets. The left-hand side of equation (6.7) is known from experimentally-determined pressure-composition isotherms (for example Figure 6.1) and so the success of a given semiempirical formalism is determined by the accuracy with which the right-hand side of equation (6.7) reproduces the experimental trends.

In modelling the right-hand side of equation (6.7) we make use of the $\Delta\mu_H^\circ$ values provided by Kuji et al[6.3]; the specific values used are displayed in Table 6.1 (see Section 6.5). In the following two sections we derive expressions for H_H^E/RT and for the *combined* entropic contribution viz. $\left[S_H^E/R - \ell n x/(b-x)\right]$, employing both our one- and two-phase models.

6.2.2 *Summary of Section 6.2*

In this section we have applied standard thermodynamic equations to the PdH_x system in equilibrium with an environment of molecular hydrogen. The equation describing the partial Gibbs free energy of hydrogen in PdH_x strictly applies only to *low* hydrogen concentrations; hence a *correction term*, referred to as the *excess chemical potential*, is added to make this equation physically acceptable at higher values of x. The correct modelling of this non-ideal correction term is the key challenge to electronic and other formalisms applied to these simple underlying thermodynamic equations. For convenience we have followed the usual procedure of combining the equations into a single equilibrium equation

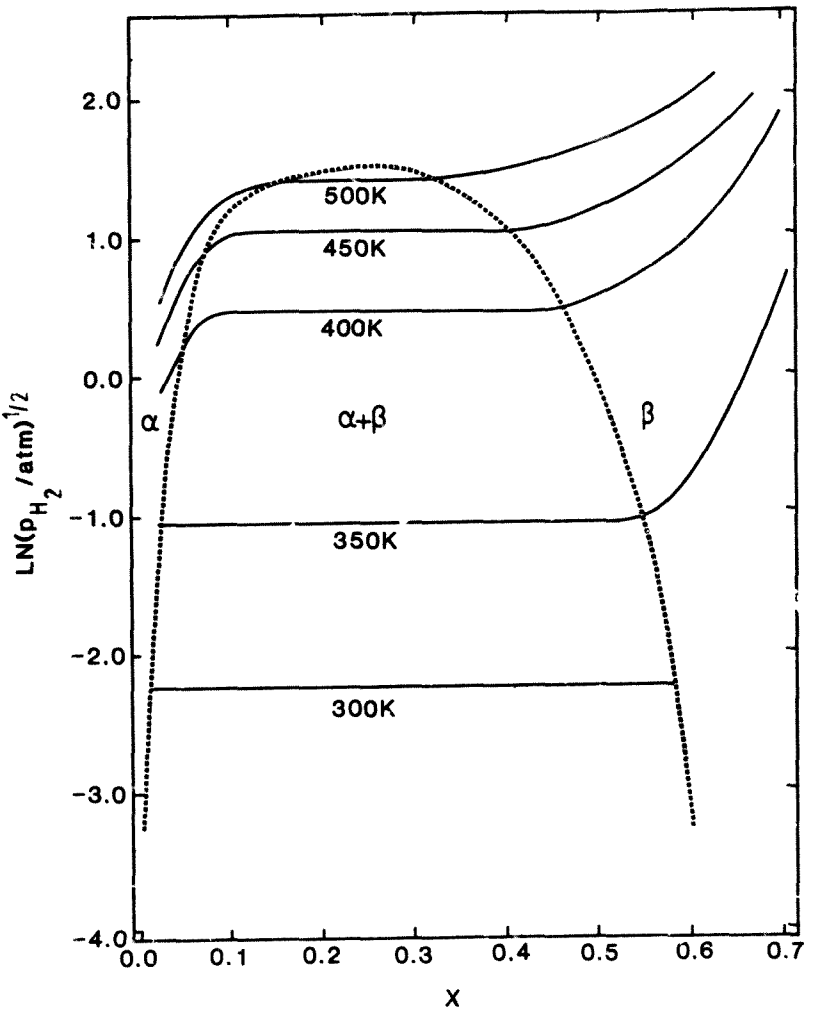

Figure 6.1 Experimental pressure-composition isotherms for PdH_x (adapted from Kuji et al[6.3] p.1794).

for the partial pressure of molecular hydrogen gas, bearing in mind that the pressure-composition isotherms are known from experiment. We have followed Kuji et al[6.3] in separating the excess chemical potential into its enthalpic and entropic parts, paving the way for the analyses in the next two sections.

6.3 PARTIAL EXCESS ENTHALPY

6.3.1 Similarities between H_H^E and our ΔH Formalism

The only enthalpy-related quantity in our formalism is the heat of formation (ΔH), and we demonstrate in a semi-quantitative manner that the partial excess enthalpy (H_H^E) can be modelled using our heat of formation expressions. Firstly, we see from Kuji et al[6.3] that H_H^E is an *excess* quantity in the sense that it tends to zero with x; both our one- and two-phase heat of formation expressions have the same property (see equations (4.20) and (5.9b) respectively). Secondly, we see from Figures 5.11 that Kuji et al's H_H^E values and our two-phase ΔH curves are similar in shape and exothermicity. Now Figures 5.11 also reveal that the minimum of Kuji et al's H_H^E curve is similar in magnitude to the minimum of Harada's *heat of formation* curve[6.4], and we recall from Figure 5.8 that Harada's values fall roughly midway between our one- and two-phase ΔH results; hence H_H^E also falls in this range, making it comparable in magnitude to our ΔH model or most values of x.

6.3.2 Summary of Section 6.3

We have found that H_H^E is compatible with our two-phase ΔH curve shown in Figure 5.8 (parameter set (a.1)), both in shape and exothermicity, and that it has values which fall between our one- and two-phase curves; further, H_H^E and our ΔH functions are all *excess* quantities. On the basis of these similarities we choose to model H_H^E by means of both our one- and two-phase heat of formation expressions (equations (4.20) and (5.9b) respectively).

We now consider the entropic contributions to the system.

6.4 ENTROPY CONTRIBUTIONS

6.4.1 Formulae and Results

In Appendix 6.1 we derive the following expression for the integral ideal configurational entropy per mole of metal atoms:-

$$S(x)/R = -\left[x \ln x - b \ln b + (b-x)\ln(b-x)\right] \qquad (6.8)$$

By taking the *derivative* of S(x) with respect to x we then obtain the following expression for the *partial* ideal configurational entropy per mole of *hydrogen* atoms:-

$$S'(x)/R = -\ln \frac{x}{b-x} \qquad (6.9)$$

which corresponds to the second entropy term in equation (6.7) Because S(x) and S'(x) are functions of x only and not of (α,p,q) we may think of them as *one-phase* quantities. Ideally we would have b=1 for the case where atomic hydrogen occupies the octahedral interstitial sites in palladium metal. It is however usually found that semiempirical models of the type described by equation (6.7) only concur with experiment for values of $b < 1$ [6.2] An entropic expression which requires $b < 1$ is consistent with the so-called *blocking model*[6.5] concept, in which short-range *electronic repulsions* between hydrogen atoms prevent the total number of interstitial sites from being occupied. This assumed existence of repulsive hydrogen-hydrogen interactions suggests that the blocking model corresponds most closely to those of our parameter sets which have $V_{hh} > 0$. However we should note at this point that the blocking concept ($b < 1$) is of only limited applicability to PdH_x because the

stoicniometric hydride, for which we require b=1, is in fact experimentally obtainable. In the present analysis we will make the simplifying assumption that blocking effects are absent altogether, and will thus work with the original set of parameters derived in Chapter 3, viz. prm.set (a.1), for which $V_{hh} = 0.0$. Neglect of the blocking model allows us to occupy all the interstitial hydrogen sites, that is we can choose b=1; substituting this into equations (6.8) and (6.9) results in the following expressions for our *one-phase* entropies:-

$$-S_{(1)}(x)/R = [x \ln x + (1-x)\ln(1-x)] \qquad (6.10)$$

and

$$-S'_{(1)}(x)/R = \ln \frac{x}{1-x} \qquad (6.11)$$

where we now place the minus sign on the left-hand side for more convenient comparison with equation (6.7).

We next consider the other entropy contribution to equation (6.7) viz. S_H^E. Kuji . al[6.3] have carried out a detailed analysis of their experimentally-measured S_H^E values and conclude that the dominant contribution to S_H^E is *configurational* in nature; they refer to this dominant term as the *non-ideal* configurational entropy. Hence the combined entropic contribution to equation (6.7) is essentially *configurational* in nature, consisting chiefly of one *ideal* and one *non-ideal* configurational entropy term. On the basis of this observation we will firstly approximate the *combined* entropy terms of equation (6.7) by means of our one-phase configurational formalism (equation (6.11)), and secondly by means of a purely configurational *two-phase* entropy formalism which we will now derive.

We recall from Section (5.2) that our two-phase model is based on the following reaction equation:-

$$PdH_x = \alpha\, PdH_p + (1-\alpha) PdH_q \qquad (6.12)$$

where p and q are the concentrations of the two constituent phases and α and $(1-\alpha)$ are the respective fractional amounts of these two phases.

In Appendix 6.2 we apply combinatorial arguments to the two-phase model and thereby obtain the following expression for the integral two-phase configurational entropy:-

$$-S_{(2)}(\alpha,p,q)/R = \alpha\left[p\ \ell n\ p + (1-p)\ell n(1-p)\right] + (1-\alpha)\left[q\ \ell n\ q + (1-q)\ell n(1-q)\right] + \alpha\ \ell n\ \alpha + (1-\alpha)\ell n(1-\alpha) \qquad (6.13)$$

Taking the appropriate *partial derivatives* and allowing for the mathematical singularities at p=q, p,q=0 and p,q=1 (Appendix 6.2), we obtain the following expressions for the partial two-phase configurational entropy of hydrogen:-

$$-\left[S'_{(2)}(\alpha,p,q)/R\right]_{\substack{p\neq q,\,p,q\neq 0,\\ p,q\neq 1}} = \frac{S_{(1)}(p)-S_{(1)}(q)}{p-q} + \frac{1}{p-q}\,\ell n\,\frac{\alpha}{1-\alpha} + \ell n\,\frac{p}{1-p} + \ell n\,\frac{q}{1-q} \qquad (6.14a)$$

where $S_{(1)}(p) = p\ \ell n\ p + (1-p)\ell n(1-p)$

and $S_{(1)}(q) = q\ \ell n\ q + (1-q)\ell n(1-q)$

$$-\left[S'_{(2)}(\alpha,p,q)/R\right]_{\substack{p=q,\ p,q=0\\ \text{or } p,q=1}} = -S'_{(1)}(x)/R = \ell n\,\frac{x}{1-x} \qquad (6.14b)$$

For our plots of $-S_{(2)}(\alpha,p,q)/R$ and $-S'_{(2)}(\alpha,p,q)/R$ versus x we employ the same (α,p,q) values as were used to obtain the two-phase total electronic energy curve in Figure 5.7.

In Figure 6.2 we show plots of the integral configurational entropies (multiplied by -1) versus x for our one- and two-phase models (equations (6.10) and (6.13) respectively). We observe that the one-phase curve is symmetrical about x = 0.5, whereas this is not so for the two-phase curve which reaches a minimum just below x = 0.5 (cf Figure 9 of Kuii et al[6.3]), in which their *ideal* integral configurational entropy is symmetrical about x = 0.5 whereas their *total* integral entropy curve lacks this symmetry).

Plots of our one- and two-phase partial configurational entropies (multiplied by -1; see equations (6.11) and (6.14) respectively) appear in Figure 6.3, where we note that the one-phase curve is an odd function about x = 0.5 whereas the two-phase curve lacks any such symmetry; we do however observe that both curves pass through zero at x = 0.5. The two-phase values are generally greater in magnitude than the one-phase values by roughly a factor of three; the significance of the greater magnitude of the two-phase values will become evident in Section 6.5.

PRM.SET(A.1)

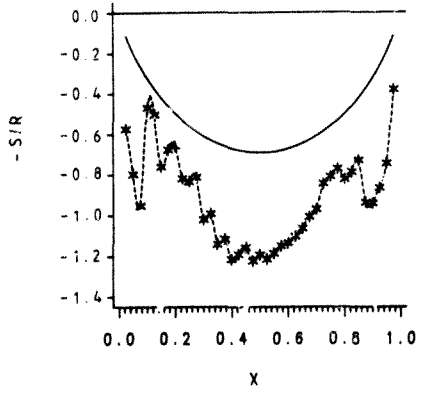

Figure 6.2 Integral configurational entropies vs x for prm.set (a.1). Full curve: one-phase model; broken curve with stars: two-phase model.

PRM.SET(A.1)

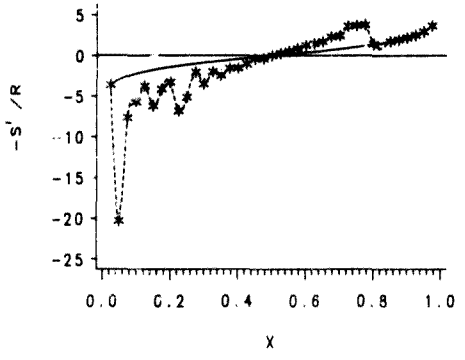

Figure 6.3 Partial configurational entropies vs x for prm.set (a.1). Full curve: one-phase model; broken curve with stars: two-phase model.

3.4.2 *Summary of Section 6.4*

In this section we have derived one- and two-phase entropy expressions with which to model the combined entropy contribution to the semiempirical partial pressure equation (equation (6.7)). We are able to approximate the combined entropy by means of our purely *configurational* one- and two-phase formalisms because we have seen that the entropy of PdH_x is predominantly configurational in nature. The *integral* two-phase entropies are found to be asymmetric about $x = 0.5$ (in qualitative agreement with the experimentally-derived results of Kuji et al[6.3]), while the *partial* two-phase entropies are found to be larger in magnitude than the corresponding one-phase values by roughly a factor of three, the significance of which will be appreciated in Section 6.5.

We are now in a position to write down our one- and two-phase partial pressure equations.

6.5 APPLICATION OF OUR MODELS TO THE SEMIEMPIRICAL EQUATION

6.5.1 Partial pressure Equations

We recall that in Section 6.2 the following semiempirical partial pressure equation was derived:-

$$\ell n(p_{H_2}/p_{atm})^{\frac{1}{2}} = \frac{\Delta\mu_H^o}{RT} + \frac{H_H^E}{RT} - \left[\frac{S_H^E}{R} - \ell n\,\frac{x}{b-x}\right] \qquad (6.7)$$

where we have chosen a b-value of unity and where $p_{atm} = 101.3$ kPa (the various energy terms on the right-hand side being expressed in kJ).

We now subscitute the results of Sections 6.3 and 6.4 into equation (6.7) to obtain one- and two-phase partial pressure equations, viz.:-

ONE-PHASE:-

$$\ell n(p_{H_2})^{\frac{1}{2}} = \ell n(101.3)^{\frac{1}{2}} + \frac{\Delta\mu_H^o}{RT} + \frac{\Delta H^{(1)}(x)}{RT} - \frac{S'_{(1)}(x)}{R} \qquad (6.15)$$

TWO-PHASE:-

$$\ell n(p_{H_2})^{\frac{1}{2}} = \ell n(101.3)^{\frac{1}{2}} + \frac{\Delta\mu_H^o}{RT} + \frac{\Delta H^{(2)}(\alpha,p,q)}{RT} - \frac{S'_{(2)}(\alpha,p,q)}{R} \qquad (6.16)$$

where $\Delta H^{(1)}(x)$ and $\Delta H^{(2)}(\alpha,p,q)$ are given by equations (4.20) and (5.9b) respectively and where $S'_{(1)}(x)$ and $S'_{(2)}(\alpha,p,q)$ are given by equations (6.1') and (6.14) respectively For the partial entropies we employ the values displayed in Figure 6.3, and the heat of formation values are the same as those appearing in Figure 5.8. Our $\Delta\mu_H^o$ data are displayed in Table 6.1 and are taken from Kuji et al[6.3]).

T(K)	$\Delta\mu_H^o$ (kJ mol^{-1}H)
300	7.05
350	9.68
400	12.26
450	14.80
500	17.35

Table 6.1 $\Delta\mu_H^o$ values used in the present study (from Kuji et al[6.3]).

6.5.2 Results and comparison with experiment

It is clear from equations (6.15) and (6.16) that each of our partial pressure formalisms requires us to provide both enthalpic and entropic terms. In order to evaluate the relative importance of these contributions, we plot the isotherms of each model for the case of *zero* partial entropy in addition to $S' \neq 0$. The case of zero entropy (as opposed to zero enthalpy) is considered because entropic considerations are introduced for the first time in this chapter and it is thus of interest to examine their particular contribution.

In Figures 6.4 a-d we present the *one-phase* results; specifically, Figure 6.4a is obtained from equation (6.15) for the case $S'_{(1)}(x) = 0$ and Figure 6.4b for the case of $S'_{(1)}(x) \neq 0$, while Figures 6.4c and d are simply numerically-smoothed versions of Figures 6.4a and b respectively (a combined spline-least-squares fitting routine was employed[6.6]). The *two-phase* isotherms (equation (6.16)) are similarly presented in Figures 6.5a-d, where Figure 6.5a represents the case for which $S'_{(2)}(\alpha,p,q) = 0$,

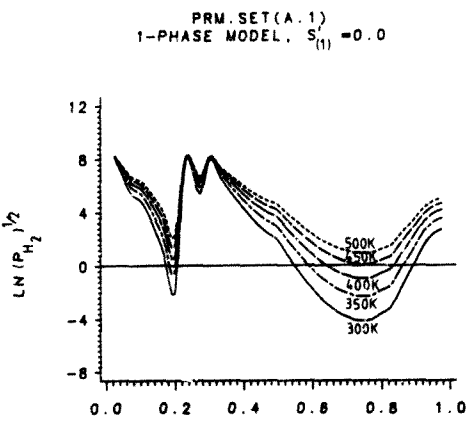

Fig. 6.4a

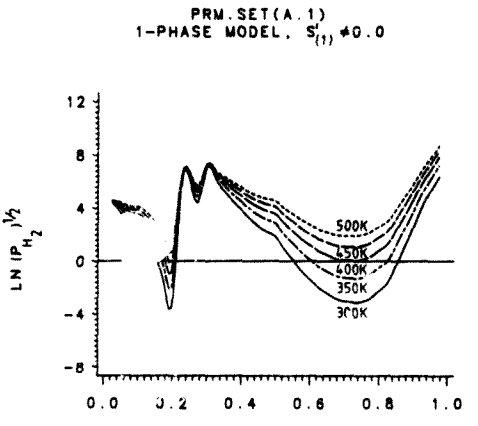

Fig. 6.4b

Figures 6.4a&b Pressure-composition isotherms for the one-phase model, using prm.set (a.1).
Fig.6.4a: zero entropy;
Fig.6.4b: non-zero entropy.

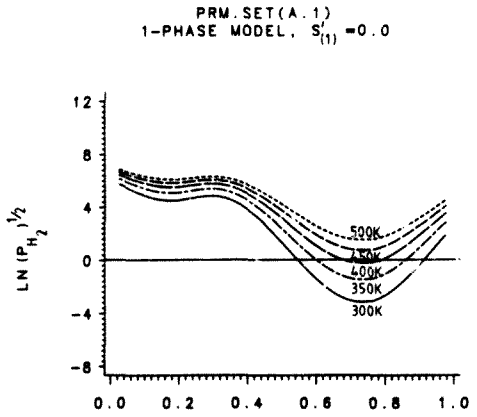

Fig.6.4c

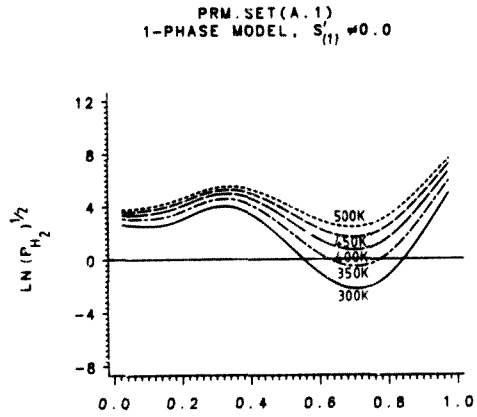

Fig.6.4d

Figures 6.4c&d Pressure-composition isotherms for the one-phase model, using prm.set (a.1).
Fig.6.4c: zero entropy (smoothed isotherms);
Fig.6.4d: non-zero entropy (smoothed isotherms).

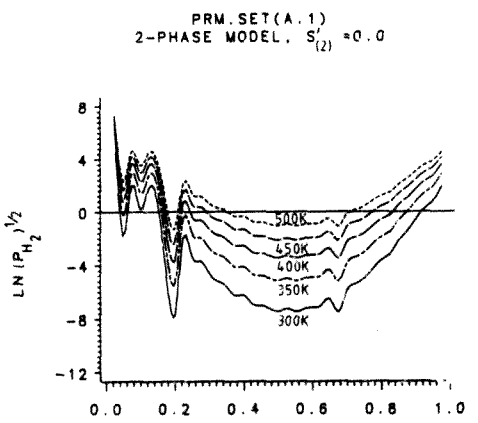

Fig.6.5a

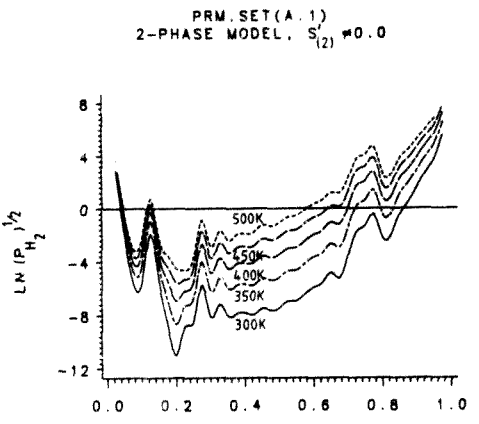

Fig.6.5b

Figures 6.5a&b Pressure-composition isotherms for the two-phase model, using prm.set (a.1).
Fig.6.5a: zero entropy;
Fig.6.5b: non-zero entropy.

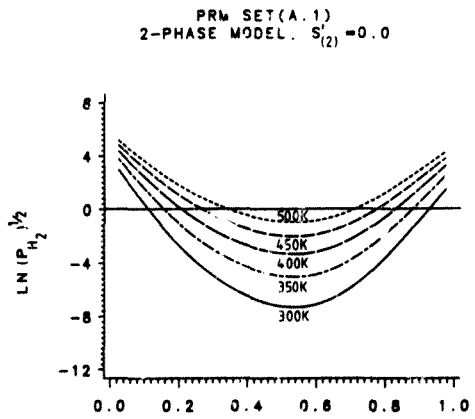

Fig.6.5c

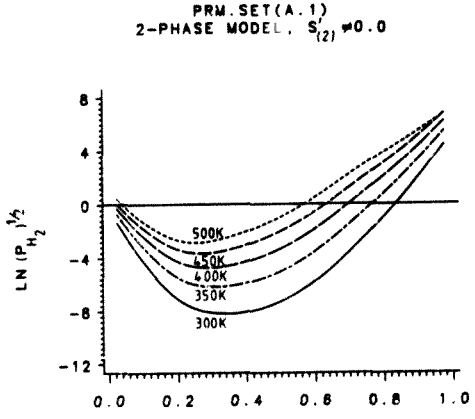

Fig.6.5d

Figures 6.5c&d Pressure-composition isotherms for the two-phase model, using prm.set (a.1).
Fig.6.5c: zero entropy (smoothed isotherms);
Fig.6.5d: non-zero entropy (smoothed isotherms).

Figure 6.5b the case for which $S'_{(2)}(\alpha,p,q) \neq 0$, and where Figures 6.5c and d are the respective smoothed isotherms.

Comparison of Figures 6.4 with the experimental isotherms displayed in Figure 6.1 reveals that the one-phase model breaks down for $x \leq 0.7$, that is over the entire two-phase region $(0.01 \leq x \leq 0.6)$, as we would expect of a single-phase formalism. We notice that for $x \geq 0.7$ the non-zero entropy contribution results in steeper (and hence more acceptable) isotherms than the $S'_{(1)} = 0$ case, thus confirming the validity of including an entropic contribution in our one-phase model.

In contrast to the one-phase findings, we observe from Figures 6.5 that the two-phase isotherms are in substantial qualitative agreement with experiment for $x \geq 0.2$. More specifically we note that the non-zero entropy contribution ($S'_{(2)}$ in this case, see Figure 6.3) again improves the shape of the isotherms, giving a slightly steeper rise for higher x; it also lowers the isotherms in the region $x \leq 0.5$, making them more compatible with the *plateau region* clearly discernible in Figure 6.1. With reference to the case $S'_{(2)} \neq 0$ we have qualitative agreement with experiment in the following specific features:-

- fairly flat regions (known as plateaus) in the isotherms for intermediate x values (corresponding to the two-phase region of the hydride), followed by sharp rises at higher concentrations;

- the isotherms do not cross, and the higher-temperature isotherms always remain above the lower temperature ones;

- the spacing between the isotherms decreases with increasing temperature.

The chief quantitative differences between our two-phase isotherms and experiment have to do with the *depth*, *width* and *absolute position* of the plateau region, and the behaviour for $x \leq 0.2$:-

- *depth of plateau region*. By "depth" we mean the separation between the 300 and 500 K isotherms in the plateau region ($x = 0.5$). By comparing Figures 6.5 and 6.1 we see that our two-phase depth is greater than the experimental one by roughly a factor of two, a difference which is largely attributable to the factor two deviation in our two-phase heats of formation (see Figure 5.8). A comparison of Figures 6.5a and b reveals that the entropic contribution has very little effect on the depth of our two-phase plateau region, confirming that the discrepancy is chiefly enthalpic in origin. To keep this deviation in its proper perspective we should bear in mind that the agreement of our two-phase heats of formation with experiment to within a factor of two or three (Section 5.4.4) is in fact a remarkable achievement in the light of the considerable cancellation effects involved (Section 4.5.3).

- *width of plateau region*. This remains constant for all our isotherms whereas the experimental plateau region diminishes with increasing temperature, disappearing at a well-defined critical temperature. Our model lacks this feature because both our enthalpy and entropy terms are independent of temperature, resulting in isotherms of unvarying shape.

- *absolute positions of isotherms in the plateau region.* Taking our isotherm values at $x \simeq 0.5$ as the rough plateau positions we observe that our plateaus do not coincide with the experimental ones; this is partly a consequence of the greater depth of our plateau region discussed above, which causes our isotherms to be more spread out than the empirical ones. The fact that our plateaus are not completely flat is a further source of error in that the actual plateau position cannot be unambiguously defined; we note from a comparison of Figures 6.5a and b that the entropy term has a considerable influence on the flatness of the plateaus (although we have seen that it does not significantly affect the *depth* of the plateau region). We finally point out that our theoretical isotherms need to be lowered by a *constant* term ($\ln(p_{atm})^{\frac{1}{2}} \simeq 2.31$, see equation (6.16)) when comparing them with the experimental isotherms of Figure 6.1.

- *behaviour at low x.* Figures 6.5 indicate that our two-phase model breaks down for $x \lesssim 0.2$ in that it does not predict the sharp downswing in the isotherms at low x revealed by experiment (Figure 6.1). Comparison of Figures 6.5c and d (or Figures 6.5 a and b) shows that the presence of the non-zero two-phase entropy term *noticeably improves* our model at low x, suggesting that the enthalpic contribution is at fault in this concentration range. Indeed it is clear from Figure 5.8 that although our two-phase heat of formation model is distinctly better than its one-phase counterpart, it nevertheless exhibits considerable instabilities at low x, including physically-incorrect endothermic behaviour for certain concentrations. Thus the partial pressure isotherms

simply highlight the fact that our heat of formation models are least successful in the low-concentration regime.

6.5.3 Thermodynamic stability of two-phase Model

Finally we briefly report on some observations related to the stability of PdH_x as a function of temperature. Our two-phase theory (see equation (6.16)) gives us:-

$$\Delta\mu_H = \Delta\mu_H^o + \Delta H^{(2)} - TS'_{(2)} \qquad (6.17)$$

In Figures 6.6 we show smoothed isotherms of $\Delta\mu_H$ versus x calculated using equation (6.17) and with prm.set (a.1); we recall from Section 3.7 that this set constitutes the best choice of interaction parameters. In particular we compare $\Delta\mu_H$ for the case of zero two-phase entropy (Figure 6.6a) with that of non-zero two-phase entropy (Figure 6.6b).

The important point is that the system is *exothermic* (and hence *stable*) when $\Delta\mu_H < 0$ while being *endothermic* (and therefore *unstable*) for $\Delta\mu_H > 0$. We are thus interested in concentrations at which $\Delta\mu_H = 0$; these can readily be obtained from Figures 6.6 and are displayed in Table 6.2 along with some experimental values deduced from Noji et al[6.3].

Our theoretical results indicate firstly that the hydride becomes *less* stable with increasing temperature (that is the isotherms become less negative, see Figures 6.6) and secondly that the highest stable concentration attainable decreases with increasing temperature (Figures 6.6 and Table 6.2); both these observations are physically sound because we expect that for a given value of x the hydride will become less stable as its thermal energy (which is proportional to temperature) increases. Furthermore, our

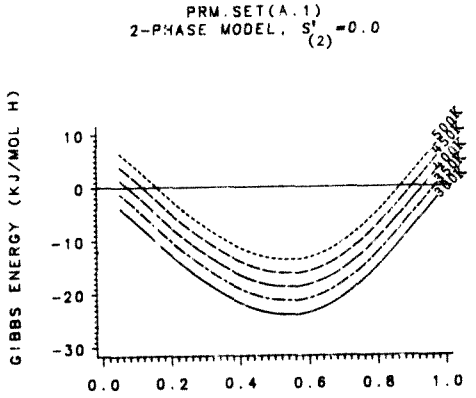

Fig.6.6a

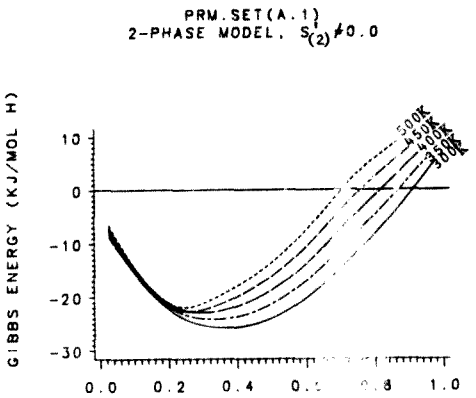

Fig.6.6b

Figures 6.6a&b Isotherms of Gibbs energy vs x for the two-phase model, using prm.set (a.1).
Fig.6.6a: zero entropy (smoothed isotherms);
Fig.6.6b: non-zero entropy (smoothed isotherms).

T(K)	x ($\Delta\mu_H$ = 0)		
	2-phase theory, prm. set (a.1)		Experiment
	$S'_{(2)} = 0$	$S'_{(2)} \neq 0$	(Kuji et al[6.3], Fig.4)
300	∿1.0	0.91	∿0.8
350	0.97	0.87	-
400	0.94	0.82	∿0.6
450	0.90	0.76	-
500	0.87	0.70	-

Table 6.2 Concentrations (x > 0.5 only) below which the PdH_x system is exothermic, as a function of temperature.

theoretical predictions are in reasonable agreement with the experimental results of Kuji et al[6.3] (see their Figure 4 and our Table 6.2), our *non-zero* two-phase entropy model again proving superior to our zero-entropy formalism (Table 6.2). Our two-phase theoretical model is thus once again consistent with experiment.

6.5.4 *Summary of Section 6.5*

We have derived one- and two-phase partial pressure equations, finding that the one-phase formalism generates incorrect isotherms over the entire two-phase concentration region, while the two-phase model is qualitatively correct for x ≥ 0.2. Specifically, the two-phase isotherms have a fairly flat plateau region followed by a sharper rise at higher values of x, and the isotherms do not cross but become more closely packed with increasing temperature.

For both one- and two-phase models the isotherms were also plotted for the case of *zero* configurational entropy, resulting in a shallower rise at high concentrations and an elevation of the isotherms for lower x; because both these changes lead to physically less-satisfactory results, the present calculations reveal that the configurational entropy plays an important part in our partial pressure models.

The two-phase formalism is *quantitatively* inaccurate in the following respects: firstly, its plateau region is too deep by a factor of two, corresponding closely to a similar discrepancy in our two-phase heat of formation curve; secondly, its plateau region is constant in width (instead of diminishing as temperature increases) because our heats of formation and entropies are temperature-independent; thirdly, the absolute positions of the isotherm plateaus are incorrect because our two-phase heat of formation curve differs from experiment in both shape and depth, and possibly also because of inaccuracies in the concentration-independent terms of our two-phase equation; and fourthly, the two-phase model breaks down for $x \leq 0.2$ as a consequence of instabilities in the corresponding heat of formation in the low x regime.

Finally, we find that the temperature dependence of the stability of the hydride follows experimentally-established trends.

6.6 SUMMARY OF CHAPTER 6

We have successfully employed our two-phase model for the heat of formation of PdH_x (described in Chapter 5) to obtain pressure-composition isotherms in substantial qualitative agreement with experiment. This was achieved by applying our formalism to a standard thermodynamic equation for the partial pressure of hydrogen gas in equilibrium with PdH_x; specifically, we were required to provide enthalpic and entropic contributions for this expression.

We firstly demonstrated a number of similarities between our heats of formation and the enthalpy results employed by Kuji and coworkers in their partial pressure formalism; hence we chose to model the enthalpic contribution to the partial pressure equation by means of our one- and two-phase heats of formation.

We next established that the entropic contribution is predominantly configurational in nature, and so proceeded to derive one- and two-phase configurational entropy expressions to model this contribution.

To complete our models we made use of standard chemical potential data provided by Kuji and coworkers.

We have found that our one-phase partial pressure equation produces incorrect isotherms for $x \lesssim 0.7$, that is, over the entire two-phase region of the hydride, as would be expected for a single-phase formalism. However our two-phase results are in qualitative agreement with experiment for $x \gtrsim 0.2$. In particular we notice that the presence of the configurational entropy term improves the shape of the isotherms at high and low x. The

quantitative shortcomings of the two-phase isotherms are closely related to discrepancies between the depth and shape of our two-phase heat of formation curve and the experimental results, and also to the lack of temperature dependence in both our heat of formation and entropy expressions. The breakdown in the two-phase model for $x \leq 0.2$ correlates closely to instabilities in the corresponding heats of formation for this concentration range.

Finally, the temperature dependence of the thermodynamic stability of the hydride is found to follow experimental trends.

In this chapter we have demonstrated the qualitative applicability of both our two-phase heat of formation model and our two-phase configurational entropy expression to the experimentally well-known pressure-composition isotherms of PdH_x; we have also confirmed that our two-phase formalism is of wider applicability than its one-phase counterpart.

APPENDIX 6.1

IDEAL CONFIGURATIONAL ENTROPIES

Consider a metal hydride MH_x consisting of one mole of metal atoms, with b interstitial sites available per atom (we assume $b > x$). This gives us $N_A b$ interstitial sites with $N_A x$ hydrogen atoms available to occupy them (where N_A is Avogadro's number). The total number of possible configurations is obtained in the usual combinatorial manner as follows:-

$$W = \binom{N_A b}{N_A x} = \frac{(N_A b)!}{(N_A b - N_A x)!\,(N_A x)!} \qquad (A6.1.1)$$

The ideal configurational entropy is given by:-

$$S = k_B \ln W \qquad (A6.1.2)$$

where k_B is Boltzmann's constant.

Further, for large integers n we obtain the following simplifying equation via Stirling's approximation:-

$$\ln(n!) \simeq n \ln n - n \qquad (A6.1.3)$$

Substituting equation (A6.1.1) into equation (A6.1.2) and using equation (A6.1.3) gives us the following entropy expression:-

$$S = k_B \left[(N_A b)\ell n(N_A b) - (N_A b) - (N_A b - N_A x)\ell n(N_A b - N_A x) + \right.$$

$$\left. + (N_A b - N_A x) - (N_A x)\ell n(N_A x) + (N_A x)\right]$$

$$= - k_B N_A \left[x \ell n\, x - b \ell n\, b + (b-x)\ell n(b-x)\right] \qquad (A6.1.4)$$

Noting that the ideal gas constant $R = k_B N_A$ we rewrite equation (A6.1.4) as follows to obtain our expression for the ideal *integral* configurational entropy per mole of *metal* atoms:-

$$S(x)/R = - \left[x \ell n\, x - b \ell n\, b + (b-x)\ell n(b-x)\right] \qquad (A6.1.5)$$

We finally evaluate the ideal *partial* configurational entropy per mole of *hydrogen* atoms by taking the *derivative of S(x) with respect to x*, giving us the following expression:-

$$S'(x)/R = - \ell n \frac{x}{b-x} \qquad (A6.1.6)$$

APPENDIX 6.2

TWO-PHASE CONFIGURATIONAL ENTROPIES

In deriving our two-phase entropy expression we use the combinatorial approach of Appendix 6.1 in conjunction with the following equation from our two-phase model:-

$$PdH_x = \alpha\ PdH_p + (1-\alpha)PdH_q \qquad (A6.2.1)$$

which is equivalent to:-

$$x = \alpha p + (1-\alpha)q \qquad (A6.2.2)$$

We start by assuming that the parameter b of Appendix 6.1 has the value b=1, as expected for an ideal fcc palladium lattice with only octahedral interstitial sites available for occupation; thus for a mole of palladium atoms there are N_A interstitial sites available for occupation by $N_A x$ hydrogen atoms.

We must now evaluate the total number of ways of distributing these hydrogen atoms between the two phases of concentrations p and q as well as amongst the N_A available sites.

Firstly, with reference to equations (A6.2.1) and (A6.2.2) we see that the number of ways of partitioning the N_A sites between the two phases is given by:-

$$\binom{N}{\alpha N} = \frac{N!}{[(1-\alpha)N]![\alpha N]!} \qquad (A6.2.3)$$

where we have dropped the subscript from N_A.

Secondly, the number of ways of distributing "p"-phase atoms amongst the αN sites available to this phase is obtained as follows:-

$$\binom{\alpha N}{\alpha p N} = \frac{(\alpha N)!}{[\alpha(1-p)N]!(\alpha p N)!} \qquad (A6.2.4)$$

and similarly, the number of ways of distributing the "q"-phase atoms amongst the $(1-\alpha)N$ sites available to this phase is given by:-

$$\binom{(1-\alpha)N}{(1-\alpha)qN} = \frac{[(1-\alpha)N]!}{[(1-\alpha)(1-q)N]![(1-\alpha)qN]!} \qquad (A6.2.5)$$

With reference to equations (A6.2.3), (A6.2.4) and (A6.2.5) we obtain the following expression for the *total* number of ways of distributing "p"-phase and "q"-phase atoms amongst the N available sites:-

$$W = \frac{N!}{(\alpha p N)![\alpha(1-p)N]![(1-\alpha)qN]![(1-\alpha)(1-q)N]!} \qquad (A6.2.6)$$

Hence

$$\ell nW = \ell n(N!) - \{\ell n(\alpha pN)! + \ell n[\alpha(1-p)N]! + \ell n[(1-\alpha)qN]! + \ell n[(1-\alpha)(1-q)N]!\} \qquad (A6.2.7)$$

Now by Stirling's approximation we have:-

$$\frac{1}{N}\ell n(\alpha pN)! \simeq \alpha p \ell n \alpha p - \alpha p + \alpha p \ell n N \qquad (A6.2.8)$$

so that by substituting equation (A6.2.8) and similar expressions into equation (A6.2.7) we obtain:-

$$\frac{1}{N} \ln W = \ln N - 1 - \left[\alpha p \ln \alpha p + \alpha(1-p) \ln \alpha (1-p) + \right.$$

$$\left. + (1-\alpha)q \ln (1-\alpha)q + (1-\alpha)(1-q) \ln (1-\alpha)(1-q)\right]$$

$$- \left[\alpha p + \alpha(1-p) + (1-\alpha)q + (1-\alpha)(1-q)\right](\ln N-1) \quad \text{(A6.2.9)}$$

$$\text{Now } \alpha p + \alpha(1-p) + (1-\alpha)q + (1-\alpha)(1-q) = \alpha + (1-\alpha) = 1 \quad \text{(A6.2.10)}$$

Substituting equation (A6.2.10) into equation (A6.2.9) and simplifying the resultant expression gives us the following formula for our two-phase *integral* configurational entropy per mole of palladium atoms:-

$$S_{(2)}(\alpha,p,q)/R = - \{\alpha\left[p \ln p + (1-p)\ln(1-p)\right] +$$

$$+ (1-\alpha)\left[q \ln q + (1-q)\ln(1-q)\right] + \alpha \ln \alpha + (1-\alpha)\ln(1-\alpha)\}$$

(A6.2.11)

where $R = k_B N_A$.

We observe that equation (A6.2.11) consists of a weighted sum of one-phase entropy terms in p and q (each term being analogous to equation (A6.1.5) for the case b=1), as well as a similar expression in α.

As in Appendix 6.1 we next evaluate the *partial* entropy per mole of *hydrogen* atoms, by taking the *derivative* of $S_{(2)}(\alpha,p,q)$ *with respect to* x:-

$$\frac{\partial s}{\partial x} = \left(\frac{\partial s}{\partial \alpha}\right)_{p,q}\left(\frac{\partial \alpha}{\partial x}\right)_{p,q} + \left(\frac{\partial s}{\partial p}\right)_{\alpha,q}\left(\frac{\partial p}{\partial x}\right)_{\alpha,q} + \left(\frac{\partial s}{\partial q}\right)_{\alpha,p}\left(\frac{\partial q}{\partial x}\right)_{\alpha,p}$$

(A6.2.12)

where we have dropped the subscript from $S_{(2)}$.

By referring to equation (A6.2.2) we obtain the following partial derivatives:-

$$\left(\frac{\partial x}{\partial \alpha}\right)_{p,q} = p-q$$

$$\left(\frac{\partial x}{\partial p}\right)_{\alpha,q} = \alpha$$

$$\left(\frac{\partial x}{\partial q}\right)_{\alpha,p} = 1-\alpha$$

which when substituted into equation (A6.2.12) give :-

$$\frac{\partial s}{\partial x} = \frac{1}{p-q}\left(\frac{\partial s}{\partial \alpha}\right)_{p,q} + \frac{1}{\alpha}\left(\frac{\partial s}{\partial p}\right)_{\alpha,q} - \frac{1}{1-\alpha}\left(\frac{\partial s}{\partial q}\right)_{\alpha,p} \qquad \text{(A6.2.13)}$$

where we assume $p \neq q$.

Now we refer to equation (A6.2.11) to evaluate the following partial derivatives:-

$$\left(\frac{\partial s}{\partial \alpha}\right)_{p,q}/R = -\left\{\left[p \ln p + (1-p)\ln(1-p)\right] - \left[q \ln q + (1-q)\ln(1-q)\right] + \right.$$

$$\left. + \ln\frac{\alpha}{1-\alpha}\right\}$$

$$\left(\frac{\partial s}{\partial p}\right)_{\alpha,q}/R = -\alpha \ln\frac{p}{1-p}$$

$$\left(\frac{\partial s}{\partial q}\right)_{\alpha,p}/R = -(1-\alpha)\ln\frac{q}{1-q}$$

We substitute these into equation (A6.2.13) to obtain the following expression:-

$$(\frac{\partial s}{\partial x})/R = - \{ \frac{S_{(1)}(p) - S_{(1)}(q)}{p-q} + \frac{1}{p-q} \ln \frac{\alpha}{1-\alpha} +$$

$$+ \ln \frac{p}{1-p} + \ln \frac{q}{1-q} \} \text{ for } p \neq q \qquad \text{(A6.2.14)}$$

where $S_{(1)}(p) = p \ln p + (1-p)\ln(1-p)$

and $S_{(1)}(q) = q \ln q + (1-q)\ln(1-q)$ (A6.2.15)

Now equation (A6.2.2) gives us:-

$$\alpha = \frac{x-q}{p-q} \qquad \text{(A6.2.16)}$$

We see from this equation that α and hence the two-phase model is not well-defined for p=q. However, it is clear from equation (A6.2.1) that p=q corresponds to our one-phase model, for which the partial configurational entropy is known (Appendix 6.1).

Using the notation $S'_{(2)}(\alpha,p,q) = \partial s/\partial x$, we can now rewrite and extend equation (A6.2.14) to give us our final expression for the two-phase partial configurational entropy per mole of hydrogen atoms:-

$$\left[S'_{(2)}(\alpha,p,q)/R\right]_{\substack{p\neq q,\ p,q\neq 0,\\ p,q\neq 1}} = - \{ \frac{S_{(1)}(p) - S_{(1)}(q)}{p-q} + \frac{1}{p-q} \ln \frac{\alpha}{1-\alpha} +$$

$$+ \ln \frac{p}{1-p} + \ln \frac{q}{1-q} \} \qquad \text{(A6.2.17a)}$$

where $S_{(1)}(p)$ and $S_{(1)}(q)$ are given by equations (A6.2.15);

$$\left[S'_{(2)}(\alpha,p,q)/R\right]_{\substack{p=q,\ p,q\neq 0,\\ p,q\neq 1}} = S'_{(1)}(x)/R = - \ln \frac{x}{1-x} \qquad \text{(A6.2.17b)}$$

where we have used equation (6.11); and

$$\left[S'_{(2)}(\alpha,p,q)/R\right]_{\substack{p,q=0 \text{ or}\\ p,q=1}} \equiv S'_{(1)}(x)/R = - \ln \frac{x}{1-x} \qquad \text{(A6.2.17c)}$$

We comment that equation (A6.2.17c) is *defined* purely for computational convenience; however it is *not* physically sound, because both a hydrogen-free phase (say p=0) and a stoichiometric phase (say p=1) would for general x (say $0 < x < 1$) result in a *two-phase* hydride ($p < x < q$ for the p=0 case and $- < x < p$ for the p=1 case). For *prm.set (a.1)* we have p=0 for x=0.0 and 0.025 and p=1 for all our x values between 0.85 and 1.0 inclusive; hence the first star and the last six stars on the broken curve of Figure 6.3 should strictly be ignored. A rough estimate of the *true* derivatives at these points can be obtained by taking the *gradient* of the broken curve in Figure 6.2 at the same x values.

In examining Figures 6.5 we should therefore bear in mind that the first data point (corresponding to $x = 0.025$) and the data points for $x \geq 0.85$ are not strictly correct. Specifically, by examining the gradient at these x values in Figure 6.2, we expect the first point to be somewhat lower and the points for $x \geq 0.9$ to be somewhat higher, but we comment that any such corrections would make very little difference to the overall trend of the data.

REFERENCES (CHAP. 6)

6.1) Wicke E and Brodowsky H 1978 *Hydrogen in Palladium and Palladium Alloys* in *Topics in Appl. Phys.* 29 73 (Ed.s: Alefeld G and Völkl J; publ.: Springer-Verlag)

6.2) Oates W A 1982 *J. Less-Common Met.s* 88 411

6.3) Kuji T, Oates W A, Bowerman B S and Flanagan T B 1983 *J. Phys. F: Met. Phys.* 13 1785

6.4) Harada S 1983 *J. Phys. F: Met. Phys.* 13 607

6.5) Boureau G 1984 *J. Phys. Chem. Solids* 45 973

6.6) *SAS/GRAPH User's Guide* 1981 pp.15-16 (SAS Institute Inc.)

CHAPTER 7

CONCLUSION

We have noted that the various theoretical approaches to non-stoichiometric palladium hydride usually belong to one of two distinct categories, namely *semiempirical formalisms* on the one hand and *band structure techniques* on the other. In the first category we have models characterized by physically-transparent simplifying assumptions and based on experimental results (for example the so-called Rigid Band Model); their chief shortcoming is that they are in general oversimplistic and hence have only limited ranges of physical validity. At the other extreme we have the band structure methods (for example the APW and KKR techniques) in which the one-electron Schrödinger equation is accurately solved for the case of a periodic crystal potential; these approaches have three important shortcomings: firstly, they require very considerable computational resources; secondly, their results are expressed in terms of interpolation schemes which require large numbers of fitting parameters; and thirdly, they are based on the assumption that the solid has a perfect crystalline structure (that is, *long-range order*), which is not the case for *random* systems such as non-stoichiometric metal hydrides.

In response to these physical shortcomings and computational restrictions we have formulated a *Cluster-Bethe-Lattice* model for non-stoichiometric metal hydrides which incorporates the following appealing features: firstly, it models the hydride from the viewpoint of *local environment* and *short-range order* instead of long-range order; secondly, it results

in *closed, analytical* expressions for the *Local Densities of States* which give us considerable insight into the *band structure* of the hydride as well as facilitating extensive electronic energy calculations; thirdly, it requires only a few *physically-meaningful parameters;* and fourthly, the model allows us to develop a physically-transparent formalism for the *multiphase nature* of the hydride. Our Local Densities of States are found to be in good agreement with the essential features of both *band structure calculations* and *photoemission spectroscopy results,* giving us confidence in the physical applicability of our model.

In the present work we have concentrated on evaluation of the experimentally-accessible *heat of formation* of PdH_x ($0 \leq x \leq 1$), thereby retaining the emphasis of our papers on this metal hydride[4.12),5.1),5.3)]. Specifically, we have found that our *one-phase* model[4.12)] generates heats of formation which agree quite well with experiment for $x \geq 0.5$ though not for $x \leq 0.5$. However our *two-phase* heats of formation[5.1)] are seen to improve on the one-phase results for $x \leq 0.5$, while remaining substantially the same for $x \geq 0.7$. It is important to recall at this stage that at room temperature PdH_x consists of *two coexisting phases* for $0.01 \leq x \leq 0.6$ and of only one phase (the β-phase) for $x \geq 0.6$. Now we have found that our one- and two-phase models for the heat of formation are in good agreement with each other and with experiment in the β-phase region, while only the two-phase model is successful over the two-phase concentration range; we thus infer that our models are consistent with experiment.

Further, our one-phase model is based on the assumption that hydrogen is *randomly* distributed in the palladium lattice[4,12], and its success for higher concentrations suggests that the β-phase exhibits randomness in its *microscopic* structure. Similarly, the applicability of the two-phase model for intermediate values of x suggests that the microscopic structure of the hydride in the two-phase regime is characterized by some sort of ordering process, possibly resulting in *segregated* forms of each phase.

A *segregation parameter*[5,3] has also been defined in the context of our two-phase model, and this gives a qualitatively successful prediction of the *phase transition* at the lower end of the β-phase.

We have concluded the present work with an application of our formalisms to the *thermodynamics* of non-stoichiometric palladium hydride. One- and two-phase configurational entropy expressions have been derived and substituted, together with the corresponding heats of formation, into a semiempirical partial pressure equation. It is found that our one-phase model is only successful in the high-concentration β-phase regime, breaking down in the two-phase region as would be expected of a single-phase approach. However our *two-phase* partial pressure isotherms are in substantial qualitative agreement with experiment for $x \geq 0.2$, the breakdown at lower x being closely linked to instabilities in our two-phase heat of formation curve for $x \leq 0.2$. We have established that our *entropy contributions* play an important role in producing isotherms of the correct shape, particularly at the higher and lower extremes of concentration.

Our two-phase model for the thermodynamic stability of palladium hydride is also found to generate isotherms in reasonable agreement with experimental trends, in particular presenting some indication of the concentrations at which the hydride becomes unstable.

In short the inclusion of temperature dependence has confirmed that our two-phase formalism is of wider applicability than its one-phase counterpart, and has also revealed the importance of entropic effects.

Despite the notable successes already achieved in the present work there are nevertheless opportunities for the improvement and extension of our two-phase model. For example, our present formalism seems to break down for $x \leq 0.2$; if this shortcoming could be rectified we would be in a position to examine the *microscopic nature* of the α-*phase* ($0 < x \leq 0.01$ at room temperature). Another potential refinement is the inclusion of *vibrational terms* in our entropy theory and maybe even in our heat of formation expressions. Further, it should be possible to extend our model to other non-stoichiometric transition metal hydrides (such as nickel hydride), and perhaps to refractory metal carbides.

In summary, we have employed the Cluster-Bethe-Lattice technique to model various electronic features of non-stoichiometric palladium hydride, finding in particular that our two-phase formalism generates Local Densities of States, heats of formation and pressure-composition isotherms all in substantial qualitative agreement with experiment.

APPENDIX 1

REVIEW OF SLATER-KOSTER INTERPOLATION SCHEME (See Section 3.3)

Slater and Koster[A1.1] work within an LCAO (Linear Combination of Atomic Orbitals) formalism, which is based on the assumption that wave functions in a periodic solid can be well approximated to by linear combinations of the isolated atomic wave functions. Specifically, consider a set of atomic orbitals $\{\phi_l(\underline{r} - \underline{R}_j)\}$, where l refers to the orbital type (for example 4d) and $\underline{R}_j$ indicates the position of the particular atom; we note that these are strictly localized states, and hence that the LCAO approximation has inherently *local* properties. To remove the localization associated with $\phi_l(\underline{r}-\underline{R}_j)$, we take the so-called *Bloch sum* B_l :-

$$B_l(\underline{k}) = \sum_j e^{i\underline{k}\cdot\underline{R}_j}\phi_l(\underline{r}-\underline{R}_j) \qquad \text{(A1.1)}$$

where the sum is strictly over the entire lattice, that is, B_l is highly delocalized. Secondly we take a weighted sum of all the Bloch sums B_l to obtain the LCAO wave function in its fullest form, *viz.*:-

$$\psi_{LCAO}(\underline{k}) = \sum_l a_l B_l(\underline{k}) \qquad \text{(A1.2a)}$$

or

$$\psi_{LCAO}(\underline{k}) = \sum_{l,j}\left[a_l e^{i\underline{k}\cdot\underline{R}_j}\right]\phi_l(\underline{r}-\underline{R}_j) \qquad \text{(A1.2b)}$$